AN EXPERIMENTAL AND A NUMERICAL INVESTIGATION OF A HIGH PRESSURE DIE CASTING ALUMINIUM ALLOY

by

Özlem Boydak

B.S., Mechanical Engineering, Yıldız Technical University, 2003

B.S., Electrical Engineering, Yıldız Technical University, 2004

Submitted to the Institute for Graduate Studies in
Science and Engineering in partial fulfillment of
the requirements for the degree of
Master of Science

Graduate Program in Mechanical Engineering

Boğaziçi University

2007

ACKNOWLEDGEMENTS

I would like to thank to Professor Mahmut A. Savaş, my thesis advisor, for his invaluable help and guidance.

I also would like to thank to Okan Deniz, the general manager of Çelikel High Pressure Die Casting Company, for his permission to use their Magmasoft programme. Also, I would like to thank to Professor İbrahim Yusufoğlu, the Dean of Engineering Faculty of İstanbul University, for his invaluable help and contact to Çelikel Company. Additionally, I wish to thank to Dr. Derya Dışpınar, the assistant of Prof. İbrahim Yusufoğlu, for his help and guidance during simulations. Moreover, I wish to thank to Mustafa Ekelik, the Magmasoft operator in the Çelikel Company, for teaching me the basic properties of the Magmasoft programme. Furthermore, I would like to thank to Uğur Osman Bozer, the prior thesis student of my professor, for his invaluable help and guidance during my experimental work.

Besides, I am grateful to my dear family for their understanding and support during my thesis work.

ABSTRACT

AN EXPERIMENTAL AND A NUMERICAL INVESTIGATION OF A HIGH PRESSURE DIE CASTING ALUMINIUM ALLOY

In the present study, a computer simulation of a high pressure die casting of aluminium alloy was performed using a sophisticated commercial software called Magmasoft and, then its results were compared with the real castings of the same aluminium alloy. The commercial aluminium alloy was Etial 150 (AlSi12Cu) that was used for a flange which was a washing machine part.

Mould filling, solidification, temperature distribution, temperature profile, air entrapment, and velocity of the liquid metal during die casting was investigated using the modelling. After this numerical model, an experimental study was carried out. The actual mould was manufactured and the alloy above was cast in the high pressure die cast machine. Comparing the experimental results with theoretical model, the microstructure and mechanical properties of the casting was discussed with the help of tensile and hardness testing specimens, and microstructure of these specimens.

Additionally, Etial 150 alloy was squeeze cast in the Material Laboratory of Mechanical Engineering Department of Boğaziçi University. Four specimens were melted at 700°C, and they were squeezed in the squeeze casting set-up under 100 MPa presssure. The temperature of the die and punch was 300°C for three castings and it was 400°C for the last casting for comparison. Moreover, six specimens of Etial 150 alloy were unsqueezely cast to the same die at 400°C. Furthermore, six more specimens of Etial 150 alloy were also unsqueezely cast to the 20°C die. All these specimens were analyzed with tensile testing, hardness testing, and microstructural investigation. Finally, all of the results were interpreted.

ÖZET

YÜKSEK BASINÇLI ALÜMİNYUM ALAŞIMI DÖKÜMÜNÜN DENEYSEL VE NÜMERİK BİR İNCELEMESİ

Bu yüksek lisans tezi çalışmasında, gelişmiş ticari bir yazılım olan Magmasoft döküm simulasyon programı kullanılarak bir alüminyum alaşımının yüksek basınçlı dökümünün simulasyonu yapılmış ve bu simulasyon aynı alüminyum alaşımının gerçek dökümü ile karşılaştırılmıştır. Ticari alüminyum alaşımı, bir çamaşır makinası parçası olan flanş için kullanılan Etial 150 (AlSi12Cu) dir.

Öncelikle, dökülecek parçanın şekli kullanılarak modelleme yapıldı. Bu modelleme ile yüksek basınçlı döküm boyunca kalıp dolumu, sıvı metalin hızı, sıcaklık dağılımı, sıcaklık profili, hava kapılması ve katılaşma incelendi.

Nümerik modelleme yapıldıktan sonra deneysel çalışma da yapıldı. Gerçek kalıp üretildi ve Etial 150 yüksek basınçlı döküm makinası SC_550'de döküldü. Teorik model ile deneysel döküm sonuçlarını karşılaştırmak üzere dökümün içyapı ve mekanik özellikleri araştırıldı.

Bunun yanında, Boğaziçi Üniversitesi Makine Mühendisliği Malzeme Laboratuarında Etial 150 alaşımına sıkıştırma döküm uygulandı. Dört numune 700°C'de ergitilip hidrolik pres ile 100 MPa basınçta sıkıştırıldı. Kalıp ve zımbanın sıcaklıkları ilk üç sıkıştırma döküm için 300°C ve dördüncü dökümde daha optimum bir sonuç için 400°C'de tutuldu. Ayrıca, altı Etial 150 numunesi 400°C'lik kalıpta sıkıştırılmadan döküldü. Altı Etial 150 numunesi de 20°C'lik kalıba sıkıştırılmadan döküldü. Bütün bu numuneler çekme testi, sertlik testi ve içyapı fotoğrafları ile analiz edildi. Bir genelleme yapabilmek üzere tüm sonuçlar karşılaştırmalı olarak irdelendi.

TABLE OF CONTENTS

LIST OF FIGURES

LIST OF TABLES

LIST OF SYMBOLS / ABBREVATIONS

B	Chvorinov constant
C	Number of components
C^i	Specific heat of the particle
C_o	Composition
C^P	Specific heat of the particles
d	Density
d_1	Primary dendrite arm spacing
d_2	Secondary dendrite arm spacing
D^M	Density of the melt
g	Gravitational acceleration
L	Liquid phase
L_f	Latent heat of fusion (J/kg)
P	Applied pressure (MPa)
P_C	Cutting force
P_h	Compressive force
P_n	Shear force
P_R	Resultant force
P_t	Thrust force
R_k	Material ratio curve parameter (μm)
R_{max}	Largest peak to valley height (mm)
R_Z	Average height of profile (μm)
r	Radius
r_c	Cutting ratio
S	Surface area of the casting
T	Temperature
T_E	Melting point
T_f	Equilibrium freezing temperature (K)
T_1	Liquidus temperature of the alloy
T_m	Monotectic temperature
T_s	Solidus temperature of the alloy

t_s	Total solidification time
V	Volume of the casting
V_1	Specific volume of the liquid
V_S	Specific volume of the solid
X	Some parameter of x
α	Solid phase
ΔH_f	Latent heat of fusion
ΔT	Temperature difference due to applied pressure
$\varepsilon_f\%$	Elongation at fracture
ϕ	Outer dimension of the test bar
μ	Viscosity
θ	Clearance angle
ρ	Calculated density
σ_{ts}	Tensile strength (N/mm^2)
σ_{uts}	Ultimate tensile strength (N/mm^2)
σ_{ys}	Yield strength (N/mm^2)
$\sigma_{0.2}$	Yield strength
σ_f	Fracture strength
ν	Cutting speed (m/min)
AlSi12Cu	Etial 150 Aluminum Silicon Alloy
ASTM	American Society for Testing of Materials
DC	Direct Casting
F	Forging
HPDC	High Pressure Die Casting
Magma	Magmasoft casting simulation programme
MagmaHPDC	Magmasoft High Pressure Die Casting simulation module
MagmaLPDC	Magmasoft Low Pressure Die Casting simulation module
MagmaTHIXO	Magmasoft Thixo Forming casting module
MMC	Metal Matrix Composite
ZA-27	Zinc-27 %wt Aluminum Alloy

1. INTRODUCTION

Die casting is a versatile process for producing engineered metal parts by forcing molten metal under high pressure into reusable steel molds. These molds, called dies, can be designed to produce complex shapes with a high degree of accuracy and repeatability. Die castings are among the highest volume, mass-produced items manufactured by the metalworking industry. Die cast parts are important components of products ranging from automobiles to toys.

Each of the metal alloys available for die casting offer particular advantages for the completed part. Zinc - The easiest alloy to cast, it offers high ductility, high impact strength and is easily plated. Zinc is economical for small parts, has a low melting point and promotes long die life [1].

Aluminum alloys are lightweight, while possessing high dimensional stability for complex shapes and thin walls. Aluminum has good corrosion resistance and mechanical properties, high thermal and electrical conductivity, as well as strength at high temperatures.

Dies, or die casting tooling, are made of alloy tool steels in at least two sections, the fixed die half, or cover half, and the ejector die half, to permit removal of castings. Modern dies also may have moveable slides, cores or other sections to produce holes, threads and other desired shapes in the casting. Sprue holes in the fixed die half allow molten metal to enter the die and fill the cavity. The ejector half usually contains the runners (passageways) and gates (inlets) that route molten metal to the cavity. Dies also include locking pins to secure the two halves, ejector pins to help remove the cast part, and openings for coolant and lubricant [2].

When the die casting machine closes, the two die halves are locked and held together by the machine’s hydraulic pressure. The surface where the ejector and fixed halves of the die meet and lock is referred to as the "die parting line." The total projected surface area of

the part being cast, measured at the die parting line, and the pressure required of the machine to inject metal into the die cavity governs the clamping force of the machine.

There are four types of dies: Single cavity to produce one component, multiple cavity to produce a number of identical parts, unit die to produce different parts at one time, and combination die to produce several different parts for an assembly.

The earliest examples of die casting by pressure injection - as opposed to casting by gravity pressure - occurred in the mid-1800s. A patent was awarded to Sturges in 1849 for the first manually operated machine for casting printing type [3]. The process was limited to printer's type for the next 20 years, but development of other shapes began to increase toward the end of the century. By 1892, commercial applications included parts for phonographs and cash registers, and mass production of many types of parts began in the early 1900s. The first die casting alloys were various compositions of tin and lead, but their use declined with the introduction of zinc and aluminum alloys in 1914. Magnesium and copper alloys quickly followed, and by the 1930's, many of the modern alloys still in use today became available.

The die casting process has evolved from the original low-pressure injection method to techniques including high-pressure casting — at forces exceeding 4500 pounds per square inch — squeeze casting and semi-solid die casting. These modern processes are capable of producing high integrity, near net-shape castings with excellent surface finishes [4].

Now**,** to achieve maximum benefits from this process, it is critical that designers collaborate with the die caster at an early stage of the product design and development.

2. LITERATURE REVIEW

2.1. Aluminium Casting Techniques

Aluminium casting processes are classified as Ingot casting or Mould casting. During the first process, primary or secondary aluminium is cast into rolling ingot (slab), extrusion ingot (billet) and wire bar ingot which are subsequently transformed in semi- and finished products. The second process is used in the foundries for producing cast products. This is the oldest and simplest (in theory but not in practice) means of manufacturing shaped components. This section describes exclusively Mould casting which can be divided into two main groups as ‘Sand casting’, and ‘Die casting’.

Other techniques such as "lost foam" or "wax pattern" processes are also used but their economical importance is considerably lower than both listed techniques. Aluminium castings are very powerful and versatile techniques for manufacturing semi- or finished products with intricate shapes. Those techniques are continuously improved and developed to satisfy the user needs and to penetrate new markets.

Innovations are mainly oriented to the automobile sector which is the most important market for castings. This continual improvement and development will ensure that aluminium castings continue to play a vital role in this field [5].

2.1.1. Sand Casting

In sand casting, re-usable, permanent patterns are used to make the sand moulds. The preparation and the bonding of this sand mould are the critical step and very often are the rate-controlling step of this process. Two main routes are used for bonding the sand moulds:

· The "green sand" consists of mixtures of sand, clay and moisture.

· The "dry sand" consists of sand and synthetic binders cured thermally or chemically.

The sand cores used for forming the inside shape of hollow parts of the casting are made using dry sand components.

In the "low pressure" sand casting technique, the melted metal is forced to enter the mould by low pressure difference. This more complicated process allows the production of cast products with thinner wall thickness.

2.1.2. Die Casting

In this technique, the mould is generally not destroyed at each cast but is permanent, being made of a metal such as cast iron or steel. High pressure die casting is the most widely used, representing about 50% of all light alloy casting production. Low pressure die casting currently accounts for about 20% of production and its use is increasing.

Gravity die casting accounts for the rest, with the exception of a small but growing contribution from the recently introduced vacuum die casting and squeeze casting process.Gravity die casting is suitable for mass production and for fully mechanised casting [6].

2.1.3. High Pressure Die Casting

In this process, the liquid metal is injected at high speed and high pressure into a metal mould. This equipment consists of two vertical platens on which bolsters are located which hold the die halves. One platen is fixed and the other can move so that the die can be opened and closed. A measured amount of metal is poured into the shot sleeve and then introduced into the mould cavity using a hydraulically-driven piston. Once the metal has solidified, the die is opened and the casting removed.

In this process, special precautions must be taken to avoid too many gas inclusions which cause blistering during subsequent heat-treatment or welding of the casting product. Both the machine and its dies are very expensive, and for this reason pressure die casting is economical only for high-volume production [1].

2.1.4. Low Pressure Die Casting

Low-pressure die casting is especially suited to the production of components that are symmetric about an axis of rotation. Pressures of up to 0.7 bar are usual. Light automotive wheels are normally manufactured by this technique.

2.1.5. Vacuum Die Casting

The principle is the same as low-pressure die casting. The pressure inside the die is decreased by a vacuum pump and the difference of pressure forces the liquid metal to enter the die. This transfer is less turbulent than by other casting techniques so that gas inclusions can be very limited. As a consequence, this new technique is specially aimed to components which can subsequently be heat-treated [7].

2.1.6. Squeeze Casting or Squeeze Forming

Liquid metal is introduced into an open die, just as in a closed die forging process. The dies are then closed. During the final stages of closure, the liquid is displaced into the further parts of the die. No great fluidity requirements are demanded of the liquid, since the displacements are small. Thus forging alloys, which generally have poor fluidities which normally precludes the casting route, can be cast by this process [8].

This technique is especially suited for making fibre-reinforced castings from fibre cake preform. Squeeze casting forces liquid aluminium to infiltrate the preform. In comparison with non-reinforced aluminium alloy, aluminium alloy matrix composites manufactured by this technique can double the fatigue strength at 300°C. Hence, such reinforcements are commonly used at the edges of the piston head of a diesel engine where solicitations are particularly high [9].

2.2. Die Casting

Die casting is a versatile process for producing engineered metal parts by forcing molten metal under high pressure into reusable steel molds. These molds, called dies, can be designed to produce complex shapes with a high degree of accuracy and repeatability. Parts can be sharply defined, with smooth or textured surfaces, and are suitable for a wide variety of attractive and serviceable finishes.

Die castings are among the highest volume, mass-produced items manufactured by the metalworking industry, and they can be found in thousands of consumer, commercial and industrial products. Die cast parts are important components of products ranging from automobiles to toys. Parts can be as simple as a sink faucet or as complex as a connector housing.

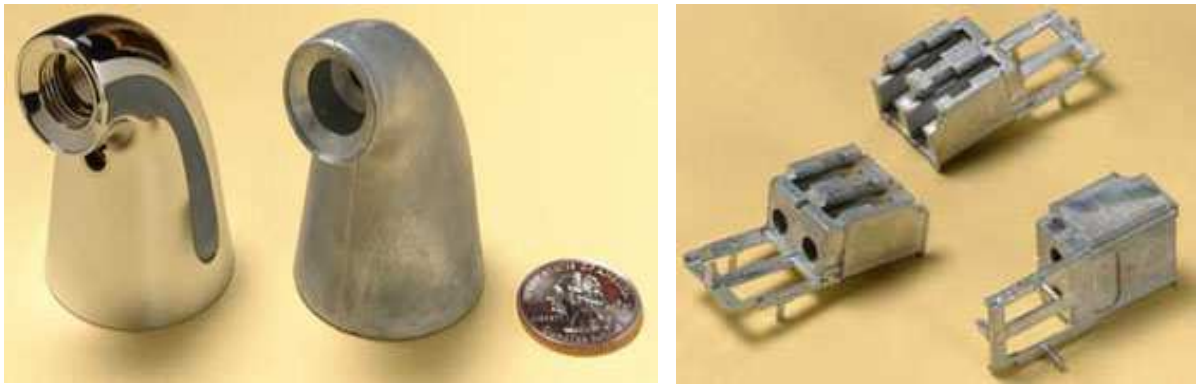

Figure 3.1. The polished, plated zinc die casting in the kitchen faucet [4]

Die cast parts are found in many places around the home. The polished, plated zinc die casting in this kitchen faucet in the Figure 3.1, illustrates one of the many finishes possible with die casting. The connector housings are examples of the durable, highly accurate components that can be produced with today's modern die casting.

2.2.1. History Of Die Casting

The earliest examples of die casting by pressure injection - as opposed to casting by gravity pressure - occurred in the mid-1800s. A patent was awarded to Sturges in 1849 for

the first manually operated machine for casting printing type. The process was limited to printer's type for the next 20 years, but development of other shapes began to increase toward the end of the century. By 1892, commercial applications included parts for phonographs and cash registers, and mass production of many types of parts began in the early 1900s.

The first die casting alloys were various compositions of tin and lead, but their use declined with the introduction of zinc and aluminum alloys in 1914. Magnesium and copper alloys quickly followed, and by the 1930s, many of the modern alloys still in use today became available [10] .

The die casting process has evolved from the original low-pressure injection method to techniques including high-pressure casting — at forces exceeding 4500 pounds per square inch — squeeze casting and semi-solid die casting. These modern processes are capable of producing high integrity, near net-shape castings with excellent surface finishes.

2.2.2. The Future Of Die Casting

Refinements continue in both the alloys used in die casting and the process itself, expanding die casting applications into almost every known market. Once limited to simple lead type, today's die casters can produce castings in a variety of sizes, shapes and wall thicknesses that are strong, durable and dimensionally precise.

Figure 3.2. A magnesium seat pan [10]

The magnesium seat pan in the Figure 3.2 shows how complex, lightweight die cast components can improve production by replacing multiple pieces.

2.2.3. The Advantages of Die Casting

Die casting is an efficient, economical process offering a broader range of shapes and components than any other manufacturing technique. Parts have long service life and may be designed to complement the visual appeal of the surrounding part. Designers can gain a number of advantages and benefits by specifying die cast parts. Die casting provides complex shapes within closer tolerances than many other mass production processes. Little or no machining is required and thousands of identical castings can be produced before additional tooling is required.

Die casting produces parts that are durable and dimensionally stable, while maintaining close tolerances. They are also heat resistant. Die cast parts are stronger than plastic injection moldings having the same dimensions. Thin wall castings are stronger and lighter than those possible with other casting methods. Plus, because die castings do not consist of separate parts welded or fastened together, the strength is that of the alloy rather than the joining process.

Die cast parts can be produced with smooth or textured surfaces, and they are easily plated or finished with a minimum of surface preparation.Die castings provide integral fastening elements, such as bosses and studs. Holes can be cored and made to tap drill sizes, or external threads can be cast [6].

2.2.4. Die Casting Process

The basic die casting process consists of injecting molten metal under high pressure into a steel mold called a die. Die casting machines are typically rated in clamping tons equal to the amount of pressure they can exert on the die. Machine sizes range from 400 tons to 4000 tons. Regardless of their size, the only fundamental difference in die casting machines is the method used to inject molten metal into a die. The two methods are hot chamber or cold chamber. A complete die casting cycle can vary from less than one second

for small components weighing less than an ounce, to two-to-three minutes for a casting of several pounds, making die casting the fastest technique available for producing precise non-ferrous metal parts.

2.2.5. Die Casting vs. Other Processes

Die casting vs. plastic molding - Die casting produces stronger parts with closer tolerances that have greater stability and durability. Die cast parts have greater resistance to temperature extremes and superior electrical properties.

Die casting vs. sand casting - Die casting produces parts with thinner walls, closer dimensional limits and smoother surfaces. Production is faster and labor costs per casting are lower. Finishing costs are also less.

Die casting vs. permanent mold - Die casting offers the same advantages versus permanent molding as it does compared with sand casting.

Die casting vs. forging - Die casting produces more complex shapes with closer tolerances, thinner walls and lower finishing costs. Cast coring holes are not available with forging.

Die casting vs. stamping - Die casting produces complex shapes with variations possible in section thickness. One casting may replace several stampings, resulting in reduced assembly time.

Die casting vs. screw machine products - Die casting produces shapes that are difficult or impossible from bar or tubular stock, while maintaining tolerances without tooling adjustments. Die casting requires fewer operations and reduces waste and scrap [4].

2.2.6. Choosing the Proper Alloy

Each of the metal alloys available for die casting offer particular advantages for the completed part. Zinc is the easiest alloy to cast, it offers high ductility, high impact

strength and is easily plated. Zinc is economical for small parts, has a low melting point and promotes long die life.

Aluminum is lightweight, while possessing high dimensional stability for complex shapes and thin walls. Aluminum has good corrosion resistance and mechanical properties, high thermal and electrical conductivity, as well as strength at high temperatures.

Magnesium is the easiest alloy to machine, magnesium has an excellent strength-to-weight ratio and is the lightest alloy commonly die cast.

Copper possesses high hardness, high corrosion resistance and the highest mechanical properties of alloys cast. It offers excellent wear resistance and dimensional stability, with strength approaching that of steel parts.

Lead and Tin offer high density and are capable of producing parts with extremely close dimensions. They are also used for special forms of corrosion resistance [10].

2.2.7. Die Construction

Dies, or die casting tooling, are made of alloy tool steels in at least two sections, the fixed die half, or cover half, and the ejector die half, to permit removal of castings. Modern dies also may have moveable slides, cores or other sections to produce holes, threads and other desired shapes in the casting. Sprue holes in the fixed die half allow molten metal to enter the die and fill the cavity. The ejector half usually contains the runners (passageways) and gates (inlets) that route molten metal to the cavity. Dies also include locking pins to secure the two halves, ejector pins to help remove the cast part, and openings for coolant and lubricant.

When the die casting machine closes, the two die halves are locked and held together by the machine’s hydraulic pressure. The surface where the ejector and fixed halves of the die meet and lock is referred to as the "die parting line." The total projected surface area of the part being cast, measured at the die parting line, and the pressure required of the machine to inject metal into the die cavity governs the clamping force of the machine.

There are four types of dies: ‘Single cavity to produce one component’, ‘Multiple cavity to produce a number of identical parts’, ‘Unit die to produce different parts at one time’, and ‘Combination die to produce several different parts for an assembly’ [11].

2.2.8. Hot Chamber Machines

Hot chamber machines are used primarily for zinc, copper, magnesium, lead and other low melting point alloys that do not readily attack and erode metal pots, cylinders and plungers.

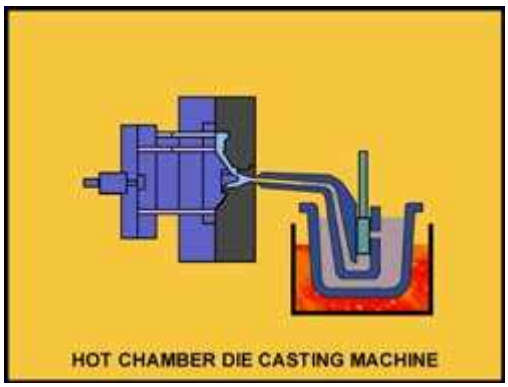

Figure 3.3. Hot chamber die casting machine [6]

The injection mechanism of a hot chamber machine is immersed in the molten metal bath of a metal holding furnace. The furnace is attached to the machine by a metal feed system called a gooseneck. As the injection cylinder plunger rises, a port in the injection cylinder opens, allowing molten metal to fill the cylinder. As the plunger moves downward it seals the port and forces molten metal through the gooseneck and nozzle into the die cavity. After the metal has solidified in the die cavity, the plunger is withdrawn, the die opens and the casting is ejected.

2.2.9. Cold Chamber Machines

Cold chamber machines are used for alloys such as aluminum and other alloys with high melting points. The molten metal is poured into a "cold chamber," or cylindrical sleeve, manually by a hand ladle or by an automatic ladle. A hydraulically operated plunger seals the cold chamber port and forces metal into the locked die at high pressures.

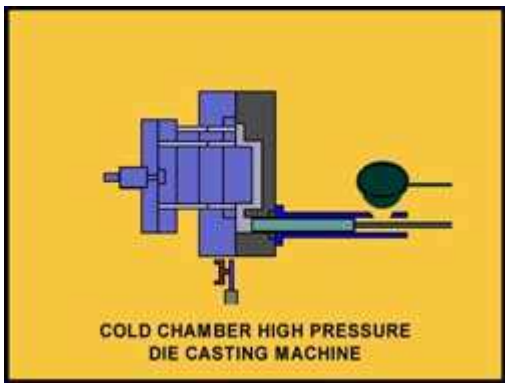

Figure 3.3. Hot Chamber Die Casting Machine [10]

2.2.10. High Integrity Die Casting Methods

There are several variations on the basic process that can be used to produce castings for specific applications. These include: squeeze casting, which is a method by which molten alloy is cast without turbulence and gas entrapment at high pressure to yield high quality, dense, heat treatable components.

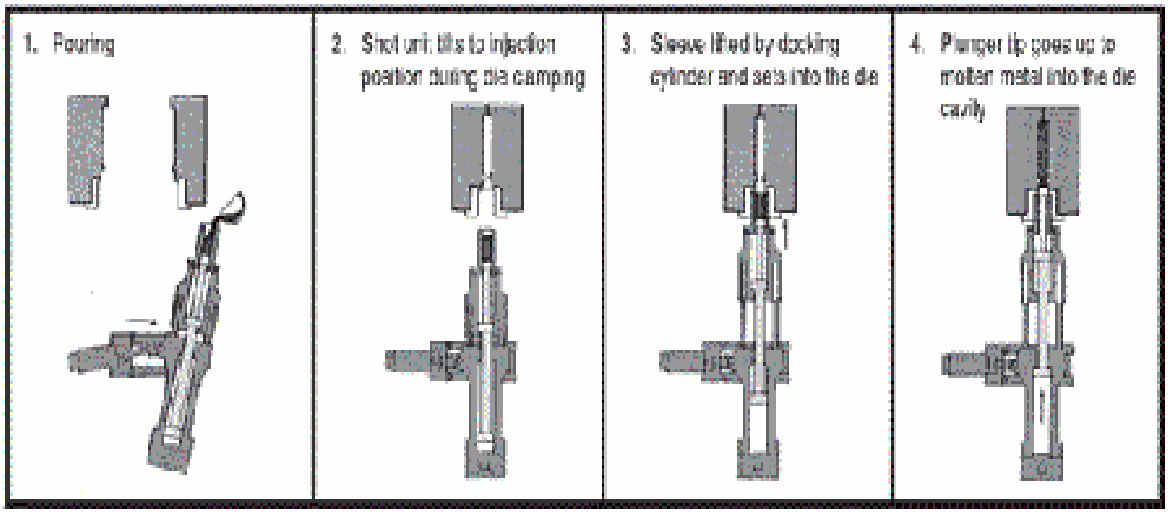

Figure 3.4. Squeeze casting steps [11]

Semi-solid molding - A procedure where semi-solid metal billets are cast to provide dense, heat treatable castings with low porosity.

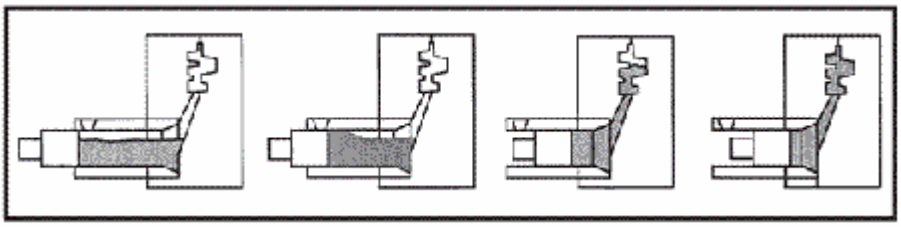

Figure 3.5. Semi-solid molding steps [12]

2.2.11. Automation and Quality Control

Modern die casters use a number of sophisticated methods to automate the die casting process and provide continuous quality control. Automated systems can be used to lubricate dies, ladle metal into cold chamber machines and integrate other functions, such as quenching and trimming castings. Microprocessors obtain metal velocity, shot rod position, hydraulic pressure and other data that is used to adjust the die casting machine process, assuring consistent castings shot after shot. These process control systems also collect machine performance data for statistical analysis in quality control [13].

2.2.12. Die Casting Design

Die casting is one of the fastest and most cost-effective methods for producing a wide range of components. However, to achieve maximum benefits from this process, it is critical that designers collaborate with the die caster at an early stage of the product design and development. Consulting with the die caster during the design phase will help resolve issues affecting tooling and production, while identifying the various trade-offs that could affect overall costs.

For instance, parts having external undercuts or projections on sidewalls often require dies with slides. Slides increase the cost of the tooling, but may result in reduced metal use, uniform casting wall thickness or other advantages. These savings may offset the cost of tooling, depending upon the production quantities, providing overall economies [14].

Alloy properties are one of the first steps in designing a die cast component is choosing the proper alloy. The cost of materials is another important design consideration.

Accurate comparisons require looking beyond the cost per pound or cost per cubic inch to fully analyze the advantages and disadvantages of each competing process. For instance, the relatively greater strength of metals generally allows thinner walls and sections and consequently requires fewer cubic inches of material than plastics for a given application.

2.3. High Pressure Die Casting

The pressure die casting process has its origins in typecasting machines, which had reached a high level of automation and mechanical efficiency by the mid-1800's. By the end of the 19th century variants of the typecasting machines were being used to produce components for cash registers and gramophones, and by the beginning of the current century die cast bearings were being produced for automotive applications. Although the technology of the process continued to evolve during the early part of the 20th century, it was not until the 1920's that the forerunners to the modern hot chamber and cold chamber machines were developed [1]. These processes have been refined to the extent that tiny zinc alloy castings can be produced in a one-second cycle on fully automated hot chamber machines. The cold chamber process is used predominantly for the production of aluminium alloy components, which include complex castings weighing in the region of 15kg (30lb), for the automotive industry. For such components the cycle time would be about two minutes.

2.3.1. Process Outline

2.3.1.1. Hot Chamber Process

A schematic diagram of a hot chamber pressure die casting machine is shown in Figure 3.3. The metal for casting is maintained at an appropriate temperature in a holding furnace adjacent to, if not part of, the machine. The injection mechanism is located within the holding furnace and a substantial part of it is therefore in constant contact with the molten metal. Pressure is transmitted to the metal by the injection piston, which forces it through the gooseneck and into the die [15]. On the return stroke metal is drawn into the gooseneck for the next shot. In this process there is minimum contact between air and the metal to be injected, thus minimising the tendency for turbulent entrainment of air in the

metal during injection. However, there is prolonged contact between the metal and parts of the injection system, which effectively restricts this process to zinc-base alloys.

2.3.1.2. Cold Chamber Process

The essential feature of this process is the independent holding and injection units. In the cold chamber process metal is transferred by ladle, manually or automatically, to the shot sleeve. Actuation of the injection piston forces the metal into the die. This is a single-shot operation. This procedure minimises the contact time between the hot metal and the injector components, thus extending their operating life. However, the turbulence associated with high-speed injection is likely to entrain air in the metal, which can cause gas porosity in the castings. The cold chamber process is used for the production of aluminium and copper base alloys and has been extended to the production of steel castings.

The advantages of the pressure die casting processes are the ability to produce castings with close dimensional control, the ability to produce castings with a good surface finish, the ability to produce castings with thin walls, and therefore of reduced weight, and the ability to produce castings at a high rate of production.

Against these advantages the disadvantages are high capital plant costs, high tooling costs, restrictions on the range of alloys which can be cast, and restrictions on the maximum size of casting that can be cast [16].

3. SIMULATION

3.1. Magmasoft Simulation Software

Magmasoft® is a comprehensive simulation tool for the technological and quality focused production of castings worldwide. The simulation capabilities of Magmasoft show the way by providing a better understanding of mold filling, solidification, mechanical properties, thermal stresses and distortions, and much more. Magmasoft® provides a complete solution for design, production, and quality departments with fully menu-driven with an integrated solid modeler, CAD interfaces, and extensive databases.

Magmasoft® provide a roadmap to casting quality and optimization. Magmasoft® helps to avoid gating and feeding problems, predict casting quality, aids permanent mold design and reduces fettling costs [17].

Magmasoft® offers solutions for all casting needs. MAGMAiron is able to predict the microstructure and resulting mechanical properties in iron castings, considering the specific metallurgical and metal treatment practices. For steel foundrymen the extended capabilities of MAGMAsteel, allow greater understanding of the effects of macrosegregation and provide information, which supports process layout as well as assists in the optimization of heat treatment. The design and process optimization of non-ferrous castings in permanent molds is supported through the process specific modules MAGMAlpdc, MAGMAwheel, MAGMArotacaster and MAGMAtilt. In high-pressure and low-pressure die casting applications, MAGMAhpdc and MAGMAlpdc support the construction of sound dies and tooling before the first castings are produced. The product development cycle can be shortened through the early prediction of residual stresses and part distortion.

3.1.1. Hardware and Software Requirements

Hardware - Although earlier it was often necessary to have expensive workstations to carry out intensive simulation, today many calculations can be completed using common

PC's. Good PC’s are now standard hardware for casting simulation. Nonetheless, computers are never fast enough - more and more physics is considered in the programs, the models become more and more complex, and the answers need to be there earlier and earlier. When simulation programs are parallelized, it is possible to take advantage of the extreme power of parallel computers. These “clusters” cost less than workstations used earlier. With the appropriate software installed on a cluster, “experimentation on the monitor” or automatic optimization becomes reality.

All projects performed by Magma Engineering Service are time-critical. So Magma's most powerful hardware is installed at Magma Engineering Service. From Linuxs' Cluster over multi-processor UNIX workstations and fast dual processor PC's to laptops; the hardware resources enable Magma Engineering Service to respond as fast as possible on customer requests. And more than that: Magma Engineering Service buffers Magmasoft® users peak loads by offering to run their projects, often over night, on powerful hardware.

Software - Finally, the foundry man needs a trustworthy simulation program, which is continuously tested, maintained and improved. From the generation and completion of geometry models to the engineering collaboration on common internet based platforms many CA-technologies are required. Magma Engineering Service is fully equipped: model repair tools, 3D CAD, FE- and CV-mesh generators and FE-Analysis are installed and integrated with Magmasoft®. Magma Engineering Service uses all released Magmasoft® modules as well as special process or material related modules for certain applications.

3.1.2. Casting Design Support

Castings are always competitive, if the design fully exploits their potential for superior functionality and performance. In the design process for such castings, information related to the manufacturing process are clearly needed: Residual stress and local mechanical properties must be taken into consideration. The complete development process including design, FE analysis, prototyping, tooling and series production planning will be improved, when casting simulation is integrated [18].

At Magma Engineering Service, the key competences are two-fold. The foundry engineers, mechanical engineers, metallurgists and toolmakers have practical experience. At the same time they worked for years in casting simulation and FE-analysis. This combination enables them to understand the casting technologies, management processes and business models of the clients of the Magma Engineering Service. Magma Engineering Service engineers analyze processes, do feasibility studies, propose and perform the layout or optimization of casting designs and casting processes. With more than thirty engineers with these skills worldwide, Magma Engineering Service is a center of excellence for the application of simulation in casting processes. And more than that: together with the partners in strategic alliances, the complete process chain from casting development is covered over FE-analysis, lifetime calculations, reverse engineering, prototyping, tool and pattern making to series production processes [19].

3.1.3. MAGMAhpdc

MAGMAhpdc provides a comprehensive simulation of the High-Pressure Die Casting (HPDC) process using detailed process and boundary conditions. In MAGMAhpdc, all important parameters influencing heat flow and the die thermal balance of the die can be considered, such as ejection time, die opening sequence, delay time (simulating effect of cycle interruptions on the thermal balance), die closing sequence, less time until the beginning of the next cycle, individual control of each cooling or tempering channel, definition of die spraying procedure, venting and vacuum, local squeezing definition.

MAGMAhpdc also supports the setup of shot sequence by a comprehensive shot calculator module, considering the casting demands and the die casting machine capabilities. The shot calculator provides information for the simulation setup of the recommended first and second phase shot profile [17].

3.1.3.1. Basics and use

Innovations and modifications in the techniques of high pressure die casting or tooling are forced by trends in part design, part load as well as by costs and times for development and manufacturing processes. All current trends require continuous improvement in planning of part performance and production processes. The quality of parts and the efficiency of development and manufacturing processes are primarily depending on the quality and accuracy of the planning process.

Generally, there are two crucial factors that secure the reliability of planning: Experiences from past projects that can be used in future projects, and Modeling of processes based on general physical laws. As die castings and casting processes get more and more complex, it becomes increasingly difficult to use experience from past projects in future projects. At the same time, due to restructuring processes in the casting industry, less information is documented and stored and thus not available in the future [20].

In high pressure die casting the term ‘modeling’ means the reproduction of the casting process in simulation programs. In this method, the very detailed process flow is specified as a boundary condition in a calculation. The result is the representation of die filling, solidification, formation of microstructure and properties, as well as development of residual stress and distortion in the castings. The simulation results can be displayed on screen, printed as color graphics, or represented threedimensionally and thus are excellent records of the anticipated results of the die casting process. As this is the quickest and most cost-effective method to develop a high-value product, die casting modeling gets more and more important.

3.1.3.2. Model specifications

In the numerical simulation of casting processes, three-dimensional differential equations are used as mathematical-physical models. Mass flow, heat flow, or development of stress are coupled to the casting process and can be modeled by coupling the respective differential equations. For die filling, e.g., there are equation systems, which are able to describe occurring phenomena like turbulent three-phase flow with possible phase transitions. However, simulations that use such detailed model specifications require very long computing

times, even on supercomputers. But it is not always necessary to use a very detailed description for the practical use of the simulation. In order to get a basic understanding of the processes during phase transition it is also possible to use other simulation techniques.

Basically, the term ‘modeling’ means the idealized replication of an object or of a process. A good model mirrors the essential characteristics of the original, but at the same time uses valid and clever simplifications. The modeling of a complex, technical operation like the high pressure die casting process means to define, to quantify, and to take into consideration the characteristic values and influential mechanisms of the process.

The simulation of die casting needs to replicate the following typical problems: Patterns and temperatures in the melt flow: last filled areas, venting of the die, aggregation of die agents, ‘dead areas’ in the runner, turbulences in the melt, disintegration of the melt and merging of melt fronts, cold shuts, or weld lines. Temperatures of the die: the complete die filling (especially during thin-wall casting), cycle times, core wear, adhesive tendency, or heat loss when spraying [21].

Solidification of the casting: the creation of shrinkage cavities and pores, hot tears, microstructure formation, possible feeding in the final pressure phase or during local squeezing, as well as the formation of residual stress and consequently arising distortion. The integration of the simulation results into the decision making processes during casting design or in the foundry assumes that the calculations generally last no longer than one day, counting from the availability of an accurate 3D-CAD-model of a casting including ingates to the creation of the documentation of the calculation. With these factors in mind, there are the following models and examples to review:

In the majority of cases the Navier-Stokes equation is used to describe pressure-driven flow. This equation needs to be solved coupled with the Fourier heat conduction equation in order to consider the heat loss of the melt during die filling. Regarding flow, basic approaches for single phase and laminar flow are used. With specific extensions of the models,

further phases like air and solidified melt are considered. The phenomena of turbulences are taken into account by using k/ε approaches.

The Fourier heat conduction equation is used for these models. Here, phase transformation enthalpies like melt heat need to be considered according to the solidification laws. Effects like the different precipitation of solidification phases in dependency on supercooling are increasingly in use. If the used modeling approaches consider values calculated during heat flow simulation, like local solidification time, cooling rate, or temperature gradient, the formation of microstructures can be computed.

The formation of residual stresses in castings is very complex, especially in the area of high temperatures. Non-linear, elastoplastic approaches are very sophisticated. It is difficult to describe phenomena like the formation of hot tears as the material laws in combination with high temperatures are not well enough known yet. Further, it is difficult to consider the contact conditions between die and casting, which has a substantial influence on the formation of stresses, especially in high pressure die casting [18].

3.1.3.3. Phases of a simulation project

In order to run a casting simulation, the following fundamental steps need to be carried out.

Basis for the simulation is a three-dimensional geometry model of the raw casting or the machined part. The casting developers in the automotive industry focus on maintaining a centrally managed and up-to-date record of geometries that exclusively consists of 3D-CAD data. This way it is nearly impossible that such model doesn’t exist in the automotive industry. In other industries it might happen that a model is not existent and it needs to be developed based on drawings. The geometries of ingates and overflows, as well as of die segments including cooling/heating lines are prepared as 3D-models and need to be available for the simulation, too [19].

The complete 3D-model, which consists of the raw casting, ingates, overflows and/or vacuum channels, as well as die segments including cooling/heating lines need to be enmeshed for the mathematical calculation. Depending on the operation method, these meshes are exclusively automatically generated (finite volume method), or automatically generated and manually reworked (finite elements method). The completion of the 3D-models and the enmeshment are known as ’preprocessing’ [17].

Before starting the calculations, the required process parameters need to be entered via interactive user interfaces. These process parameters are shot curve, temperatures of melt, thermal regulation medium and die, as well as the chronological sequence of the whole casting process including the spraying of the die agent. Some simulation programs include subroutines that automatically forecast and propose appropriate process parameters.

The actual calculation can be carried out on various hardware platforms. The complete calculations usually run overnight on powerful machines, but with the use of cluster computers and appropriate simulation programs, the calculation can be completed within minutes.

‘Postprocessors’ prepare the results in colored graphics or movies that visualize and document the calculated operations during die filling, solidification, formation of microstructure and properties, as well as the formation of residual stress and distortion.

The time needed for the run of the simulation is depending on various parameters and can range between 30 minutes (for the determination of the ingate position and the requirements for thermal balancing of the die) and two days (for the calculation of die filling, solidification, and formation of residual stress with more cycles for a complexly structured casting) [20].

3.1.3.4. Automated numerical optimization

With the help of simulations it is possible to ‘x-ray’ the casting process that was elaborated by qualified personnel. The results of the simulations support the decision-making-

process in order to implement improvements. Thus, the use of casting simulations is always dependent on the employment of qualified personnel. The labor costs in a simulation project increases in correlation with the velocity of the available hardware. This raises the question on how the simulation can be more effective in respect to the use of personnel.

Thus, the qualified user needs a tool that helps him to implement his knowledge in the areas of error diagnostics and optimization. This ‘second generation’ of simulation tools aims to use the knowledge of the user to formulate the purpose of optimization and assessment criteria for the simulation process. The above mentioned steps of a single simulation project (change of CAD-geometries, process parameters, start of a simulation, and evaluation of the results) can indeed be carried out by a computer according to appropriate pre-settings.

The rapid development of computer processors and memory generates increasingly powerful hardware. Today, it should be possible to simulate hundreds of variations of a casting process overnight. However, the definition of these variations would take some time and the amount of generated information could hardly be evaluated within days. The advantage of the very short computing times can only be used if the evaluation and the new definition of the calculated variations would be carried out automatically by the computer. Basically, there are two different approaches.

On the one hand, there are knowledge-based systems that perform modifications or optimizations of the casting process based on stored regulations. However, a very high number of clear and unambiguous correlations between cause and effect need to be known for that purpose, which is not the case in high pressure die casting [21].

On the other hand, there is the possibility to use the survival of strong individual’s genetic components as it is practiced in nature. Genetic algorithms accept variations more or less at random where reasonable variations survive from generation to generation. The integration of such optimization algorithm into casting simulation software results in a system that is able to perform computerized and fully automated optimizations of the casting process.

Basically, this system is suitable for the solution of the following problems in high pressure die casting:

Due to turbulences and dead areas, gas is entrapped in the melt before the actual die filling. Purpose of optimization is the minimization of peak gas pressure during filling. The variables are the parameters of the CAD-design of the runner.

High temperature gradients that develop during the casting cycle in the die reduce the lifetime of the die. Purpose of optimization is the minimization of temperature gradients at certain locations of the die and at certain times of the casting cycle. The variables are the parameters of the CAD-design of the cooling/heating lines.

Dry die agents in a closed die need to evaporate in the shot chamber and to re-condense at the wall of the cavity. Purpose of optimization is to keep the temperature of the die surface on the level required for this process. The variables are the parameters of the CAD-design of the cooling/heating lines, too.

Many castings have heavy sections between thin sections. In order to avoid shrinkage cavities it is necessary to perform local squeezing. Purpose of optimization is to avoid heavy sections with pores. The variables are the exact position and the volume of the squeezers as well as the exact point in time, when the squeeze pin is pressed into the solidifying melt [22].

3.1.3.5. Die filling simulation

The die filling is often seen as the most critical and for the casting result the most influential subprocess in high pressure die casting. Apart from some exceptions that require a slow die filling (like infiltration of inserts made of ceramic fibers) the ingate velocities lie in a range between 30 and 140 m/s and the filling times are between 20 and 200 ms. These conditions lead to a turbulent flow, where, due to the geometries of the castings, the melt fronts are nearly always uneven. The flow consists of at least two phases (liquid and gas) and in some cases additionally of a solid phase during the die filling.

Due to various reasons, the gating design is very important in high pressure die casting. Regarding the design of the gate, the following needs to be taken into consideration:

• Turbulences in the melt should be reduced in order to avoid entrapped gas in the casting.

• The melt flow through the gate needs to be timed in order to allow the controlled merging of the melt fronts.

(a) (b)

Figure 3.6. (a) Turbulences in the gate due to unfavorable design, (b) Disadvantageous dimensions of the runners lead to uneven die filling. Due to the tight dimensions the right branch of the gate is filled too late [21].

• The flow velocities need to be consistent, also when using fan ingates.

• The desired ingate velocities need to be met.

• The desired direction of the melt flow into the cavity needs to be met.

The die filling simulation based on an existing design of the gating system allows to evaluate all these problems, and thus to decide if the design is usable or needs to be modified (Figure 3.6-3.7).

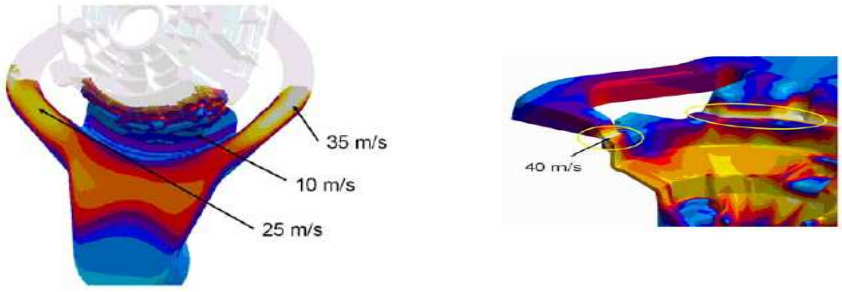

(a) (b)

Figure 3.7. (a).Fan ingate, where the flow velocities vary considerably. (b)Here, the ingate velocities are just right (40m/s) [21].

The die filling is primarily determined by the defined shot parameters. Thus, the plunger velocity and switching points need to be considered very precisely for the simulation. Generally it is assumed that the machine hydraulics is able to implement the defined parameters. In this case the volume flow of the melt as a function of time is exactly known and will be considered in the calculation accordingly (Figure 3.8).

Using the PQ^2-diagram, it can be verified if the machine hydraulics is able to convert the defined parameters (Figure 3.9). The PQ^2-diagram is calculated from the following parameters; firstly, the machine parameters that can be stored in the data base of the simulation program, classified under the corresponding machine types; and secondly, the tool parameters that are calculated from the CADmodel of the die. With the verified parameters the simulation program is able to calculate (and if necessary to optimize) various process values like filling time, gate velocity, necessary closing force, etc. (Figure 3.10).

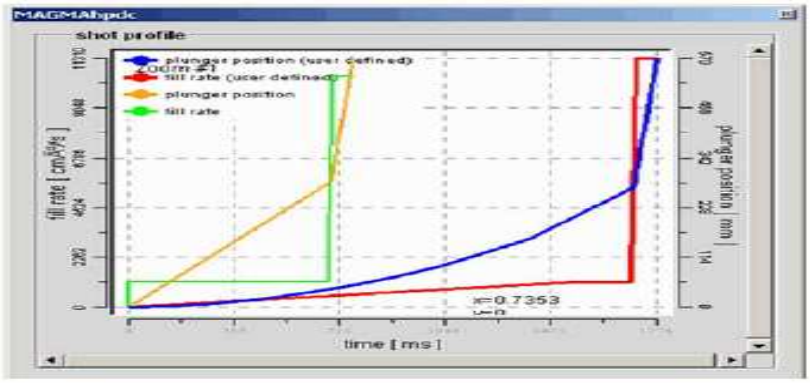

Figure 3.8. A shot profile with constant plunger velocity in the first phase and a shot profile optimized according to NADCA [17].

As seen in the Figure 3, the filling process in the simulation can be controlled by various shot profiles. This example shows a shot profile with constant plunger velocity in the first phase and a shot profile optimized according to NADCA. Based on the defined machine and die parameters, the simulation program is able to calculate an optimized shot profile.

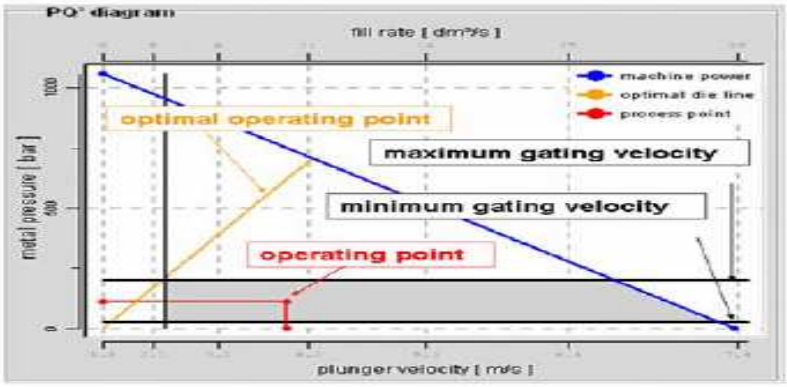

Figure 3.9. PQ²-diagram [17]

With the PQ²-diagram, the optimally adjusted operating point for machine and die can be determined as seen in the Figure 3.9.

switch over stage 1-2:	489.004	510.000	[mm]
(3a) Acceleration after "shot sleeve filled". End of acceleration before "runners filled".			
plunger, start of stage 2:	520.873	569.915	[mm]
plunger, runner full position:	577.515	577.515	[mm]
slow shot velocity:	0.702	0.250	[m/s]
fast shot velocity:	2.995	4.000	[m/s]
cavity filling time:	57.283	42.891	[ms]
optimal ingate area:	5.880	7.500	[cm²]
velocity at the ingate:	31.364	41.888	[m/s]

Figure 3.10. Manufacturing and process parameters, proposed by the simulation program, and based on the parameters of chosen machine and die [18]

The results of the mold filling simulation allow an evaluation of the chosen casting parameters and the runner in respect to the anticipated quality of the casting. The typical casting errors due to suboptimal filling are visible welding lines, cold runs, or pores as a result of entrapped air. With the help of mold filling simulation it is possible to verify the formation and development of those errors (Figure 3.11).

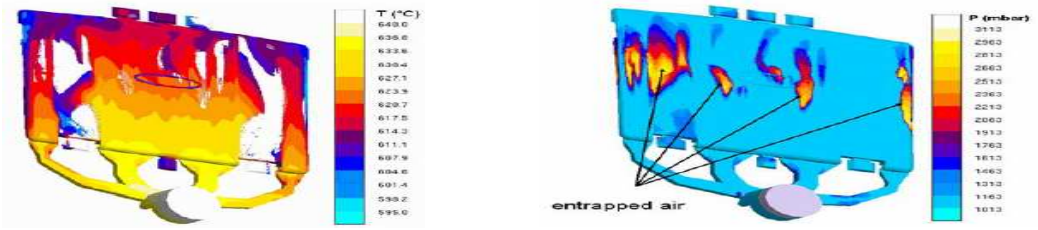

(a) (b)

Figure 3.11. (a) Gas pores (b) Stretcher lines and cold runs at thin wall castings [18]

As seen in the Figure 3.11, gas can be entrapped if the venting doesn't conform to the die filling. The pressure of entrapped air at the end of the filling results in gas pores. The simulation can precisely predict stretcher lines and cold runs at thin wall castings.

Errors like erosion of the mold are caused by the filling process, too. Generally, erosion is a result of high melt temperatures in connection with high melt velocities. Those

conditions usually occur at the gate but also at positions where the melt is redirected (Figure 3.12). Just before the ingate, the pressure is especially high during filling. This results in high wear in this area of the die.

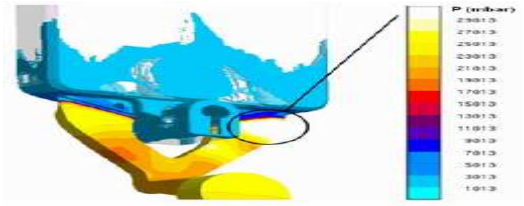

Figure 3.12. High wear just before the ingate [17]

Ideally, the die filling process is directed in a manner that the casting can directionally solidify towards the biscuit. At the same time, the volume of the gating system should be reduced as much as possible. It is often required to have a certain area of the casting with a minimal amount of entrapped gas. For this purpose the location or the design of the runner and gating system is modified, where the simulation verifies this alteration.

3.1.3.6. Simulation of the casting solidification

The solidification of the melt is characterized by a number of metallurgical-physical phenomena that eventually determine the local properties of the casting. Those need to be considered in the simulation with appropriate modeling approaches. The main aspects in high pressure die casting are the shrinkage during solidification and the microstructure formation.

The volume contraction during the solidification of the metal melt leads to shrinkage cavities and dispersed porosity depending on the alloy and the wall thickness of the casting. Heavy sections of the casting usually form a stable metal skin, whereas thin walls and especially the ingate start to freeze quickly. For this reason, feeding can only be used as a compensation of the shortfall in volume if the ingates are thicker than the wall of the casting, where further feeding is necessary (exception here is local squeezing).

The simulation allows an easy determination of areas where solidification shrinkage can lead to volume errors. The simplest criterion is the solidification time (Fig. 3.13). The possibility to partially compensate the solidification shrinkage by feeding with the plunger or with the local squeezer can also be displayed (Figure 3.14).

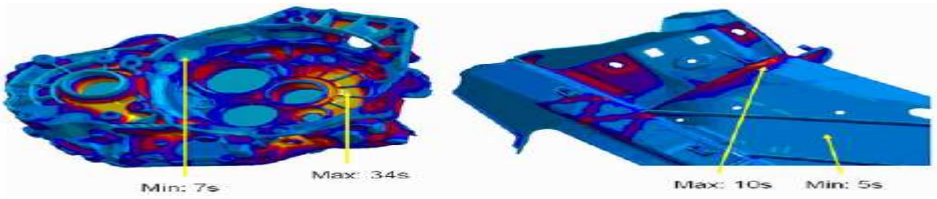

Figure 3.13. Dispersion of the solidification times [18]

Solidification times dispersion is seen in a gear box housing with different wall thicknesses (left) and in a structural component with constant wall thicknesses (right) in the Figure 3.13. Long solidification times indicate shrinkage errors.

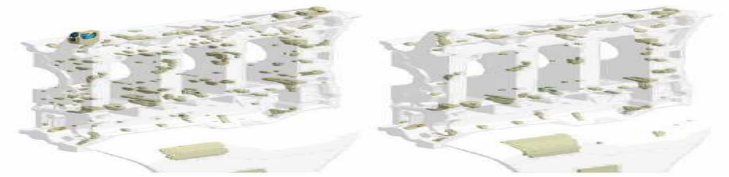

Figure 3.14. The porosity of thick-wall castings can be reduced by enlarging the ingate [16]

As seen in the Figure 3.14, using an ingate size of 0,4mm (left) leads to more porosity than a gate size of 0,7mm. However, the ingate is always one of the thinnest areas of the casting and thus freezes so quickly that only little feeding is possible.

In the past years, computer tomography (CT) has been increasingly used in the area of quality assurance. As imperfections can be exactly localized and results are very accurate, the computer tomography is a great support for casting simulation (Figure 3.15).

During the development of a gear box casting some cast prototypes were analyzed with the help of CT. At the same time, the casting process was simulated. The comparison of the results shows a vast agreement between the measured and the calculated pores.

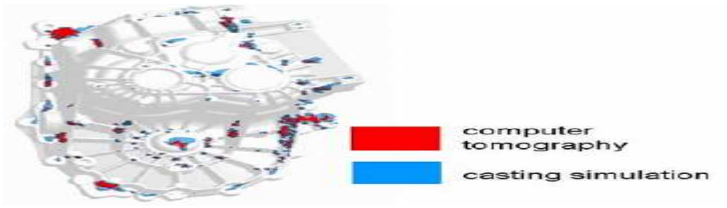

Figure 3.15. The pores calculated with MAGMASOFT® and the pores analyzed with CT [18]

As seen in the Figure 3.15, the pores calculated with MAGMASOFT® and the pores analyzed with CT (computer tomography) show the same critical areas. The display of the calculated pores is intentionally bigger than the display of the actually detected pores (FORD gear box casting, Prototype).

Shrinkage cavities are acceptable in some die castings; however, they generally cause problems during mechanical exposure and during machining of the casting. Shrinkage cavities always occur in heavy sections that are functionally necessary in many die castings. There are only a few possibilities to avoid shrinkage cavities, if the design of the casting can't be modified. One of those possibilities is local squeezing.

The example in Figure 3.16(a) presents the dimensioning of a squeezing system that should be used for the forced feeding of a critical area in the casting (Figure 3.16).

(a) (b)

Figure 3.16. (a).The maximum solidification time occurs in a thick-wall area of the casting. (b).Depending on the design of the squeezing system, shrinkage cavities can be avoided at the critical area (right) [19].

As seen in the Figure 3.16, the maximum solidification time occurs in a thick-wall area of the casting. This certainly leads to distinctive shrinkage cavities. As feeding is not possible in this area a local squeezer needs to be used. Purpose of optimization is to completely feed the critical heavy sections with a small volume squeezer. Depending on the design of the squeezing system, shrinkage cavities can be avoided at the critical area (right). Location and volume of the squeezer as well as exact point in time of the squeezing need to be determined. As shown in the left figure, insufficient parameters do not lead to the desired result.

The microstructure formation is depending on the alloy and on the local solidification conditions. A consistent solidification structure or structure after heat treatment can only be assumed for castings with an even wall thickness. All castings with different wall thicknesses inevitably show a distribution of various microstructure characteristics and thus have different local casting properties. The simulation of microstructure formation differentiates between macro- and micromodeling. Using macromodeling, microstructure characteristics can be derived from the results of the heat flow calculations. For instance, the secondary dendrite arm spacing of many aluminium alloys can be calculated from the local cooling rate and the temperature gradient (Figure 3.17). The calculation of the formation of grains, eutectics, or microscopic gas precipitations can not be implemented in praxis yet. This calculation is often based on two-dimensional calculations in microscopic scale and currently serves mainly as an instrument for the understanding of the microstructure formation.

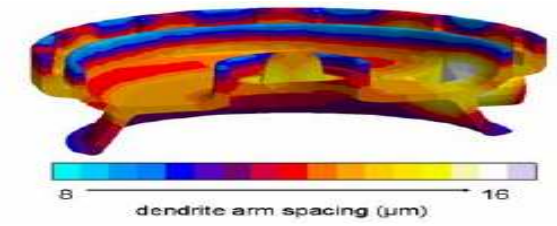

Figure 3.17. The secondary dendrite arm spacing can be calculated from the results of the solidification simulation [20].

3.1.3.7. Simulation of residual stresses in castings

Basically, in every casting with different wall thicknesses occur residual stresses. Different wall thicknesses of the casting lead to different cooling behavior after pouring as well as after heat treatment and thus result in residual stresses and in distortion of the casting. Usually, this distortion lies in an acceptable range. However, the existing residual stresses can lead to a different behavior of the casting under load. In material pairs like aluminium cylinder crank cases with cast iron sleeves, massive residual stresses can occur due to the different expansion coefficients, too.

The basic problem in the process of calculating residual stresses is the determination of laws to describe the material behavior in high temperatures. The creeping phenomenon at high temperatures, as well as the contact between die wall and casting, are often inaccurately described. These effects are currently subject of intense research projects. Therefore, the technical calculation of residual stresses is primarily based on the cooling of the casting after ejection. Regarding the processes taking place in the closed die, it is assumed that arising stresses in the casting are plastically relieved. Thus, the free shrinkage of the casting is calculated.

The locally arising von Mises equivalent stresses can be used for the evaluation of residual stresses. This equivalent stress is determined as vector product of the arising three-dimensional stresses. The development of residual stress until the removal of the ingate is initially calculated based on the results of the solidification simulation and during the cooling

of the casting. Depending on the proportion between cross section of the ingate and wall thickness of the casting, the removal time of the ingate has a significant influence on the development of residual stress as this process leads to stress transfer in the casting. Due to the occurring stress transfer, machining of the casting can also lead to distortion. The finally important value is the distortion caused by the residual stress in the machined casting [21].

Stresses in dies are basically caused by the following three reasons: The load caused by the closing mechanism of the machine, the load caused by the melt that is highly pressurized at least for a short moment in time, and the cyclically changing temperatures in the die segments that lead to cyclically changing residual stresses.

These conditions cause a highly complex and unsteady overall load, whose entirety is difficult to display in simulations, but where the single elements can be measured quite accurately.

The simulation of stress and distortion in the frame is always advisable when huge castings like engine blocks or castings with a large projected area, like structural components, are combined with tight die tolerances (due to dimensional limitations of the machine). At complex, i.e., entire models with side cores, an initial stress value is assumed at the side core locks. It can be assumed that there are little temperature gradients between the frame and the insert [22].

If the die spotting was carried out in a warm environment, the thermal residual stresses especially in the die inserts have nearly no influence on the stress in the frame. Closing force and pressure of the melt as well as a stable temperature of the frame are considered for the examination of the distortion in the frame.

For the evaluation of stress in the inserts, the thermal residual stress is a considerable part of the overall load. The thermal shocks in each cycle caused by the melt and later by the die agent in correlation with the die tempering generate inhomogeneous and cyclically unsteady temperature distributions with partially very high gradients. This results in

thermal residual stresses, where a likewise cyclically changing distortion is especially important for the lifetime of the die insert. These calculations need to be carried out with non-linear, elastoplastic model approaches, too [22].

Temperatures in a die casting tool can differ significantly. High pressure die casting dies in Aluminum applications can reach temperatures of more than 450°C near the impressions just after the filling. Temperatures close to the cooling channels are much lower. Due to the temperature gradients appearing in all high pressure dies, residual stresses arise especially in the die insert, where the tool steel load can reach the yield point. Compressive and tensile stresses successively occur due to strong temperature changes that are also caused by spraying of die agents. This leads to the development of cracks, especially in slim cores, where big changes in temperature happen due to intense heating up and cooling (spraying).

3.1.3.8. Integrating the casting simulation into development and manufacturing

A lot of information is generated during casting simulation, a lot of which would not be available when using conventional processes. To what extent this information can actually lead to a measurable improvement of casting design or processes is depending on the level of integration of the simulation into development and manufacturing processes. In this respect, it can be differentiated between firstly technical integration with focus on the communication of CAE-tools via interfaces, and secondly structural integration with focus on information management during planning and performance of operating procedures [22].

The information generated by the casting simulation is of significant importance to the constructing engineer. The local properties of the casting, like microstructure distribution, mechanical properties, or casting errors can be calculated and displayed with the help of casting simulation. Whereas the calculated distribution of casting errors is only a qualitative approximation of the local damage of the casting, FE-calculations can consider calculated, local, mechanical properties. There is the fundamental problem that different simulations, like the casting simulation and FE-analysis or crash simulation, are carried out with different calculation meshes. One mesh of a die-dashboard for casting simulation consists of two million elements whereas the mesh of the very same part for crash simulation consists of only

some hundred nodes. Thus, interfaces need to be used that transfer the calculated and interpolated value fields from one calculation mesh to the other [23].

Data and information are increasingly valuable once they are used in praxis. In the foundry, technologies like charge material calculation, thermal analysis, spectral analysis, analysis of the gas concentration, x-ray, or CT provide information, whose flow and use is determined by QA-processes. In the same way it needs to be dealt with data generated by the casting simulation, that only gain in value when implemented into design and manufacturing. There are no standardized rules in respect to the integration of casting simulation into design and manufacturing processes. However, companies with good experience in casting simulation exercise binding rules regarding the integration of simulations into existing QA-structures. Generally, the following is determined:

- Projects, where a casting simulation needs to be carried out,
- Point in time of the simulation,
- Charged cost centers,
- Documentation and back-up of the simulation results,
- Responsibility for optimization measures based on the simulation, and
- Verification of the optimization measures.

A steady improvement of development and manufacturing with the use of casting simulation can only be assured where work processes strictly follow such binding agreements.

Commercial programs for simulation of casting processes have been on the market for nearly 20 years now. Performance and credibility of software and available hardware have been drastically expanded and improved in this time. In some casting applications, like steel casting, the use of simulation had been evolved very quickly and reached a high level ten years ago. Today, there is hardly any steel casting with corresponding casting process that has not been extensively optimized with the help of casting simulation [24].

The costs of a high pressure casting die in relation to the costs of a pattern for a sand casting shows a huge potential to save costs if one succeeds in avoiding tool changes, in increasing tool lifetime, and in producing the desired quality of the casting at the first go. In many cases, costs for failed sample runs or for error correction and for rework are not consequently added to the unit costs. This results in high overhead costs that are considered as inevitable. Engineers and technicians are not exactly aware of these costs in detail and sometimes do not feel responsible for them. On the one hand, the management tolerates significant cost variances for single products, but on the other hand, the management avoids to either pay in advance for simulation or to approve expenses for improvements that assure cost reductions. The result is a declining competitiveness of the company. There is hardly a casting process, where effective and professionally used simulation is as beneficial as in high pressure die casting.

Foundries with a conventional and little changing range of products will find satisfactory solutions without the help of simulations. However, in this case simulations could help to reach improvements in a quicker and more methodical way. As the automotive industry requires a yearly price reduction for repetition parts due to constant operational optimization, room for improvement needs to be detected by simulation, and effectiveness of these improvements need to be evaluated by calculation. Everything can be tried in a simulation, including variants that are finally not implemented into the real process. For sophisticated castings, it is important that provider as well as customer know as early as possible about the reliability of the planned casting technique [24].

The validity of the physical-mathematical models as basis for the simulation has been proven in many successful projects. It is often difficult to find the exact manufacturing process conditions of a casting. In this case assumptions need to be met, where the detection of useful variations finally leads to a good agreement between the real conditions of the casting and the simulation values. This is the basis for the improvements achieved by the implemented changes. The experimentation is carried out in computerized manner. Due to the high number of parameters in high pressure die casting there are phenomena that appear in reality but are not part of the simulation model. Based on simulations, many companies have significantly

improved the accuracies of new parts so that already in the first sample line high-quality parts are produced followed by a consistently top-quality serial production.

It is difficult to defend the competitiveness of a company based on the specific knowledge of certain employees. There is probably a higher loss of this knowledge due to employee turnover than due to the transfer of simulation results between designer, foundryman, toolmaker and end user. The work of casting service providers is based on confidentiality. It is proved that simulation in one's own company leads in any case to increasing know-how rather than to the loss of technical expertise. Knowledge can be stored and internally transferred by using documentation and archiving processes. In this way, personal knowledge is much better processed and actually made available to other employees. The quality of the calculated results is significantly improved when considering know-how based on experience in the simulation. Now and in the future, the foundry specialist is needed.

The casting is designed by the design engineer without specific consideration of the manufacturing process. The toolmaker prioritizes on his own process. All problems of the whole manufacturing process are passed on to the foundryman. This applies to designing heavy sections in the casting as well as to not systematically elaborating the position of the ingates, the cooling channels, or the overflows. If the foundryman accepts those conditions without objection, he decreases to a simple metal pourer. Chances arise by the endeavor of great automotive companies to create an integrated development and manufacturing chain. This includes integral cost awareness, i.e., also the designer needs to contribute to a cost effective production. It is understandable that the designer doesn't want to perform the casting simulation by herself, especially as the designer doesn't profit from the cost reductions in the further course of them manufacturing chain. This is the chance for the foundryman to provide prompt and capable input with the use of simulation and also to point out requirements in respect to the production of new designs. This kind of assistance can also be offered by service providers. In their own interest, foundryman should be involved in and pro-actively work on the processes as early as possible [23].

Alfred T. Spada, editor of 'Modern Casting', writes regarding the reservation towards the simulation in an editorial of 'Modern Casting': 'If you are still waiting for casting

process modeling/simulation to prove itself, I'd say that you are at least a decade behind the times. If you still argue that you can't justify the cost for the technology/manpower, I'd say that you haven't done a true time or cost analysis as to what this software can save your operation. The proof is in the success that every metalcaster using the technology has had' [25].

3.2. Magmasoft Simulation Steps For A Washing Machine AlSi12Cu Flange

In this study, the Aluminum alloy AlSi12Cu, was simulated for the shape of the flange, which is used for washing machine cylinders in order to make them turn, with Magmasoft high pressure die casting simulation programme. At first, the shape of the flange was drawn with the CAD programme.

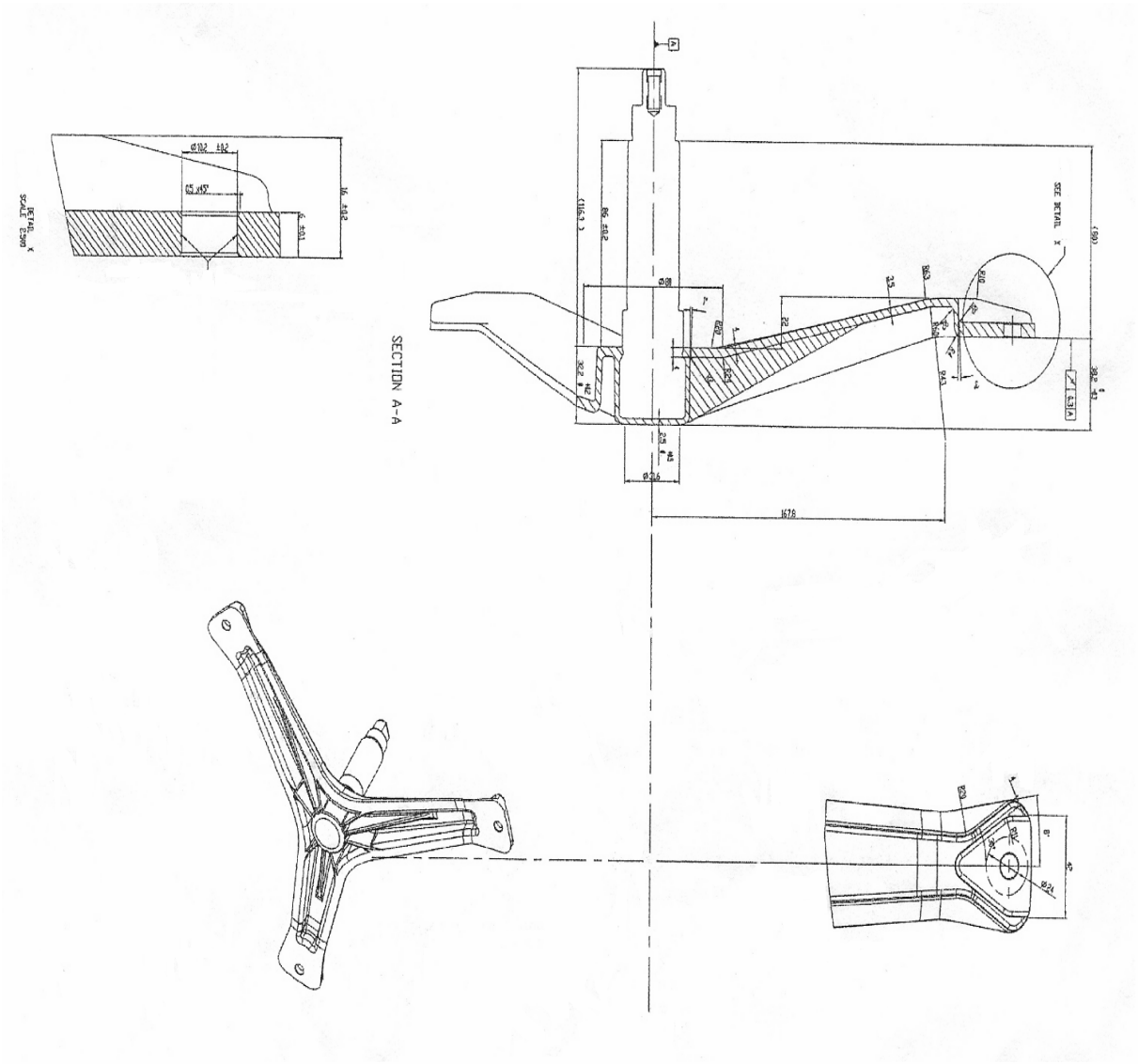

Figure 3.18. The shape of the flange designed using the Solidworks CAD software

The CAD data of the Flansch was opened at the Solidworks cad programme. It was ensured that this cad data was wholly solid at the Solidworks cad programme. Then, the cad data of the Flansh was divided in to three sections as casting, gating, and ingate with

the cut command at the Solidworks 2006. Thus, three seperate cad data of the flange was formed. These three seperate parts had to be in the same axis. Therefore, they were again united with the assembly command at the Solidworks 2006.

The cad data can only be transferred to the Magmasoft casting simulation software by saved as (*.STL) format. That's why, the prepared cad data was saved as (*.STL) with the deviation 0.05 and the angle 9°. Thus, casting.stl, gating.stl, and ingate.stl files were ready to be transfered to the Magmasoft simulation software.

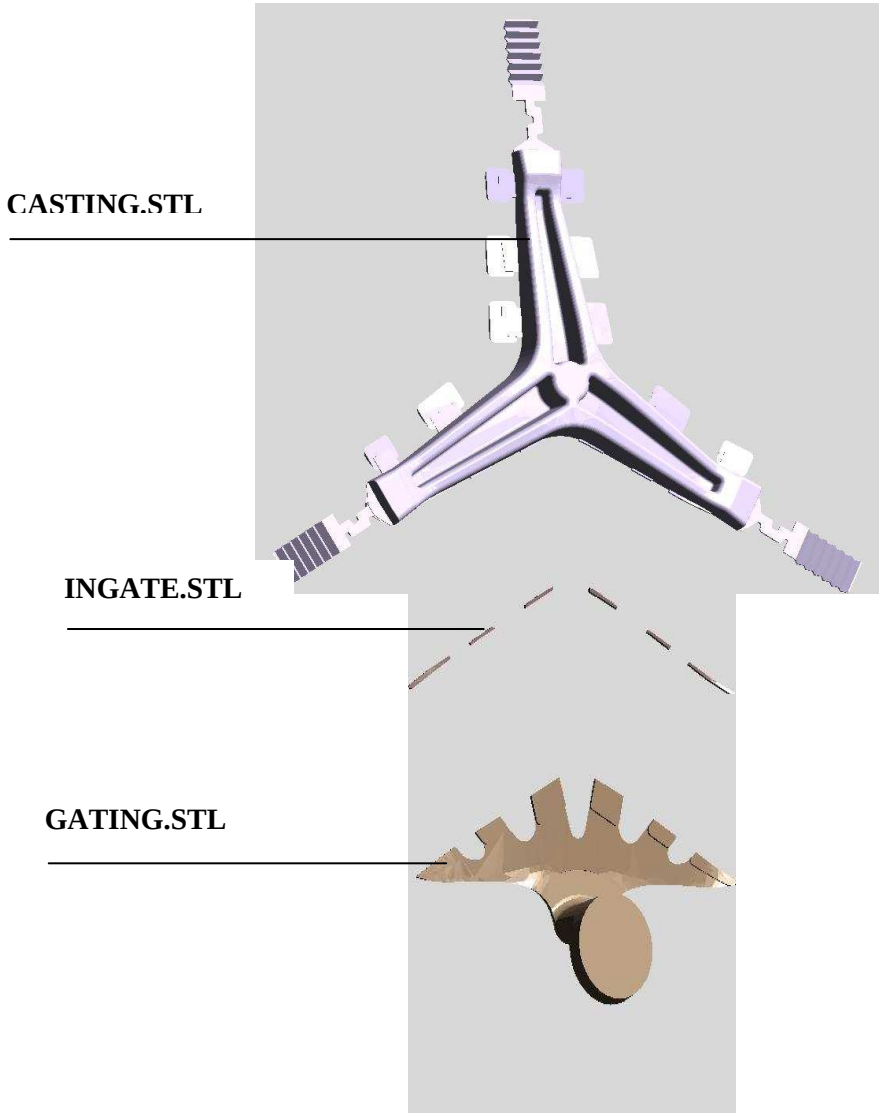

Figure 3.19. Casting, ingate and gating parts for the flange saved as (*.stl) in order to transfer Magmasoft

Thus, the cad data of the Flansch was transferred to Magmasoft simulation software. When it is clicked on the Magmasoft; Project, Preprocessor, Enmeshment, Simulation, Postprocessor, Database, Info, and Help icons are seen in the main menu of the casting simulation programme. In order to start, Create Project icon under Project headline was activated.

3.2.1. Preprocessor Steps

Then, Preprocessor icon was clicked. Material groups were selected as casting.geo, ingate.geo, and gating.geo in the preprocessor, under the headline Load Sla, which comes after the File subheading,. So, casting.geo, ingate.geo, and gating.geo were opened at the same time in the preprocessor of Magmasoft. After that, biscuit, inlate, and user defined (piston), which form pressurize planes to bottom of the gating, was defined in the preprocessor respectively.

The striking point of defining biscuit, inlate and piston is that their diameter reduces just a little from gating to piston. Additionally, biscuit goes into gating a little. Inlet goes into biscuit a little and piston goes into inlet a little.

After defining the piston, air channels was defined in the preprocessor. Thus, after clicking the Material heading at the top of the right menu of the preprocessor page, ‘Set AC’ subheading under Material heading was clicked. Air channels are always towards downwards and from moving part to outside. In order to save the air channels, ‘save sheet 0 SHEETS/air channel’ command was written.

After defining the air channels, cooling channels of the mould was defined in the preprocessor. There are two cooling channels. One of them is in the piston and the other is around the casting in the mould. The cooling channel in the piston is drawn before the other one. In order to form the cooling channels completely, the commands ‘set point 0 0 0’ and ‘set point 5 0 0’ were written. The three zeros were for defining the origin. In the Magmasoft, origin should always be defined like this at first. Five in the other command represent the diameter of the cooling channel in the piston. In order to save the cooling

channels according to these arrangements, ‘save sheet 1 SHEETS/cools’ command was written.

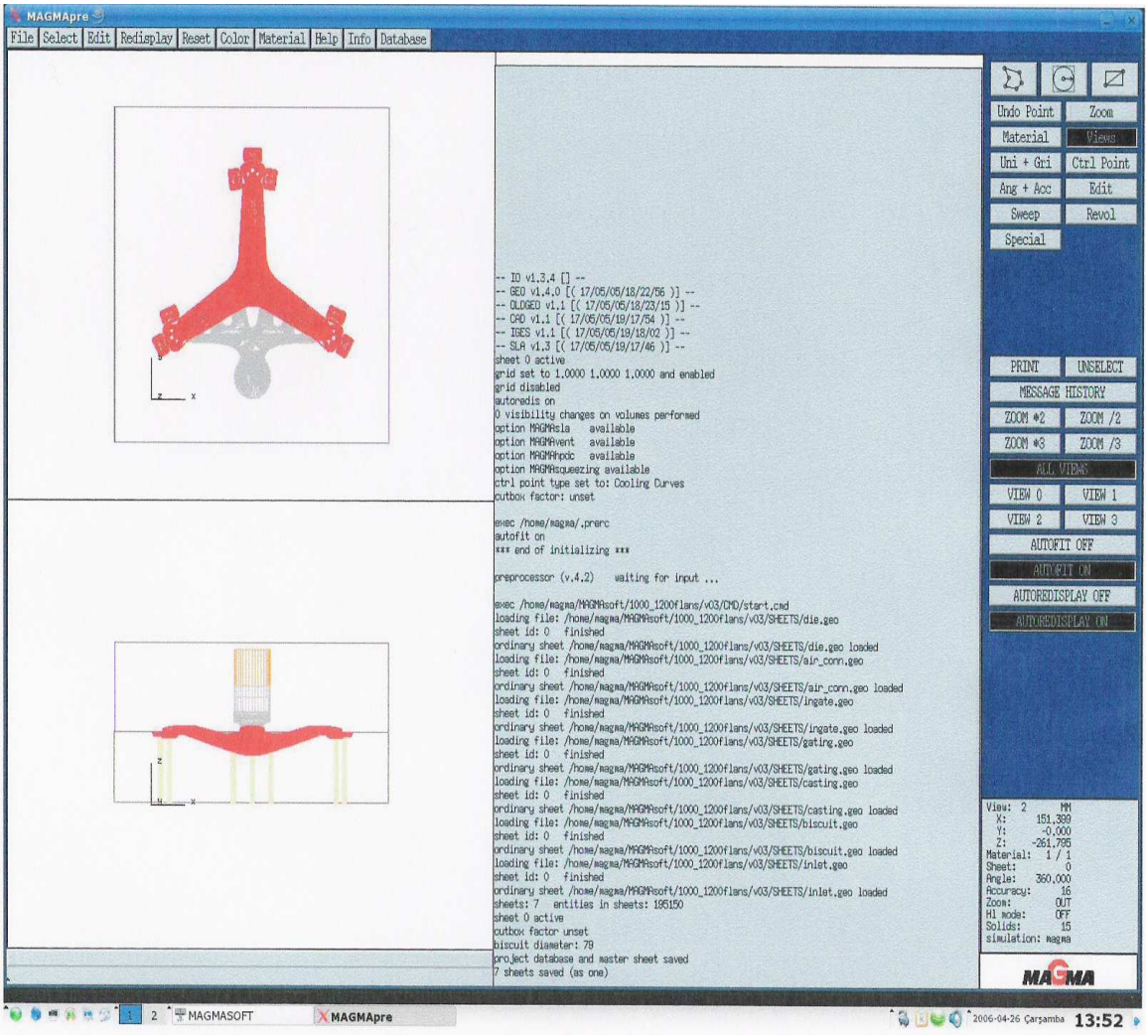

Figure 3.20. Preprocessor outline of the biscuit, inlate, piston and air channels on the Flange (casting). The casting is red, the gating is grey, the air channels are yellow, the biscuit and the inlet are also grey, the piston is orange. On the right, message history of the preprocessor is seen by clicking ‘Message History’ subheading under ‘Views’ heading.

All these adjustments were also activated together in a sheet by clicking Select Active Sheet after Select icon. If the axis are not in the right direction, their directions are changed by ‘rot sel’ command. Rot means rotation. In order to make simulation properly, z axes should be the direction of the cavity, x axes should be the direction of pressurized planes gating, biscuit, inlate, piston from –x to +x, and y axes should be the horizontal direction

on the casting. Then, ‘Save All As 1’ proceeding File icon was clicked. Thus, all the changes up to now was saved as a whole in one sheet.

Tracer points were defined by clicking with the left button of mouse on the top and side views of the biscuit part of the casting. The important point of clicking for the tracer points is that the tracer points should be chosen as possible as away from the cooling channel of the piston. And the number of the tracer points should be at least 100. Thus, tracers were saved as ‘tracer.geo’. In order to activate the definements of the sheet of tracer points, Active Sheet subheading under Select heading was clicked. In order to save all the definements from the biscuit to the tracer points, Save All As 1 subheading proceeding File heading was clicked. Thus, all arrangements were completed and saved as ‘Master.geo’ in the Preprocessor like this.

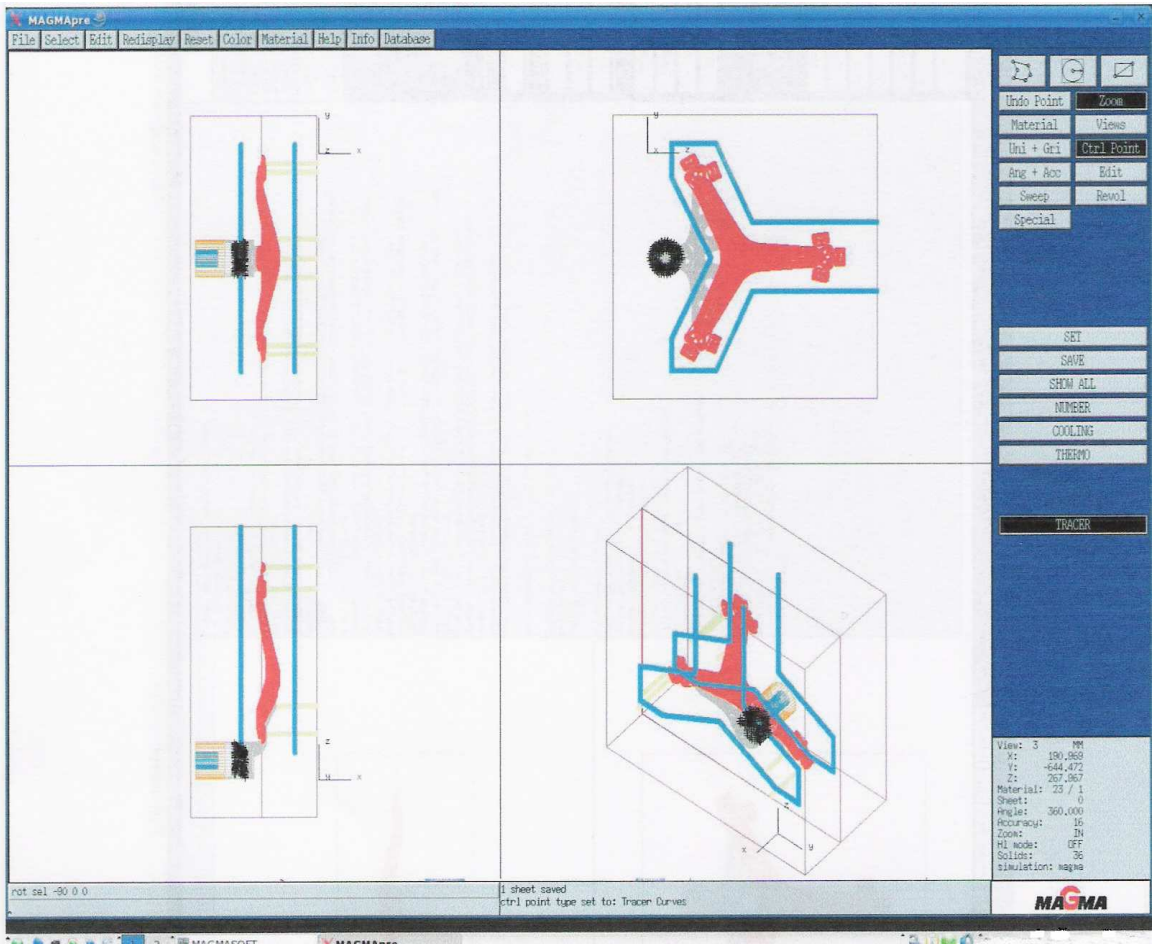

Figure 3.21. Preprocessor outline of different views of the mould i.e. the casting is red, the gating is grey, the air channels are yellow, the biscuit and the inlet are also grey, the piston

is orange, the cooling channels are blue, the tracer points are black in the biscuit. The cooling channel in the piston is circular and the cooling channels in the mould are linear. The directions of axis are seen that the casting is in the right position.

3.2.2. Enmeshment Steps

In order to start working on mesh elements, enmeshment heading in the main menu of Magmasoft was clicked. Under method subheading in the enmeshment, the applied mesh was divided into two groups as advanced and advanced 2. Advanced 2 group consisted of casting and ingate which are more important for high pressure die casting. The advanced group consisted of gating which is less important than casting and ingate for high pressure die casting.

Table 3.1. The values that were entered to Magmasoft enmeshment stage in order to provide the most accurate meshes

	Mesh Standard	**Mesh Advanced**	**Mesh Advanced2**
Accuracy			
x	3	3	3
y	3	3	3
z	3	3	3
Wall thickness			
x	10.00	2.90	0.90
y	10.00	2.90	0.90
z	10.00	2.90	0.90
Element size			
x	10.00	2.00	0.60
y	10.00	2.00	0.60
z	10.00	2.00	0.80
Smoothing	3.00	2.00	2.00
Ratio	5.00	3.00	3.00

Mesh standard values seen in the above table and the values that were seen when Accuracy subheading was clicked are the values that had previously been obtained and given by Magmasoft. In order to define the wall thickness of the casting, wall thickness subheading was clicked. Different values that were nearest to real wall thickness of the

casting were tried. But the most optimum mesh values were obtained according to these values by observing from the Postprocessor of Magmasoft since mesh results and simulation results can be observed in the Postprocessor. Thus, cube and rectangular mesh elements occured. After all of these values were defined, the Flange was meshed and the results of enmeshment were observed by clicking the Postprocessor heading in the main menu of Magmasoft.

The important point when adjusting the meshes is that there should be at least three mesh element lines from buttom to top at the cut view of the ingate while observing the enmeshment in the postprocessor. The results displayed that number of meshes in x direction was 161, number of meshes in y direction was 557, number of meshes in z direction was 516, total number of meshes was 46273332, number of cast alloy meshes was 758748. Furthermore, number of edge to edge connections were 13, number of thin walls was 424, and number of blocked cells was 0. Edge to edge connections, thin walls, and blocked cells are sensitive properties that influence the simulation negatively. Therefore, their numbers should be as small as possible. Changing the wall thickness and element size values, it was tried many times to make the least number of edge to edge connections, thin walls, and blocked cells for the best enmeshment.

3.2.3. Simulation Steps

After enmeshment had been done, the preparations to start the simulation were made. Thus, after clicking simulation headline, the window in the figure 3.22 was approved. Simulations start with calculations. That’s why high pressure die casting calculations window was opened as seen in the figure 3.22. Calculate batch production and prepare fast postprocessing were clicked, then ok icon was clicked. In the figure 3.22 the Linux subprogramme was also seen, because Magmasoft is more effective in Linux than in Windows as Magmasoft simulations occur more quickly with Linux.

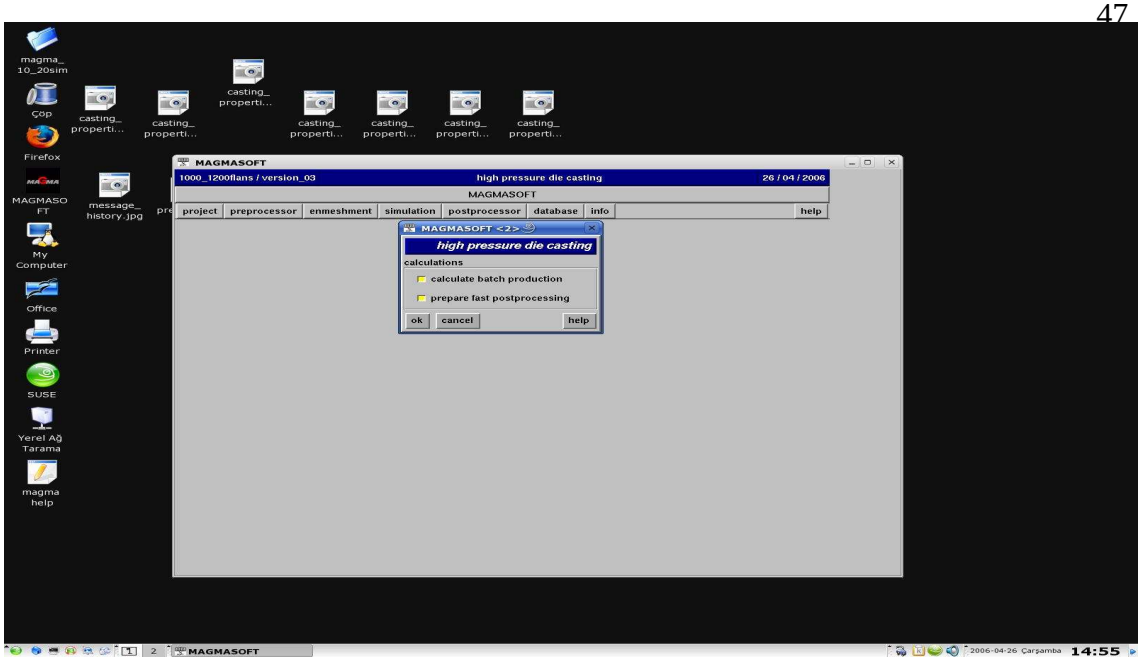

Figure 3.22. Calculations window that started the simulation steps

Initial temperature, liquidus temperature, and solidus temperature values of cast alloy, permanent mold, cooling, and user defined and their materials were defined with the help of the figure 3.23.

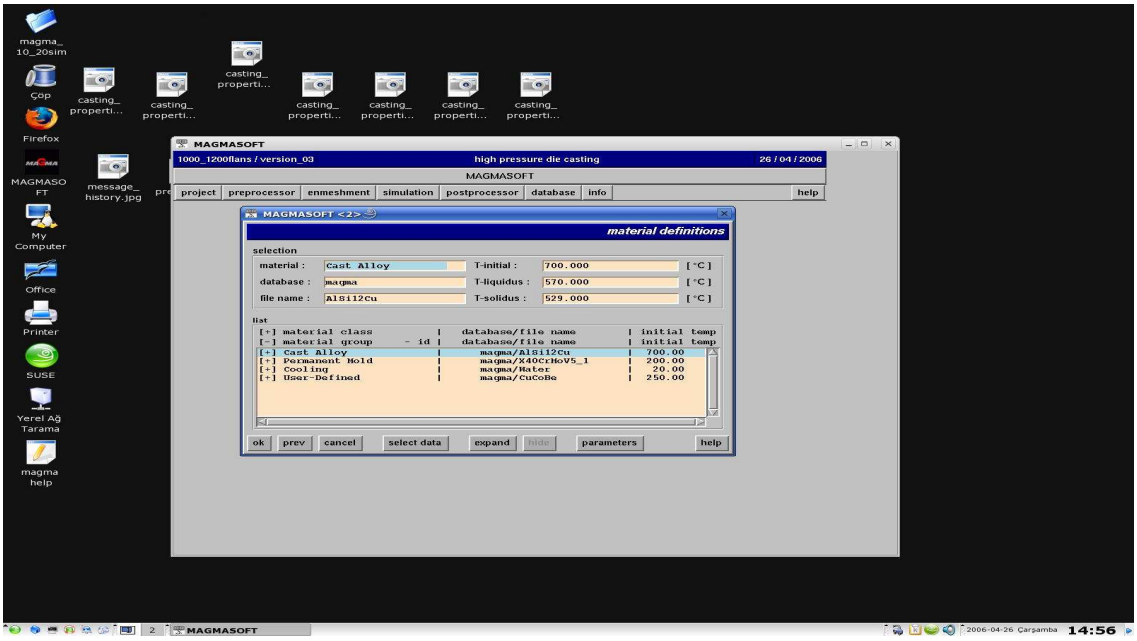

Figure 3.23. Material definitions window

For instance, cast alloy in the figure was clicked with left button of the mouse firstly. Then, the initial temperature, liquidus temperature, and solidus temperature values of cast alloy and the cast alloy material were written with the help of expand at the buttom of the material definitions table. Permanent mold, cooling, and user defined values were written in the same way by clicking on the select data button after the expand button. After all of the temperatures and materials were defined, ok button at the bottom of the material definitions table was clicked.

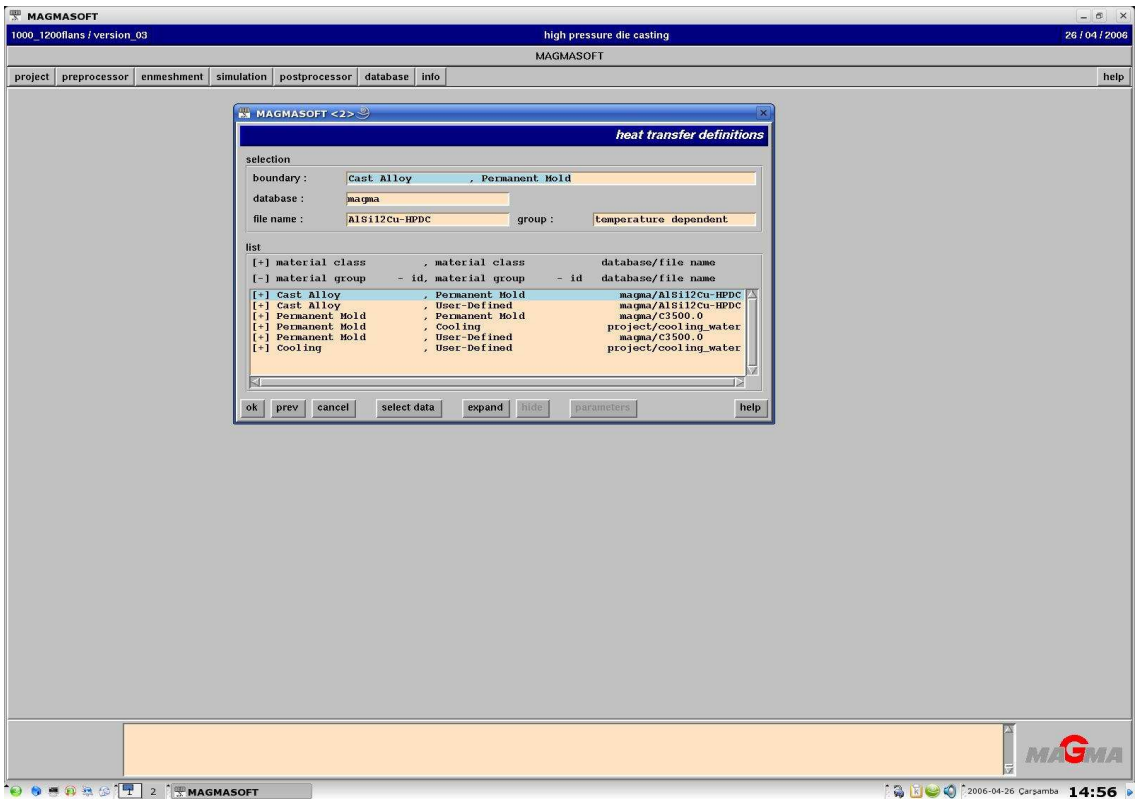

Figure 3.24. Heat transfer definitions window

After defining the material definitions, heat transfer definitions were made in the same way as seen in the figure 3.24.

When heat transfer definitions were finished, a new window in the figure 3.25 asking ‘start the HPDC calculator now?’ occured. And the calculator was started by pressing on ok at the bottom of the window with the left button of the mouse.

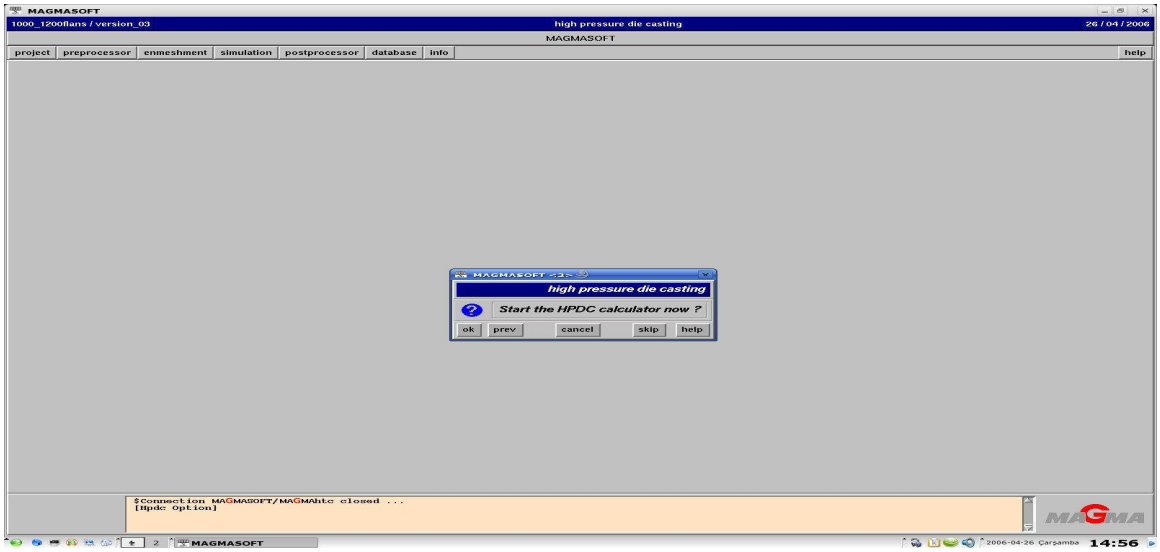

Figure 3.25. The high pressure die casting calculator starting window

Then, volume and area data were written as seen in the figure 3.26. The geometry data values seen on the left were written to the space on the right and next button was clicked with the left button of the mouse.

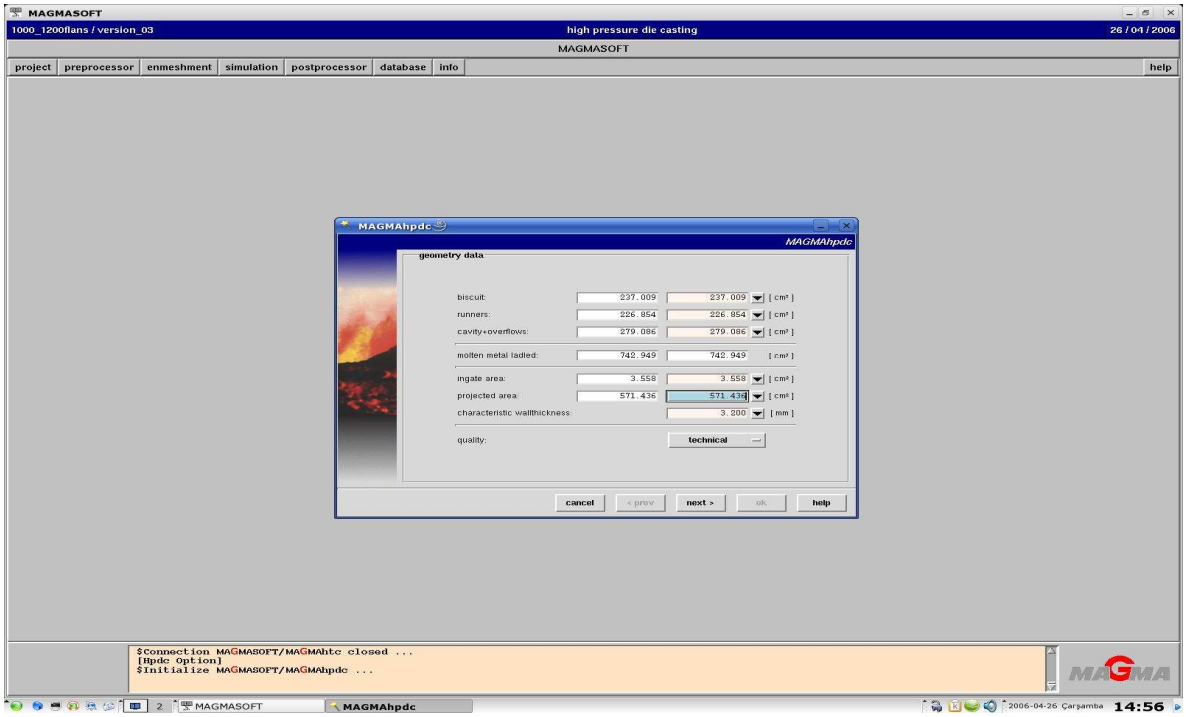

Figure 3.26. Geometry data window

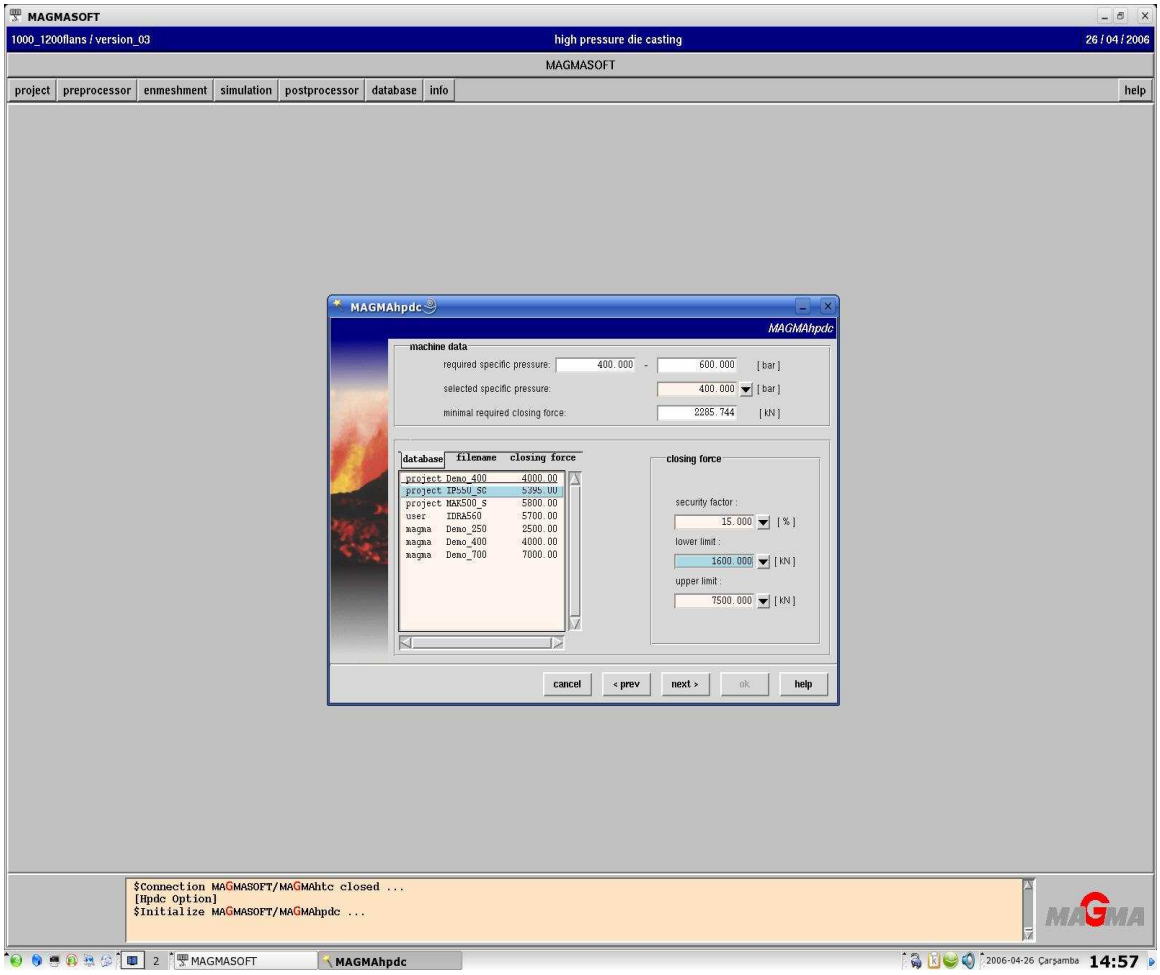

Figure 3.27. Machine data window

After defining the geometry data, machine data values, which are seen in the figure 3.27, were defined. The machine used for casting the Flange was IP550. Thus, IP550 was selected. The pressure and closing force values of the machine were approved by clicking on next.

Then, shot sleeve data values as seen on the left were written to the space on the right and next button was clicked with the left button of the mouse in the figure 3.28.

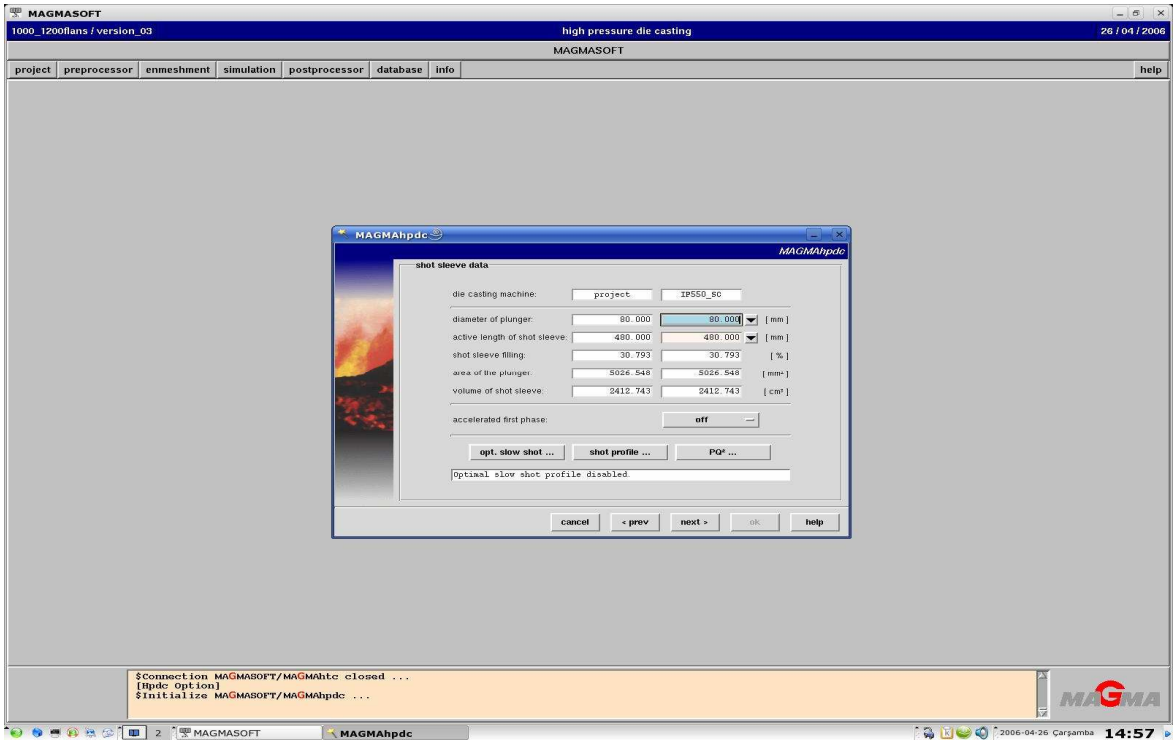

Figure 3.28. Shot sleeve data window

After defining shot sleeve data values, process data values, which are seen in the figure 3.29 were also approved by clicking on the next.

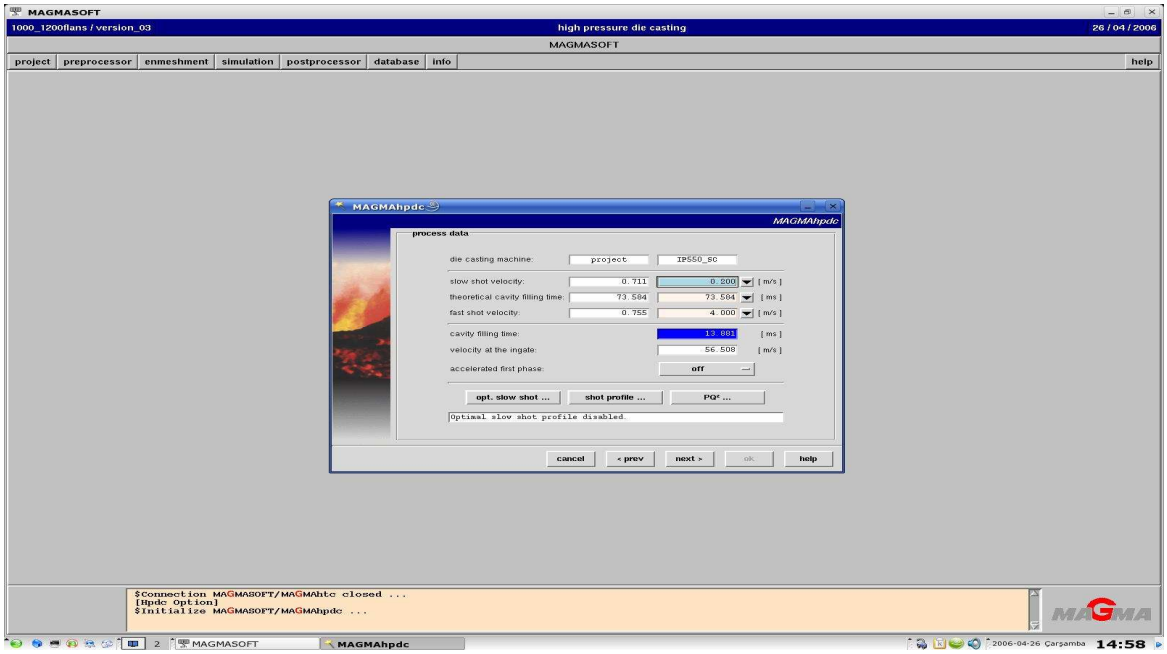

Figure 3.29. Process data window

Shot characteristics were also approved samely by clicking on the next as seen in the figure 3.30.

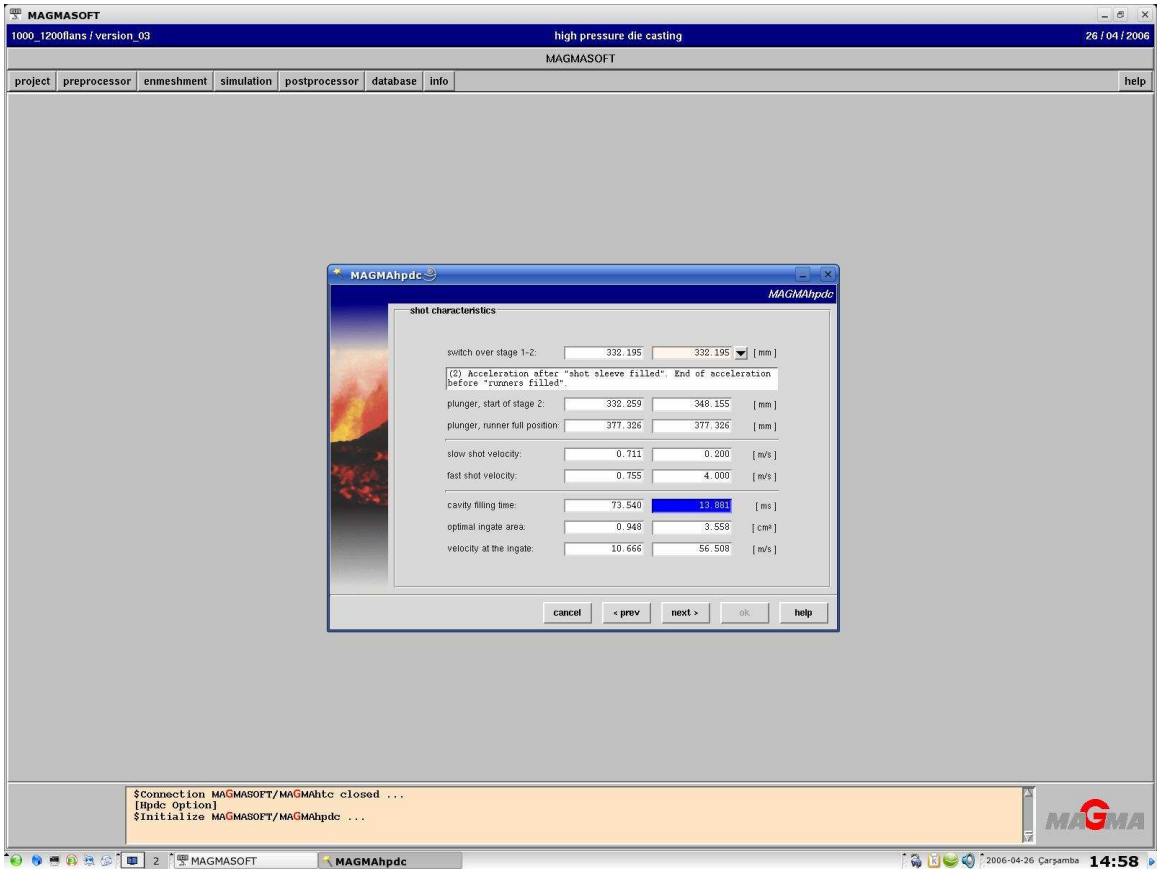

Figure 3.30. Shot characteristics window

Then, cycle definitions window in the figure 3.31 was appeared. How many cycle of casting was going to be made was written. Simulations were made for one cycle and five cycles. Do filling, fill results and solid results were made yes. Thus, cycle definitions were defined by clicking ok.

In the options window of figure 3.34, pressurize was made yes, die coating and quenching were made no since there was pressure, but there were not coating and quenching. Then, ok was clicked.

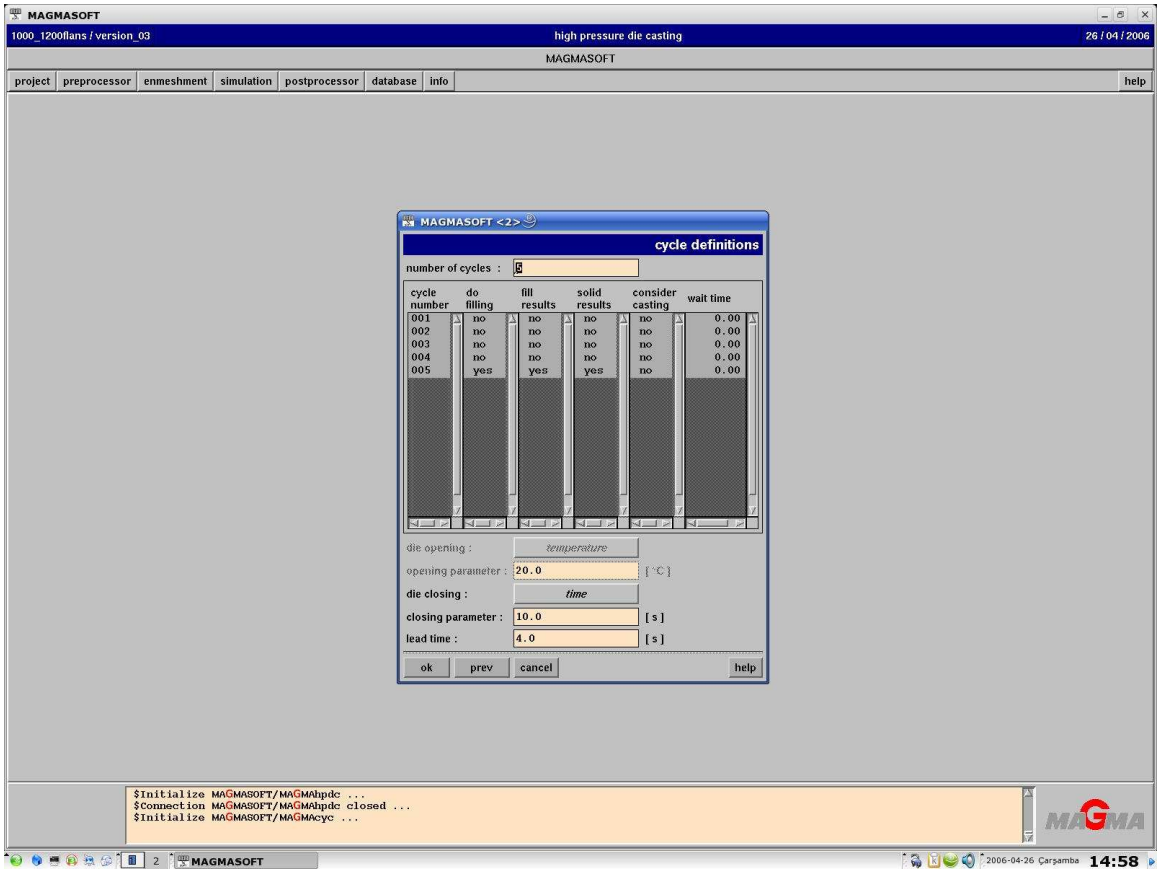

Figure 3.31. Cycle definitions window

Then, core open definitions were defined. Since there is no channel, channel definitions were leaved blank. Core open definitions and free channel definitions windows are in the Figure 3.32 and Figure 3.33.

Filling and solidification definitions were defined as seen in the Figure 3.35 and Figure 3.36. Then, OK was clicked.

The results, which were wanted to be seen after simulation, were signed in the fast postprocessing preparation window of Figure 3.37.

After clicking OK, simulation started with online job simulation control window in the figure 3.38.

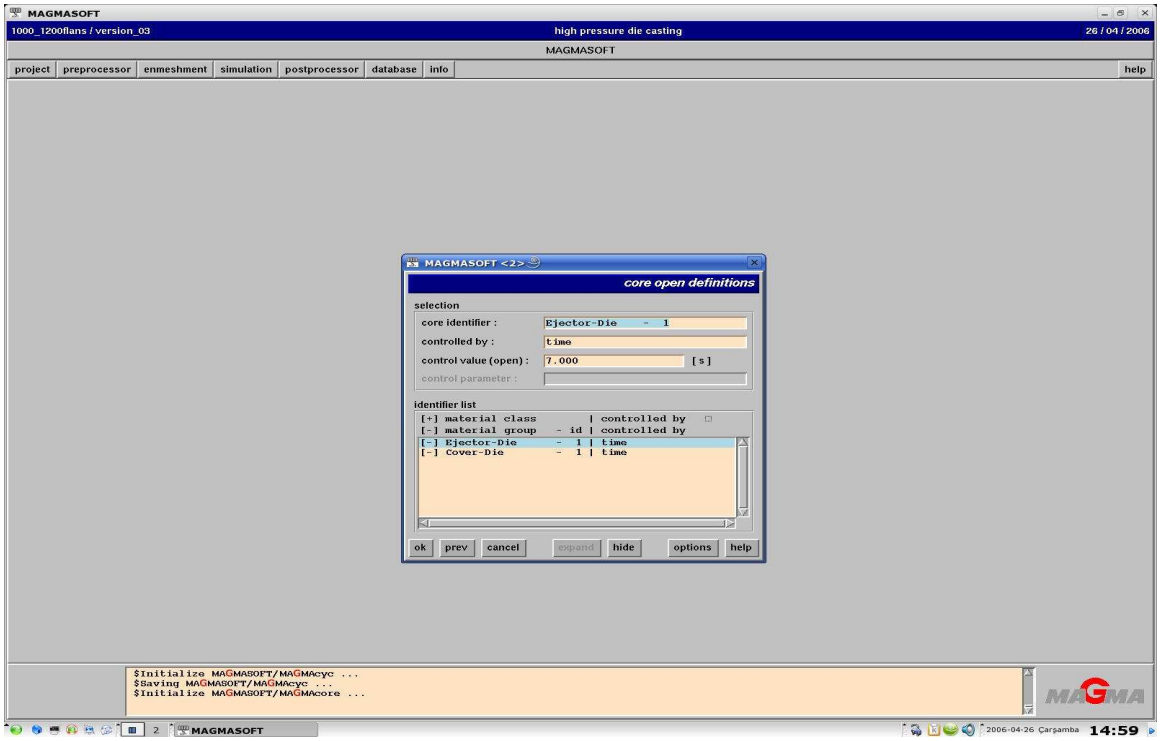

Figure 3.32. Core open definitions window

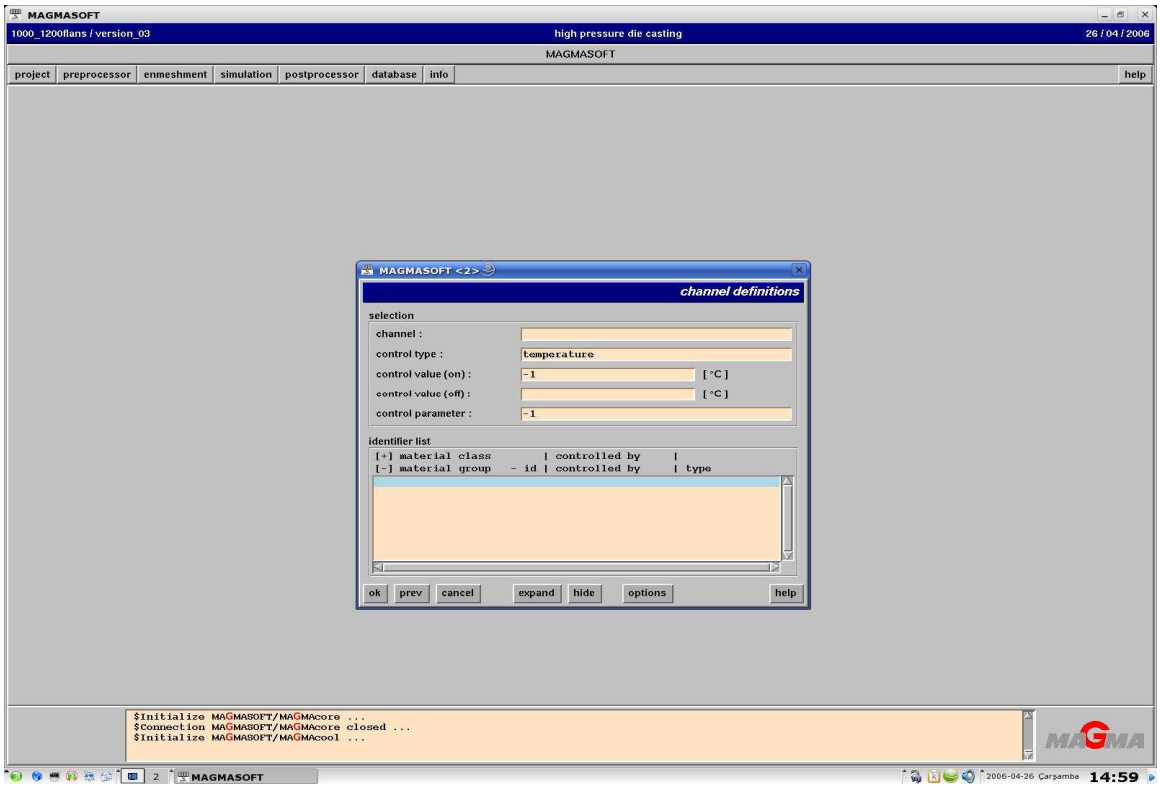

Figure 3.33. Channel definitions window

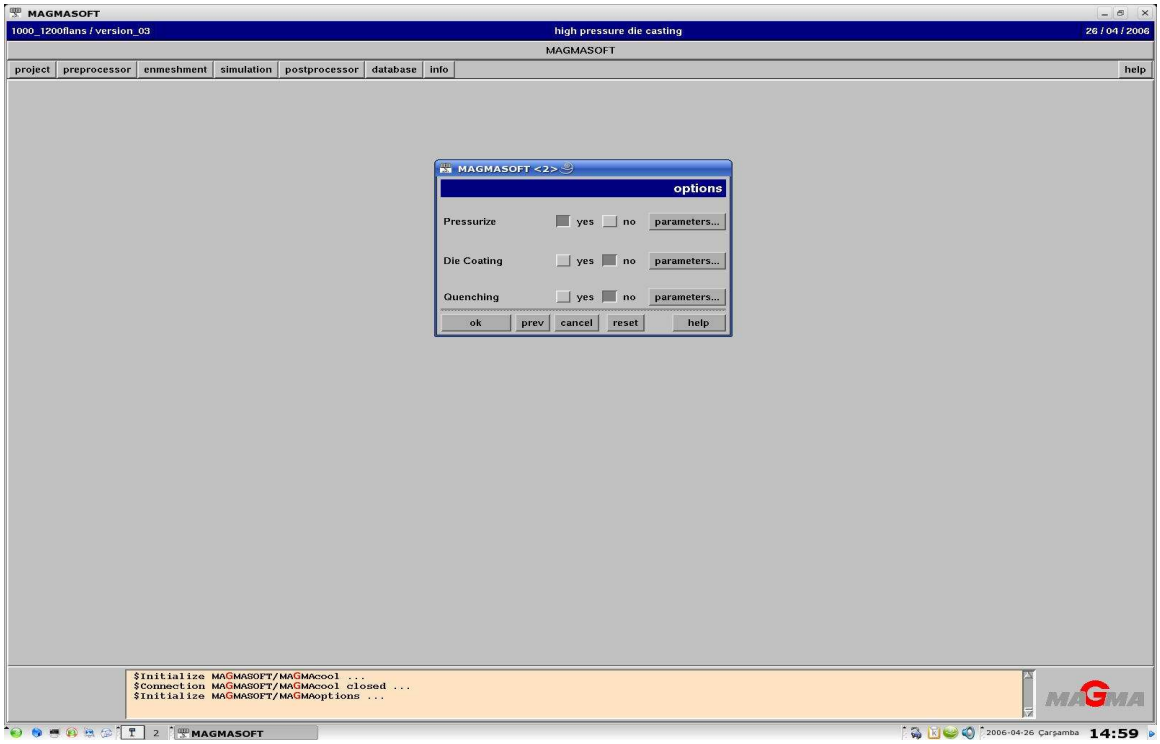

Figure 3.34. Options window

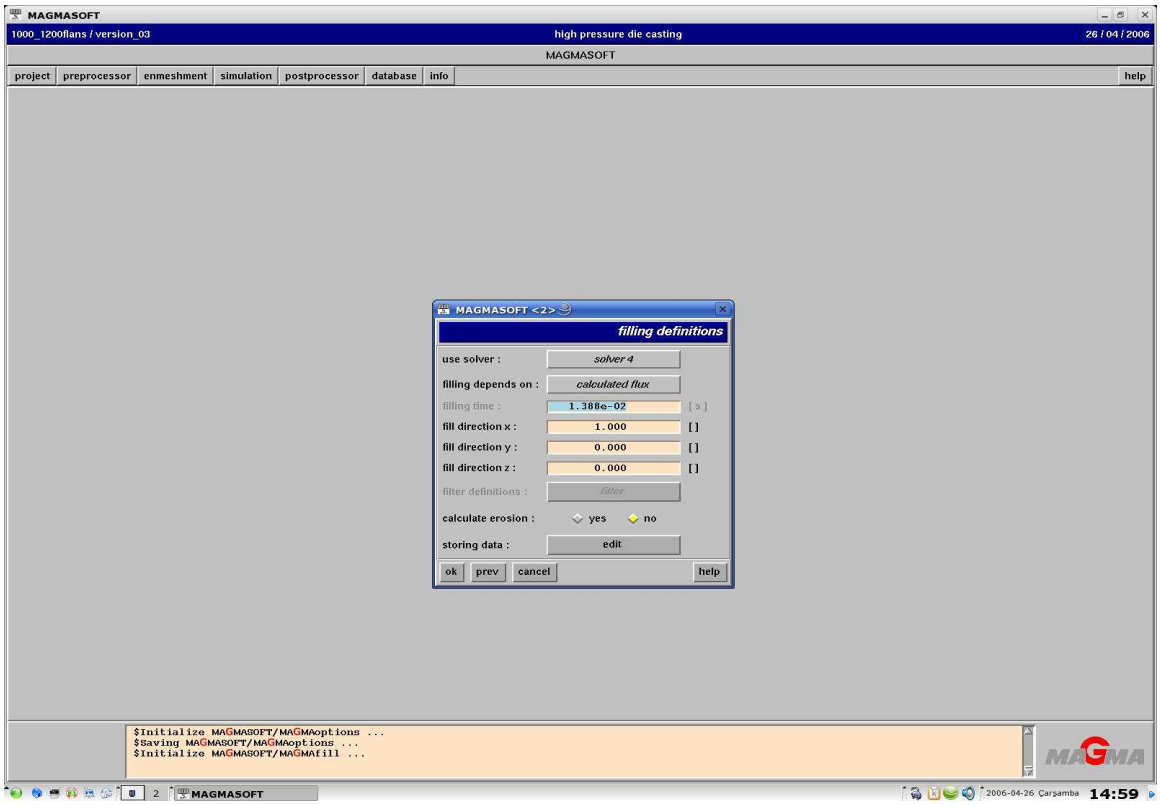

Figure 3.35. Filling definitions window

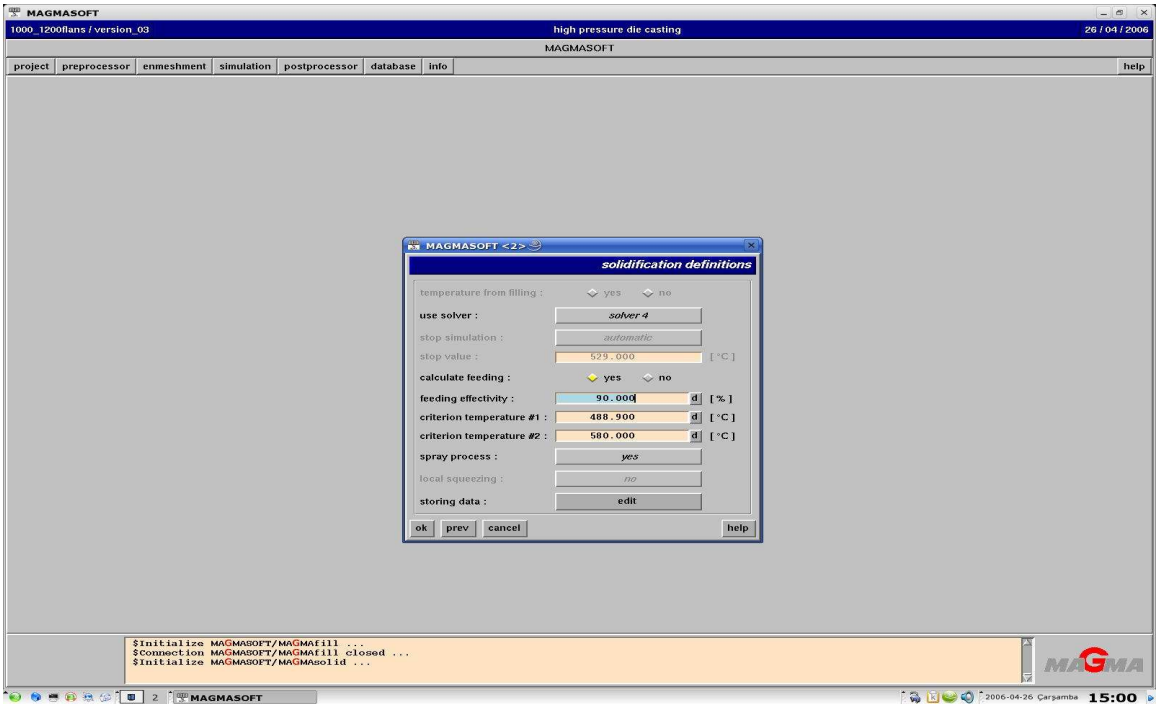

Figure 3.36. Solidification definitions window

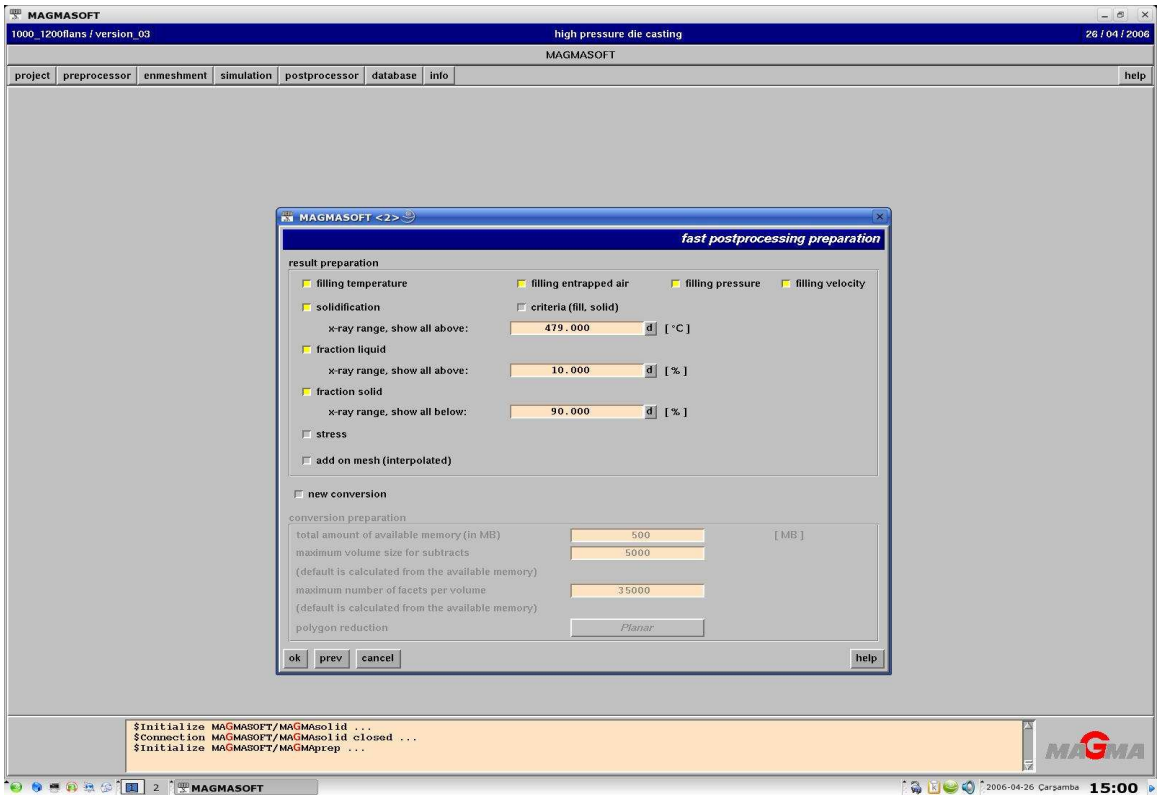

Figure 3.37. Fast postprocessing preparation window

In the figure 3.38 online job simulation control is seen for 0.1 second of the simulation. In the figure 3.39 online job simulation control is seen for approximately 46% of the simulation was made.

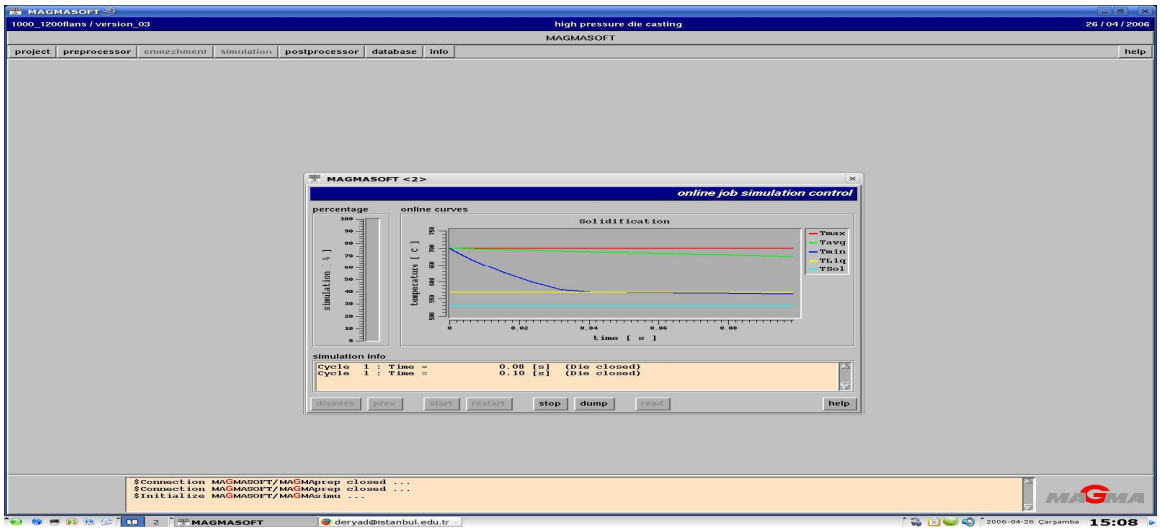

Figure 3.38. Online job simulation control window at 0.1 second of the simulation when the simulation is just started

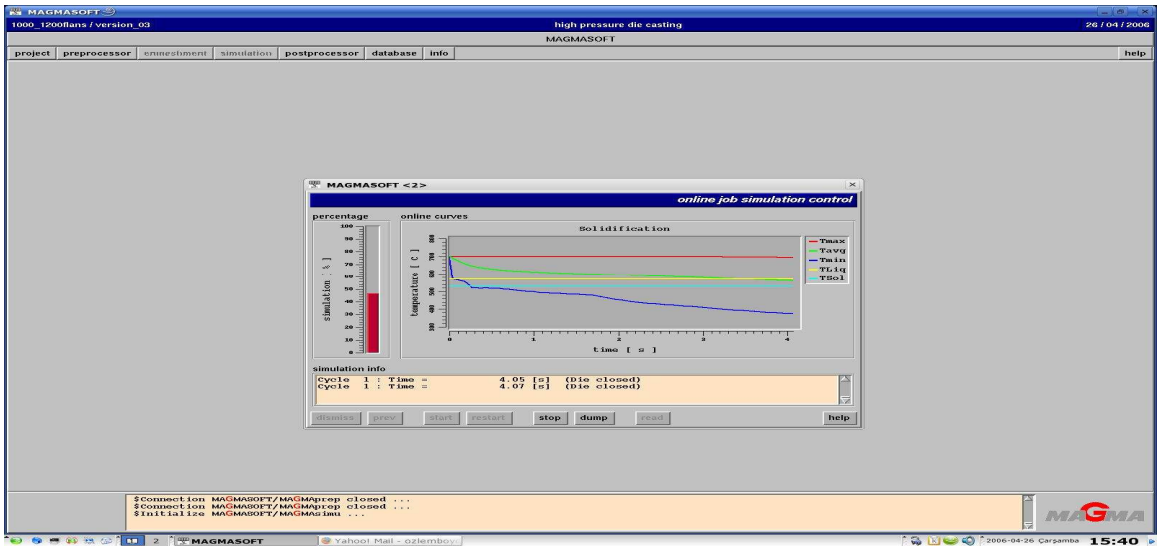

Figure 3.39. Online job simulation control window when approximately 46% of the simulation was made

3.3. Results Of The Simulation For AlSi12Cu Flange

After all the parameters were defined at the simulation step, Magmasoft programme started the simulation of the high pressure die casting alloy AlSi12Cu of the Flansch for cycle 1 and cycle 5. Results of filling temperature, filling velocity, filling pressure, filling time, air entrapment, and solidification of the casting were taken. These resullts are very accurate. Moreover, these results are not only valid but also applicable to reality. Temperature, velocity, pressure, time, and air entrapment percentage values during filling and solidification can be learned from these results. These simulation results are going to be demonstrated in the figures below from now on.

3.3.1. The Simulation Result For Our Mesh Quality

From the mesh quality simulation picture in the Figure 3.3.1, it is understood that an excellent mesh quality was done since it is also written in the simulation picture that the number of blocked cells are 0, the number of edge to edge connections are 13, and the number of thin walls are 424, which are rather small. Thin walls, edge to edge connections, and blocked cells are critical points that affect the simulation negatively. That's why their number should be as small as possible. Because at the points where there are many blocked cells the flow of melt can not demonstrate its continuity, and it is often blocked. Since number of the blocked cells is zero, flow of the liquid metal is not obstacled and the melt flew continously and freely.

Additionally, edge to edge connections obstacle the continuity of meshes. As seen in the figure 3.3.1 there are only 13 edge to edge connections, which are not at the important parts of the casting for simulation. Moreover, thin walls are weak points of the casting but there are only 424 thin walls at some of the thin sections of outer surface of the casting, at the entrance of overflows, at the gating, and at two of the ingates as seen in the figure 3.3.1. Since the thin sections, the gating, and the ingates are not at the inside of the casting, the thin walls here does not affect simulation. Since overflows are for air vents, the thin walls here does not affect simulation. Thus, these critical points thin walls, edge to edge connections, and blocked cell should be at the least important places for the casting

such as air pockets, overflows, gatings, ingates, biscuits, inlates, pistons, sections of outer surface, and etc.

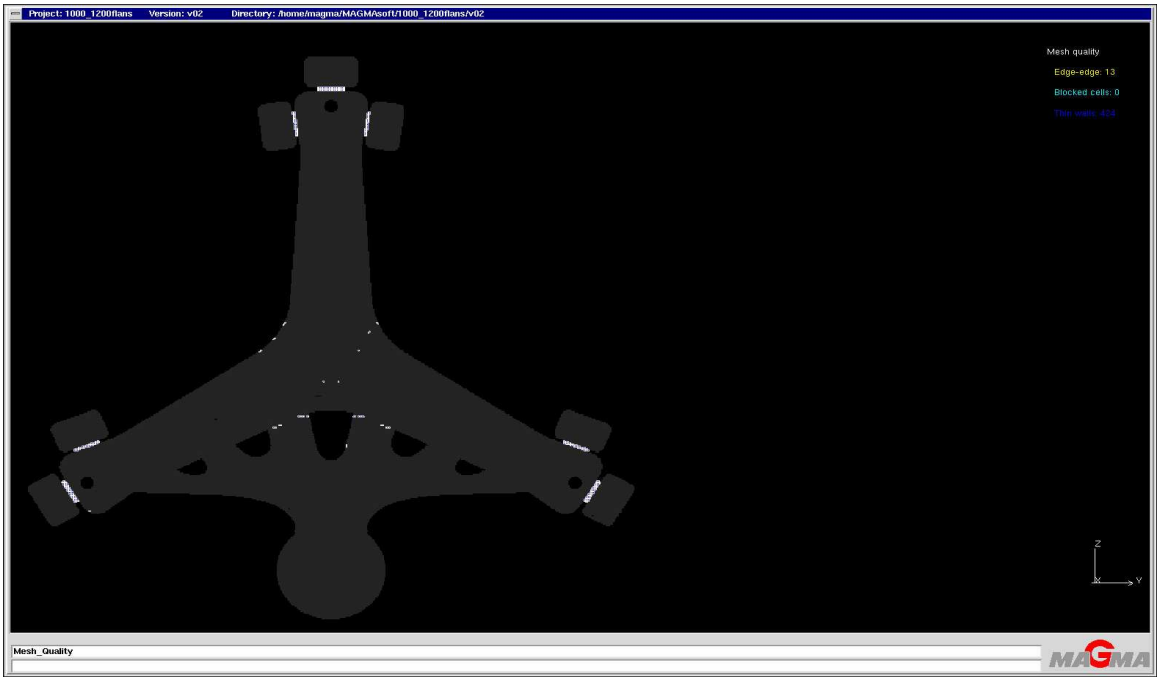

Figure 3.40. Viewing the mesh quality simulation result of the Flanch for cycle 5

3.3.2. The Simulation Result For Path Of The Tracers

In order to fulfil the simulation as well as to see the way of melt flow step by step completely, tracer particles was activated in the ‘‘options window’’ for the simulation that was defined in the preprocessor.

Tracers are the particles which define the path of liquid metal flow not dimensionally but pointally. From this simulation picture in the Figure 3.3.2, it can be understood that the melt was poured from the biscuit by comparing with the millimetric path length scale at the right side of the simulation picture. Since the tracers in the biscuit have light blue color which means the shortest path length according to the path length scale.

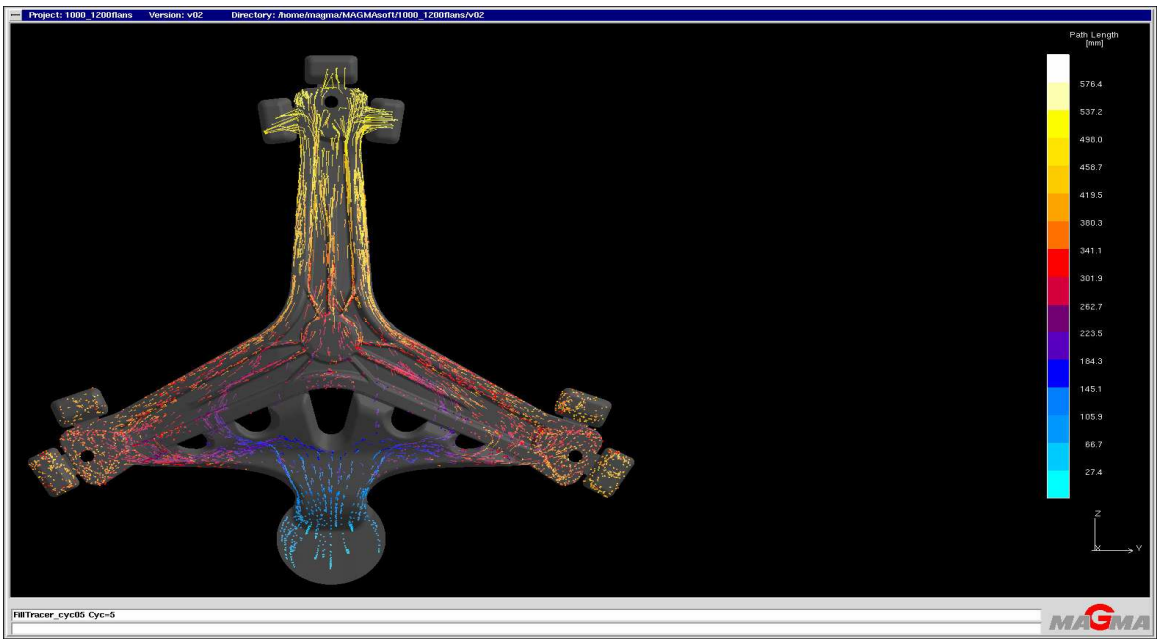

Figure 3.41. The simulation result of the path legth (mm) of tracers in order to visualize the melt flow for cycle 5

It can also be seen that the flow of melt is from the biscuit to the furthest regions than the biscuit and also the path way of melt flow can be seen step by step from the simulation picture. Accordingly, the liquid metal is flowing from biscuit to gating, runners, ingate, bottom corners of the casting, and top corner of the casting in orderly according to color change between them comparing with the path length scale. Therefore, relatively the latest filled region is the top of the Flanch since this region has light yellow color. The regions that have tones of red color are seen that they are filled before the top region, but after the blue toned biscuit region.

Thus, the path length of tracers are getting bigger from biscuit to the top corner of the Flanch as seen in the simulation picture of Figure 3.3.2. While the path length of tracers in the biscuit is approximately 27.4 mm, the path length of tracers in the gating is 145.1 mm, in the ingate is 223.5 mm, and in the casting changes from 262.7 mm to 537.2 mm towards the top of the casting according to the millimetric path length scale at the right side of the simulation picture.

3.3.3. The Simulation Result For Enter Time Step Of The Tracers

Tracer particles demonstrate the flowing of the liquid metal point by point. In the following simulations for enter time step of the tracers in the figures 3.3.3, 3.3.4, 3.3.5, 3.3.6, and 3.3.7 the entire movements of the melt can be seen clearly. Additionally, how liquid metal is flowing pointally not dimensionally can be seen in detail in these figures with time dependence not length dependence like the Figure 3.3.2. While the light yellow particles are the most active liquid metal points, the light blue particles are relatively motionless, and the red particles are more active than blue particles but less active than yellow particles as comparing with the enter time step scale in the figures 3.3.3, 3.3.4, 3.3.5, 3.3.6, and 3.3.7.

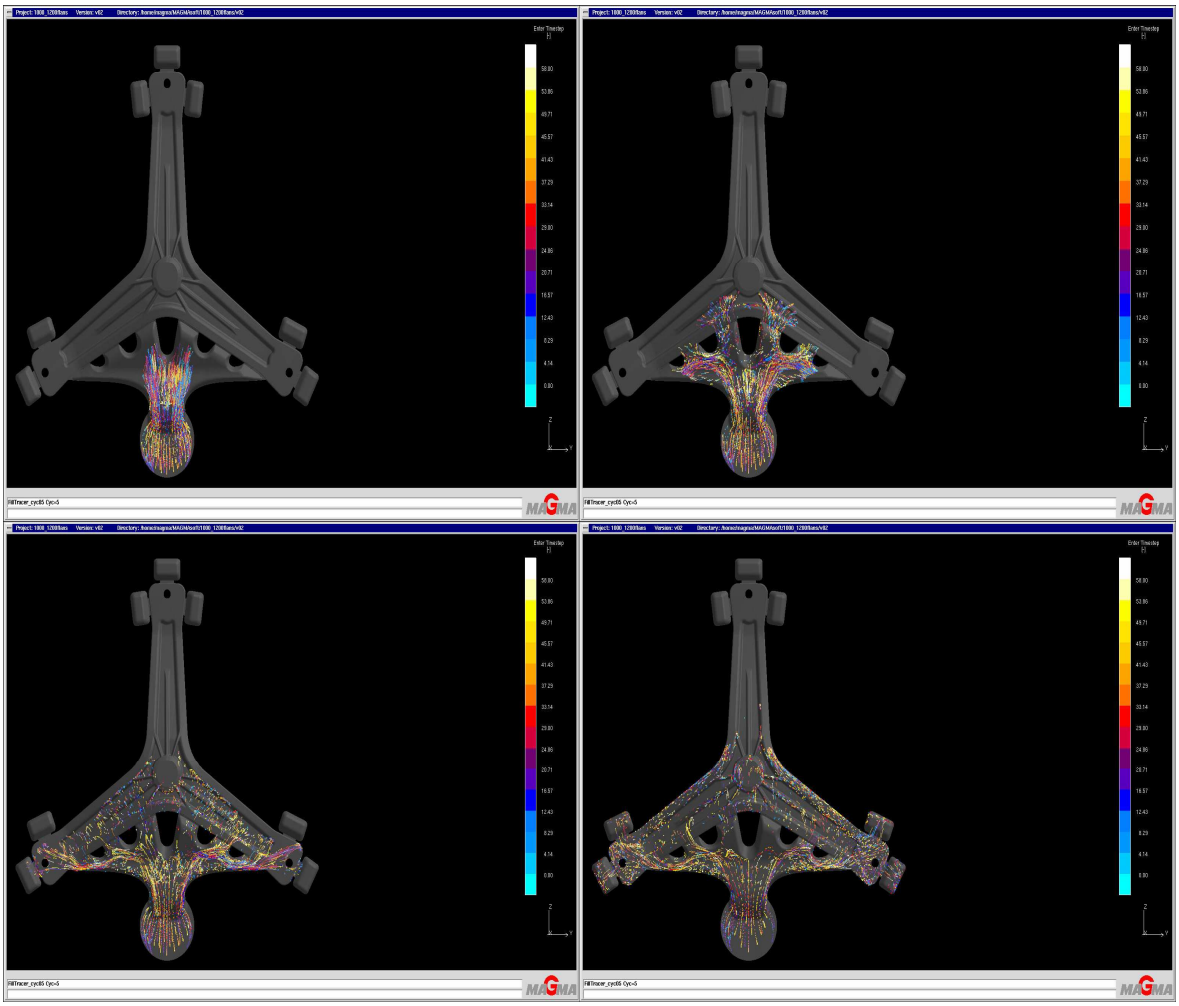

Figure 3.42. Enter time step of the tracers for 52% of filling, 65% of filling, 75% of filling, and 85% of filling was done for cycle 5, respectively

Comparing with the enter time step scale at the right side of the Figure 3.3.3, the enter time step for light yellow tracer particles is the biggest, which is 58. This means that the light yellow tracers are the most active points of the melt. The enter time step for light blue tracer particles is the smallest, which is 0. This means that the light blue tracers are motionless. The tracer particles that have colors between yellow and blue are moderate active; for example the enter time step for navy blue tracers is 12.43, for purple tracers is 20.71, and for red tracers is 29, for orange tracers is 37.29. Thus, motion of melt showed by orange tracer points are more than motion of melt showed by red tracer points, however motion of melt showed by red tracers are more than motion of melt showed by purple tracers, but motion of melt showed by purple tracers are more than motion of melt showed by navy blue tracers. These explanations are also valid for Figure 3.3.4 and only percentage of filling values change among these figures.

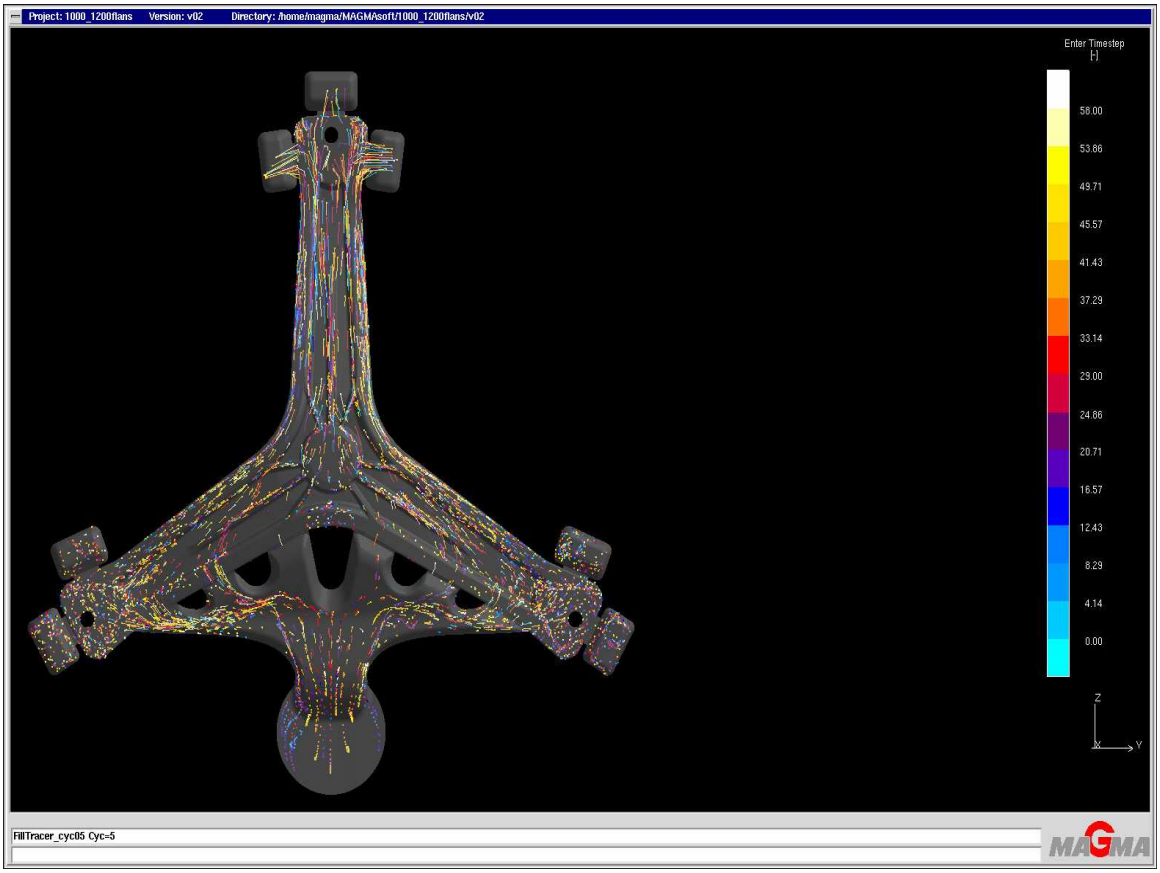

Figure 3.43. Enter time step of the tracers for nearly 100% of filling was done for cycle 5

3.3.4. The Simulation Result For The Age Of Tracers

From the simulation picture in the Figure 3.3.5, age of tracer particles after 100% of filling can be seen. According to the age scale with respect to second on the right side of the simulation picture, the youngest tracers are light blue toned tracer particules and the oldest tracers are light yellow toned tracer particules.

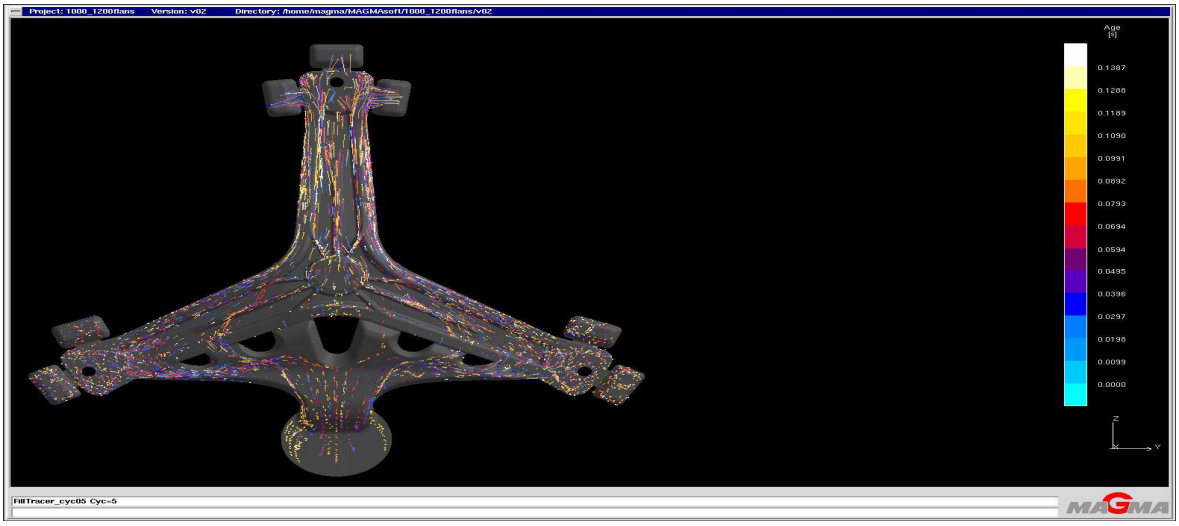

Figure 3.44. Age of the tracer particles for 100% filling, and for cycle 5

The stages of tracer age seperated by different colors on the age scale with respect to second are seen on the right of the Figure 3.3.5. According to this stages of age, the light blue tracer particles are 0 second old, and the light yellow tracer particles are 0.1387 second old; since the light blue color is at the bottom of the age scale, and the light yellow color is at the top of the age scale. The oldest light yellow tracer particles demonstrate the longest melt flow. Moreover, the youngest light blue tracer particles demonstrate the least active melt flow.

The age of other tracers between light blue and light yellow change from 0 second to 0.138 second. For instance, the purple tracer particles are 0.0495 second old, the red tracer particles are 0.0694 second, the orange tracer particles are 0.0793 second old. This means that melt flow of orange particles are longer than red tracers, melt flow of red tracer particles are longer than purple particles, melt flow of purple tracer particles are longer than blue tracers.

3.3.5. The Simulation Results For the filling Time

According to this filling simulation picture in the Figure 3.45, the casting, gating, and ingate parts are 100% filled in 1.690 second as comparing the light yellow color on these parts with the colors on the time scale. Thus, it is understood that these filling process is very fast.

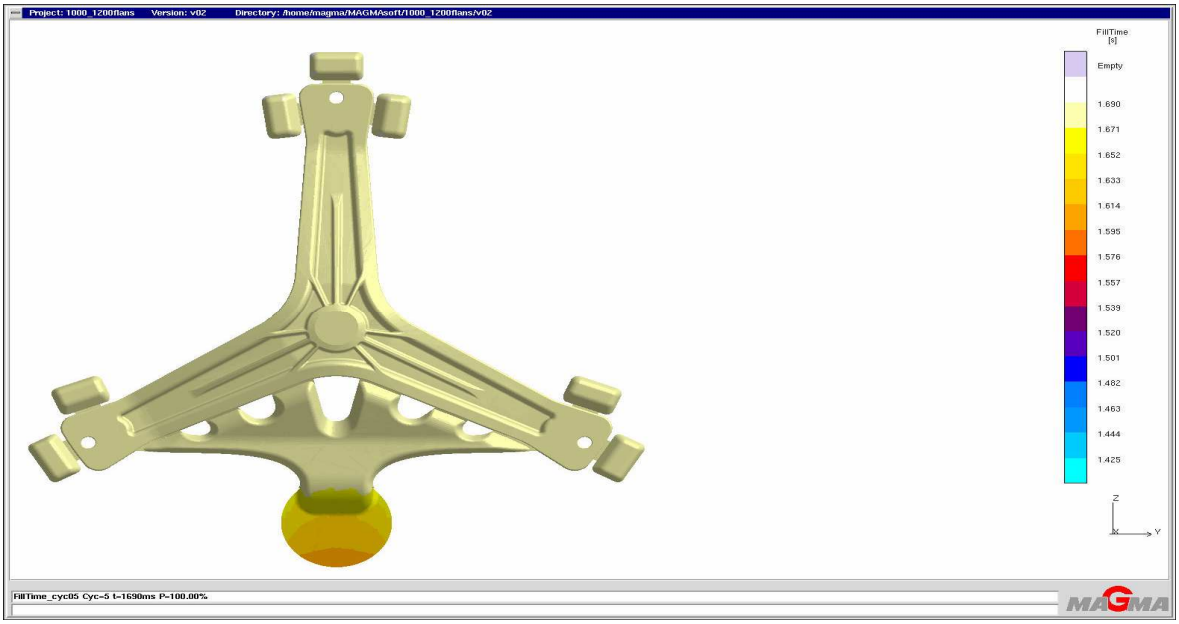

Figure 3.45. Time of 100% filling simulation result for cycle 5

Since the filling is started from the biscuit part, there is orange color presenting 1.614 second at the bottom corner of the biscuit. This means that the bottom corner of the biscuit is the firstly filled region. In the biscuit, time of filling increases step by step from the bottom corner to the gating since light orange, dark yellow, and yellow colors are seen there. Additionally, light orange represent 1.633 second, dark yellow represent 1.652 second, and yellow represent 1.671 second of filling for the biscuit part.

3.3.6. The Simulation Results For The Filling Velocity

The filling velocity simulation result for 52% of filling at 1672 millisecond is seen in the Figure 3.3.7. The velocity range changes from 625 cm/s to 7429 cm/s for 52% filling .

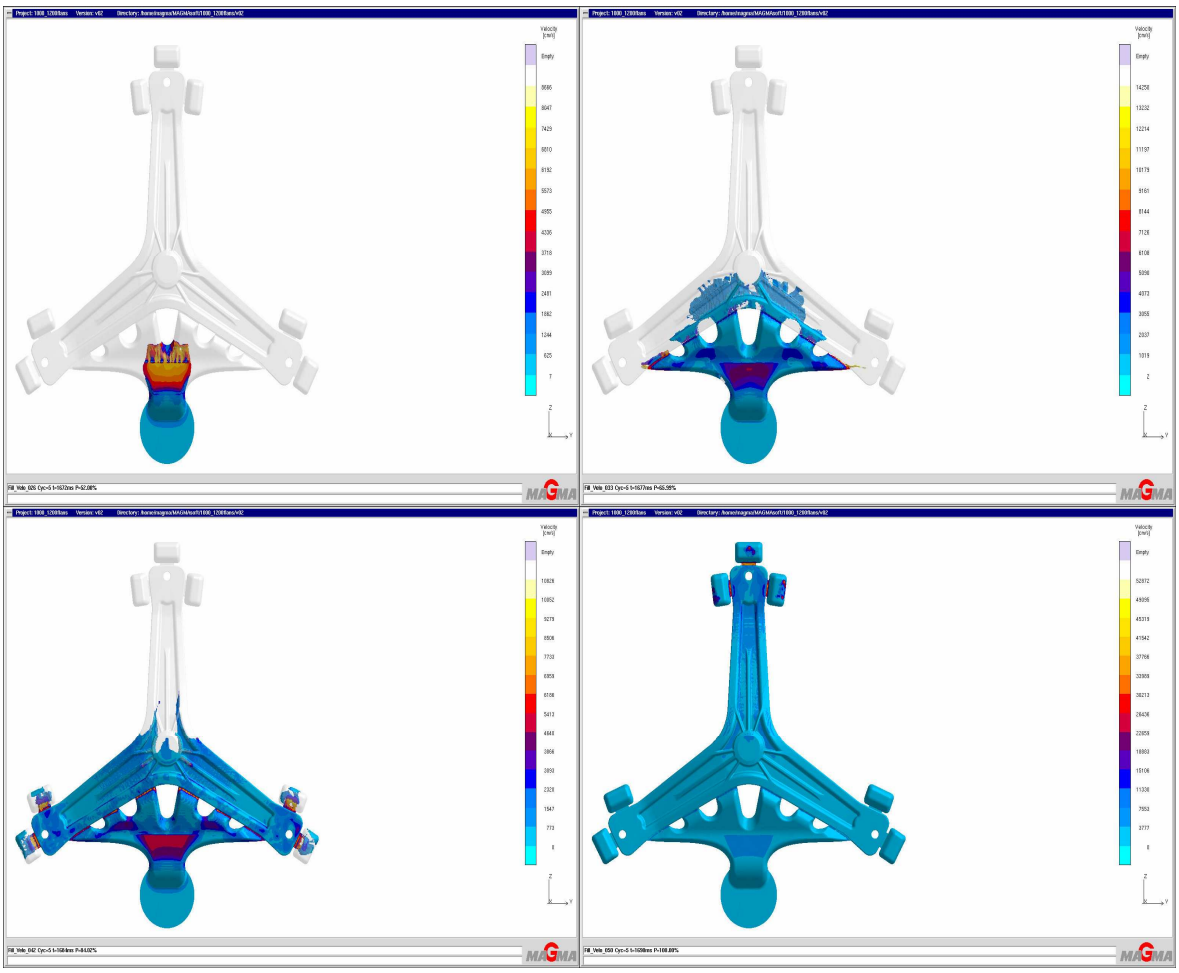

Figure 3.3.7. Representation of filling velocity simulation result for 52%, 65.99%, 84.02%, and 100% of filling for 5 cycles respectively

Since the liquid metal is poured from the biscuit, it can be seen that the melt in the biscuit has the slowest velocity 625 cm/s from the simulation picture in the Figure 3.3.7 for 52% of filling. Because the melt in the biscuit stays backward and its velocity slows down. However, the velocity of the liquid metal in the gating, proceeding from the biscuit, increases step by step because of flowing forward and there is also a velocity increase just at the end of the biscuit from 625 cm/s to 1244 cm/s. Comparing with the velocity scale with respect to cm/s on the right side of the simulation picture, the velocities in the gating are increasing from 625 cm/s to 1244 cm/s, 1862 cm/s, 2481 cm/s, 3099 cm/s, 3718 cm/s, 4336 cm/s, 4955 cm/s, 5573 cm/s, 6192 cm/s, 6810 cm/s, and 7429 cm/s respectively. Additionally, in the simulation picture of the Figure 3.3.7, the dark blue region in front of the melt might be because of crashing of the melt to the runner wall, and the melt slows

down to 1862 cm/s. Velocity of the liquid metal slows down when the fastly coming liquid metal meets an obstacle.

Filling velocity simulation result for 65.99% of filling at 1677 millisecond is also seen in the Figure 3.3.7. The general velocity, which is seen at many parts with light blue color, is 1019 cm/s comparing with the velocity scale with respect to cm/s on the right side of the Figure. However, in some regions different velocities such as 3055 cm/s in the blue colored regions, 4073 cm/s in the dark blue colored regions, 5090 cm/s in the light purple colored regions, 6108 cm/s in the purple colored regions, 7126 cm/s in the dark red colored regions, 8144 cm/s in the red colored regions, etc. can be observed from the figure. The reason why there is a velocity increase from 3055 cm/s to 7126 cm/s step by step at the center of the gating is the second heat of the piston and relatively thin volume of the gating. There is also a velocity increase from 3055 to 4073 cm/s and to 7126 cm/s in the ingates due to becoming narrow. 7126 cm/s velocity is in the left and right ingates, 4073 cm/s is in the other ingates. When a liquid metal enters into a narrow channel, firstly it slows down by crashing, then it accelerates with a jet effect going out of the channel.

Filling velocity simulation result for 84.02% of filling at 1684 millisecond is also seen in the Figure 3.3.7. The general velocity, which is seen at many parts with light blue color, is 773 cm/s comparing with the velocity scale with respect to cm/s on the right side of the Figure. However, in some regions different velocities such as 2320 cm/s in the blue colored regions, 3093 cm/s in the dark blue colored regions, 3866 cm/s in the light purple colored regions, 4640 cm/s in the purple colored regions, 5413 cm/s in the dark red colored regions, 6186 cm/s in the red colored regions, etc. can be observed from the figure due to change of flow. When the velocities of 65.99% and 84.02% filling is compared, it is seen that the velocity range of 84.02% filling is lower than the velocity range of 65.99% filling.

The reason why there is a velocity increase from 2320 cm/s to 5413 cm/s step by step at the center of the gating for 84.02% filling in the Figure 3.3.7 is the its relatively thin volume. There is also a velocity increase from 2320 cm/s to 6186 cm/s and to 8506 cm/s in the ingates due to becoming narrow. 6186 cm/s velocity is in the left and right ingates, 8506 cm/s is in the other ingates. Furthermore, there is a velocity increase from 6186 cm/s to 8506 cm/s in the narrow channels that connect the casting to the overflows at the

corners. After flowing out of these channels, the velocity decreases to 773 cm/s in the overflows by crashing of the melt to their walls in the Figure 3.3.7.

Filling velocity simulation result for 100% of filling at 1690 millisecond is also seen in the Figure 3.3.7. The general velocity, which is seen at many parts with light blue color, is 3777 cm/s comparing with the velocity scale with respect to cm/s on the right side of the Figure. However, in some regions different velocities such as 11330 cm/s in the blue colored regions, 15106 cm/s in the dark blue colored regions, 18883 cm/s in the light purple colored regions, 30213 cm/s in the red colored regions, 41542 cm/s in the orange colored regions, etc. can be observed from the figure. There is a velocity increase from 3777 cm/s to 7553 cm/s at the center of the gating due to relatively thin volume of that side of the gating . The same amount of velocity increase can also be observed at the ingates due to becoming narrow. At the upper side of the casting, some amount of velocity increases from 3777 cm/s to 7553 cm/s and from 3777 cm/s to 15106 cm/s step by step are visible. Because the lastly filled zone is the upside of the Flansh. Therefore, the liquid metal coming with high pressure travelled longer distance while going to the upside. Thus, in the upside of the Flansh the liquid metal was fastened to higher speed. Moreover, there is a velocity increase from 30213 cm/s to 41542 cm/s in the narrow channels that connect the casting to the upper overflows at the corners, and the velocity increase from 3777 cm/s to 30213 cm/s can be seen at the some little parts of the overflows, but it is not so important.

Consequently, a rather uniform and accurate velocity distribution is seen at the simulation result picture for wholly filling. This uniform velocity is near to typical high pressure die casting velocity. These filling velocity simulation results demonstrate mold filling and turbulence ideally. However, turbulence is not seen in these simulation result figures of velocity. Thus, there is no turbulence in these figures.

3.3.7. The Simulation Results For The Filling Temperature

Filling temperature simulation result for 54% of filling at 1673 millisecond is seen in the Figure 3.3.8. The coldest region of the melt with 594.2°C temperature demonstrated with dark blue color is in the bottom edge of the biscuit due to crashing to the wall of the

mould and so transfering some amount of heat to the wall. From this edge to upper side, it is seen that the temperature is rising step by step to the hottest temperature 640°C demonstrated by the lightest yellow. The region of the melt demonstrated with red color in the biscuit has 612.5 °C comparing with the temperature scale seperated by colors with respect to °C on the right side of the simulation result picture. Additionally, the region of the melt demonstrated with light orange color in the biscuit has 626.3°C, the temperature of dark yellow colored melt region in the biscuit is 630.8 °C, and the temperature of yellow melt region is 635.4°C.

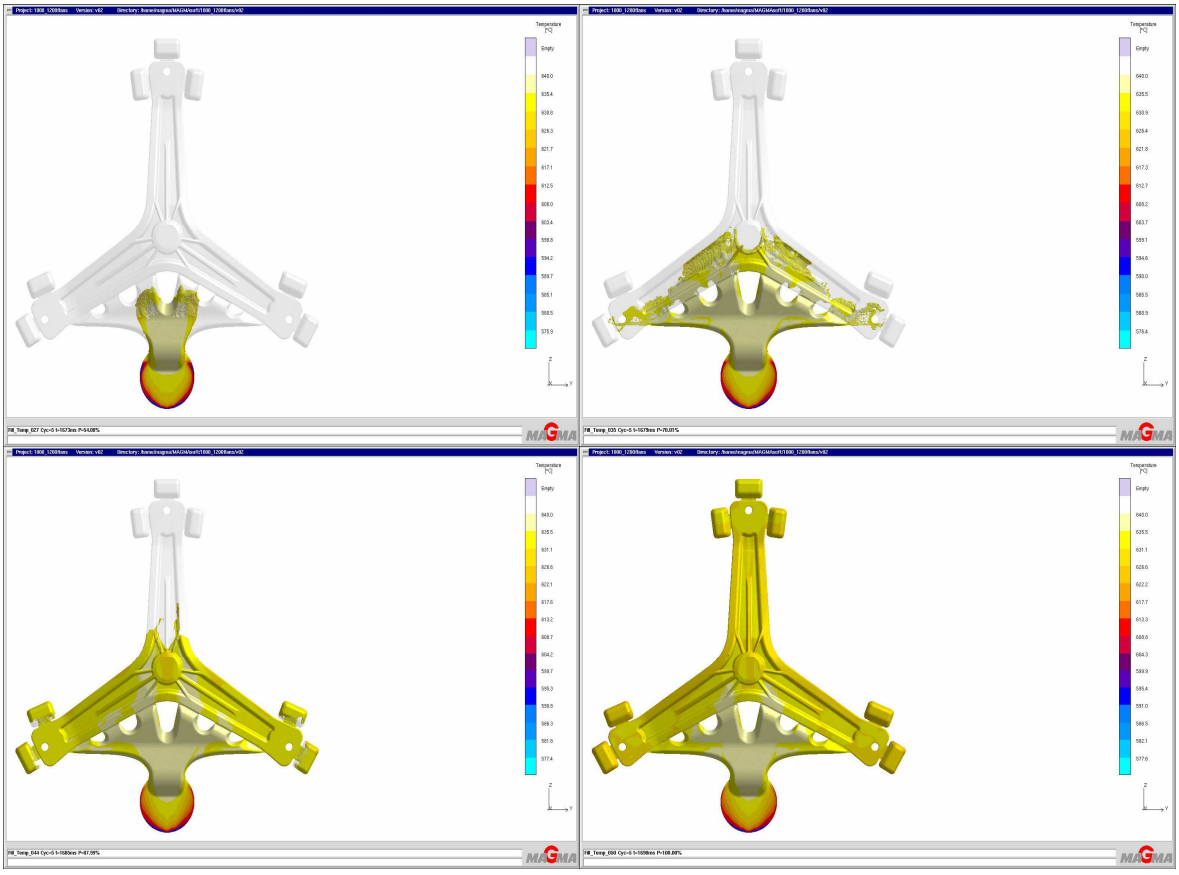

Figure 3.3.8. Filling temperature simulation result for 54%, 70.01%, 87.99%, and 100% of filling for cycle 5

Filling temperature simulation result for 70.01% of filling at 1679 millisecond is also seen in the Figure 3.3.8. The temperature distribution of 70.01% filling is like the continuation of 54% filling. There is again some amount of stepped temperature increase from the bottom side of the biscuit to the upside of the biscuit. The dark blue colored melt

in the bottom edge of the biscuit has 594.6°C temperature. The red colored melt just on the dark blue melt region has 612.7°C. The orange colored melt just on the red melt region has 621.8°C. The light orange colored melt just on the orange melt region has 626.4°C. The dark yellow colored melt just on the light orange melt region has 630.9°C. The yellow colored melt just on the light orange melt region has 635.5°C. The light yellow colored melt just on the yellow melt region has 640°C. Apart from the biscuit, the general temperature of the liquid metal seen in the gating, ingates, and exit of the ingates is 640°C. However, in some regions 635.5°C temperature value can also be seen for 70.01% filling in the Figure 3.3.8.

Filling temperature simulation result for 87.99% of filling at 1685 millisecond is also seen in the Figure 3.3.8. The temperature distribution of 87.99% filling is like the continuation of 70.01% filling. There is again some amount of stepped temperature increase from the temperature of bottom edge of the biscuit 595.3°C represented by dark blue color to the temperature of the top edge of the biscuit 640°C represented by light yellow color. The temperature value steps between these temperatures can be seen from the Figures by comparing the colors with the temperature scales. Apart from the biscuit, the general temperature of the liquid metal seen in many sides of the gating, ingates, and exits of the upper four ingates is 640°C. However, the general temperature in many sides of the casting is 635.5°C represented by yellow color.

Filling temperature simulation result for 100% of filling at 1690 millisecond is also seen in the Figure 3.3.8. The temperature distribution of 100% filling is like the continuation of 87.99% filling. In the biscuit region, there is again some amount of stepped temperature increase from the temperature of bottom edge of the biscuit 595.4°C represented by dark blue color to the temperature of the top edge of the biscuit 640°C represented by light yellow color. Because there is piston, which pushes the liquid metal into the mould, just behind the biscuit. This piston works with grease since the piston is cooled against corrosion. In order to impede thermal expansion, the piston is also cooled with water. Therefore, the biscuit becomes cool due to these effects. Thus, there is approximately 50°C temperature difference in the biscuit. However, the important part is the casting part not the biscuit part for us since the biscuit, gating, and ingate will be cut

away after casting was completed. Thus, the changes in the biscuit, gating, and ingate do not disturb us.

Apart from the biscuit, the general temperature of the liquid metal in many sides of the gating, upper two ingates, and exits of the upper two ingates is 640°C for 100% filling as seen in the Figure 3.3.8. Moreover, the general temperature in many sides of the casting is 635.5°C represented by yellow color. However, 631.1°C temperature demonstrated by dark yellow color can also be seen in some regions of the casting such as edges, overflows, and navel due to the geometry.

Consequently, a uniform temperature distribution is seen at the temperature simulation results especially the result for 100% filling in the Figure 3.3.8 since there is not different color than yellow tones in the casting part. Thus, this uniform temperature distribution demonstrates that the solidification will be also uniform.

3.3.8. The Simulation Results For the filling Pressure

The filling pressure simulation result for 52% of filling at 1672 millisecond is seen in the Figure 3.3.9. From the figure, it is seen that the biggest pressure is in the biscuit and in the exit of the biscuit colored with the lightest color representing 3000 mbar (300 MPa) according to the pressure scale, at which every color represent a pressure value with respect to mbar, on the right side of the Figure. Since the liquid metal is started to be poured from the biscuit, the biggest pressure is seen in the biscuit. From the exit of the biscuit, pressure is step by step decreasing to 1155 mbar, which is still a high pressure, in the region colored with light blue.

There is also a pressure decrease to 1865 mbar in the small region of the bottom corner of the biscuit colored with yellow, dark yellow, red, and dark purple, respectively. The change of the pressure is related to the change of the cut side of the specimen directly. When the cut side of the Flansh widens, the pressure decreases. When the cut side of the specimen become narrow, the pressure increases. Therefore, the pressure is in inverse relation with the velocity since the pressure decreases when the velocity increases. Furthermore, the pressure of the region between two top runners is also 3000 mbar. The other dark grey regions are empty (not filled) regions of the casting as seen in the Figure 3.3.9 for 52% filling .

The filling pressure simulation result for 63.99% of filling at 1676 millisecond is also seen in the Figure 3.3.9. The biggest pressure, which is 3000 mbar, is in the biscuit, gating, and in the exit of top four ingates shown with the lightest color as seen in the Figure 3.3.9 for 63.99% filling. 1155 mbar pressure can also be observed in some small regions of the gating, ingate, and the casting represented with light blue color as seen in the figure. The other dark grey regions are empty regions. Needless to say, the pressure scale on the right side of the figure demonstrates the pressure steps according to colors in order to compare with the casting.

The filling pressure simulation result for 80% of filling at 1682 millisecond is also seen in the Figure 3.3.9. The gating has only the lightest color, which means there is only

3000 mbar pressure in the gating according to the pressure scale on the right side of the figure.

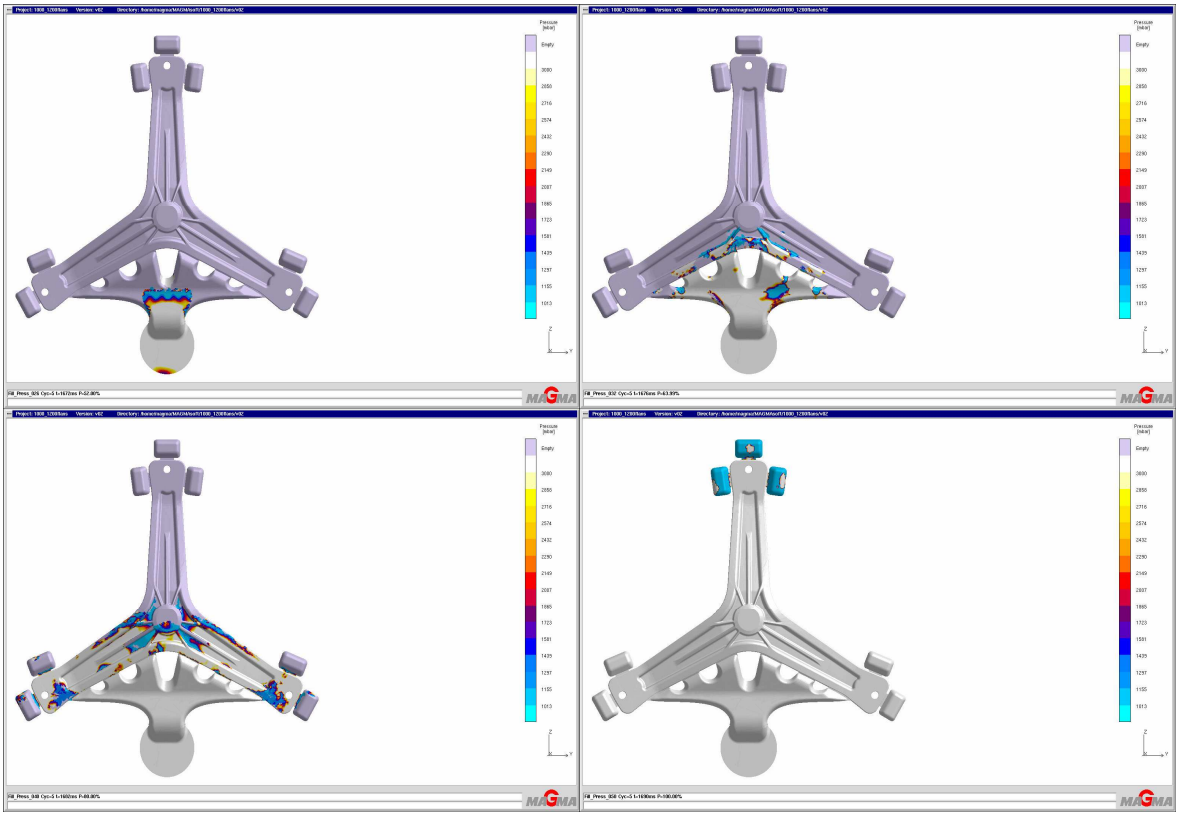

Figure 3.3.9. Filling presure simulation for 52%, 80%, 63.99%, and 100% of filling for 5 cycles

However, some different colors can be seen in the ingates, which means there is pressure change in the ingates. The general color of the casting is same as the color of the gating. Therefore, the general pressure is also 3000 mbar in the casting. Yet, some pressure change can also be observed in some regions of the casting with different colors. Thus, the light blue regions in the casting has 1155 mbar pressure, the blue regions in the casting has 1439 mbar pressure, and the red regions in the casting has 2007 mbar pressure, and very small yellow regions in the casting has 2858 mbar pressure. These pressure changes might occur due to the geometry and velocity changes. Samely, a little amount of pressure changes are also seen in the overflows and in the narrow regions that connect the casting to the overflows in the Figure 3.3.9 for 80% filling.

The filling pressure simulation result for 100% of filling at 1690 millisecond is also seen in the Figure 3.3.9. The very light grey color is seen all the parts of the gating, ingate, and casting. Therefore, the unique pressure in the gating, ingate, and casting is 3000 mbar. The only different color, which is light blue, is seen in the upper overflows in the Figure 3.3.9 for 100% filling. The overflows are air vents, and they are not as important as the casting part since they are cut after solidification. Thus, pressure change from 3000 mbar to 1155 mbar in the overflows is not so crucial. Consequently, the pressure distribution for 100% filling is very homogen and accurate. So, there will be no problem.

3.3.9. The Simulation Results For The Air Entrapment

The filling air entrapment simulation result for 56% of filling at 1674 millisecond is seen in the Figure 3.3.10. Air entrapment means forming of air during casting operation. Voids also take form physically due to air entrapment. It is seen from the Figure 3.3.10 that the biscuit has generally turcuise color. Comparing this turcuise color with the air entrapment scale on the right side of the simulation picture, turcoise color represents 0% air entrapment. Therefore, there is no air entrapment (0%) in the most parts of the biscuit region. Additionally, light blue color seen at some little parts of the biscuit and most parts of the gating apart from the biscuit, demonstrates 7.2% air entrapment.

The dark yellow color representing 78.6% air entrapment is only seen at three very small regions in the runners. The air entrapment increases in these small regions from 7.2% to 78.6% step by step. This dark yellow region will probably be the potential air entrapped region. However, this yellow colored region is not observed from the other proceeding figures. Therefore, it is understood that air entrapment will not form in this region. Thus, air entrapment result figures should be observed respectively as a whole from the beginning to the end not seperately in order to understand the real forming of air. The light yellow colored regions with 100% air entrapment percentage will be the possible air entrapped regions according to the air entrapment percentage scale. The other colored regions will not be air entrapped according to the scale. Therefore, especially light yellow colored regions should be examined in terms of being possible air entrapped regions, in which air and voids form in the figures of air entrapment.

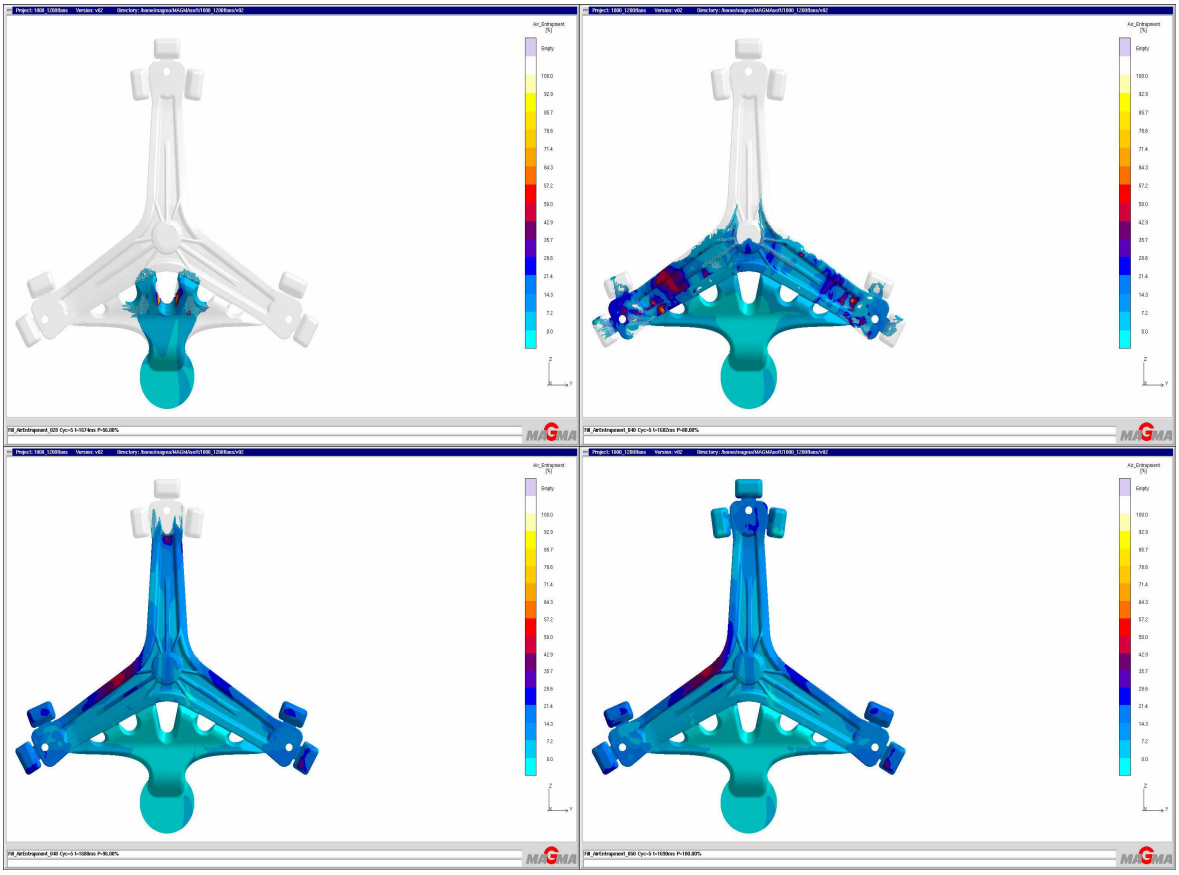

Figure 3.3.10. Filling air entrapment simulation result for 56%, 80%, 96%, and 100% of filling for 5 cycles

The filling air entrapment simulation result for 80% of filling at 1680 millisecond is also seen in the Figure 3.3.10. There is 0% air entrapment in most parts of the biscuit, gating, and in some parts of the casting represented with turcoise color. Yet, it is seen from the Figure 3.3.10 that there is 7.2% filling air entrapment in the small right side of the biscuit, in the runners, and in some parts of the casting colored with light blue. Additionally, the air entrapment is 14.3% in the small blue regions of the casting, and 28.6% in the small dark blue regions of the casting. In some small parts of the casting colored with red the air entrapment increases to 50% step by step, and in the smallest yellow regions of the casting the air entrapment changes to 78.6% step by step.

The dark blue, red, and purple regions will probably be the potential air entrapped regions due to the design and filling of the mould. However, these regions are not problem. Because the important point is that there should not be light yellow colored 100% air

entrapped regions since there will only be air entrapment if the region was colored with light yellow according to the scale. The filling air entrapment percentage values of different colored regions are understood with the help of the air entrapment percentage scale on the right side of the Figure 3.3.10 for 80% filling.

The filling air entrapment simulation result for 96% of filling at 1688 millisecond is also seen in the Figure 3.3.10. It is seen for 96% filling that the filling air entrapment of the gating colored with turcoise is generally 0%. However, there is 7.2% air entrapment in the small right region of the biscuit and in the two bottom runners colored with light blue. The general air entrapment in the casting is 7.2%. Yet, there is 14.3% air entrapment in the three corners of the casting colored with blue. Additionally, the air entrapment is 28.6% in some small dark blue regions of the casting, and the air entrapment is 50% in the left and top small regions of the casting shown with red. The filling air entrapment percentage values of different colored regions are understood with the help of the air entrapment percentage scale on the right side of the Figure.

The filling air entrapment simulation result for 100% of filling at 1690 millisecond is also seen in the Figure 3.3.10. The filling air entrapment simulation result for 100% filling is like the continuation of the filling air entrapment simulation result for 96% filling. It is seen from the Figure 3.3.10 for 100% filling that the filling air entrapment of the gating colored with turcoise is generally 0%. However, there is 7.2% air entrapment in the small right region of the biscuit and in the two bottom runners colored with light blue. The general air entrapment in the casting is 7.2%. Although the biggest air entrapment percentage is seen in the left small side of the casting shown with dark red representing 50%, this is not important since this region is a thin section. Dark blue colored regions representing 28.6% air entrapment are also not so important for accurate casting since some of them are thin sections and some of them are in the overflows. Consequently, the blue tones are dominating color on the casting, which demonstrate a homogen and problemless air entrapment distribution. Since there is no light yellow color representing 100% air entrapment in the figure 3.3.10, it can be said that there is not air entrapment event through the casting operation.

3.3.10. The Simulation Results For The Filling Flow Lenght

In the Figure 3.3.11, the filling flow lenght simulation result for 100% of filling at 1690 millisecond is seen. The filling flow lenght simulation demonstrate the distance of the filling flow from the biscuit to the upper overflows since the melt was poured firstly from the biscuit. It is seen from the figure 3.3.11 that the smallest filling flow lenght is 7.8 cm in the biscuit colored with blue since blue represents 7.8 cm flow length according to the distance scale with respect to centimetre on the right side of the figure.

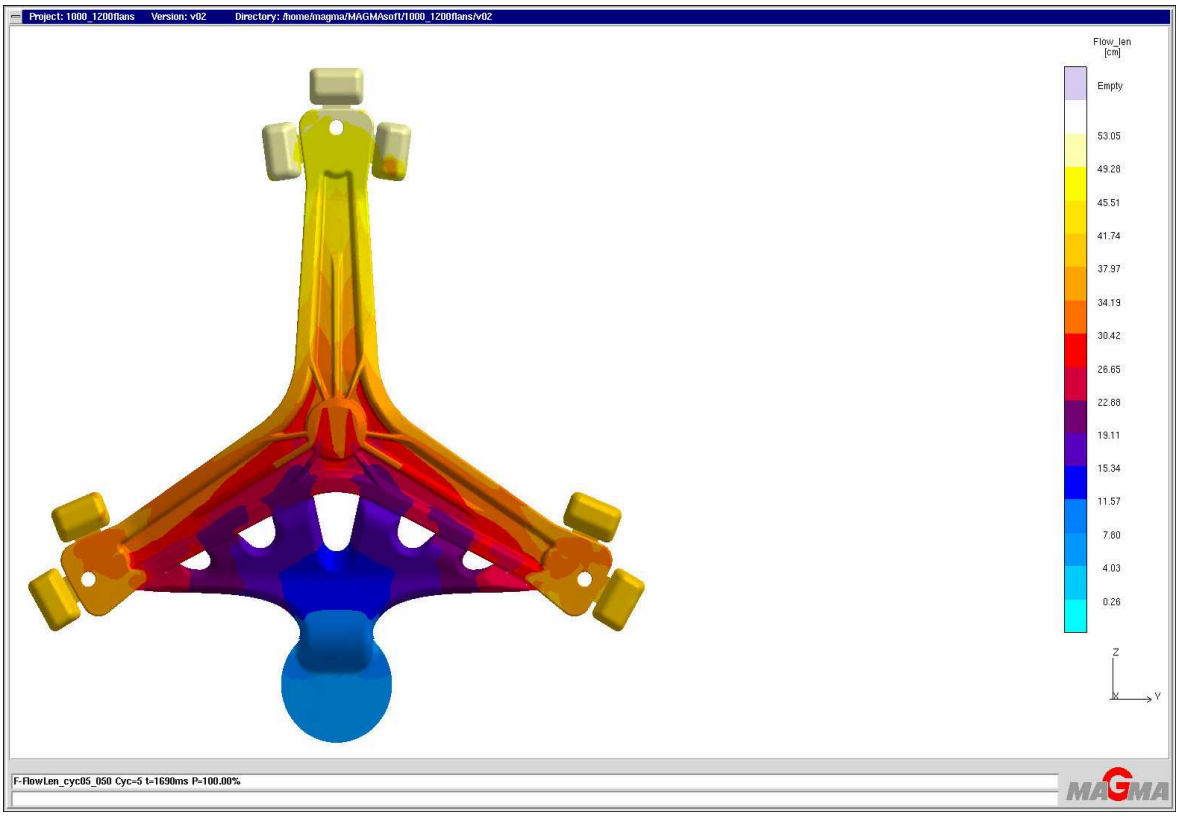

Figure 3.3.11. Filling flow lenght simulation result for 100% of filling at 1690 millisecond for five cycle

The filling flow lenght gets bigger and bigger from the biscuit to the gating, ingate, and the casting step by step. The filling flow lenght in the dark blue colored exit of the biscuit is 15.34 cm. The filling flow lenght in the purple colored upper four ingates is 22.88 cm. The melt in the other ingates have dark red color which means 26.65 cm flow lenght.

The longest filling flow lenght is for the top of the casting and for the upper overflows shown with light yellow color, which represent 53.05 cm flow lenght. Different flow lenght distances is seen for the other sides of the casting. For instance, the red zones in the casting demonstrate 30.42 cm filling flow lenght, the orange zones in the casting demonstrate 34.19 cm filling flow lenght, the light orange zones in the casting demonstrate 37.97 cm filling flow lenght, the dark yellow regions in the casting demonstrate 45.51 cm filling flow lenght, nearly top the yellow regions in the casting demonstrate 49.28 cm filling flow lenght. The filling flow lenght gets bigger from bottom of the casting to the top of the casting step by step.

Consequently, the uniform filling flow from the biscuit to the upper sides can be seen from this simulation figure 3.3.26 clearly since the colors in the mould change with the same order as the colors of the flow lenght scale.

3.3.11. The Simulation Results For The Filling Cast Lenght

In the Figure 3.3.12, the filling cast lenght simulation result for 100% of filling at 1690 millisecond is seen. The filling cast lenght simulation demonstrate the way of the liquid metal at the time of mould filling.

The liquid metal was firstly poured from the biscuit. Therefore, the liquid metal in the bottom of the biscuit has blue color which represent 7.5 cm filling cast lenght. The cast lenght gets bigger from the bottom of the biscuit to the ingates step by step as comparing the different colors at this region with the cast lenght scale with respect to centimetre on the right side of the Figure 3.3.12.

The cast lenghts in the ingates shown with turcoise are 0 cm since the melt slowed down and stopped when it came through the ingate and as if the movement of the melt started again from the ingates to the casting. Thus, the cast lenght starts to increase from the ingates to the top of the casting after the biscuit.

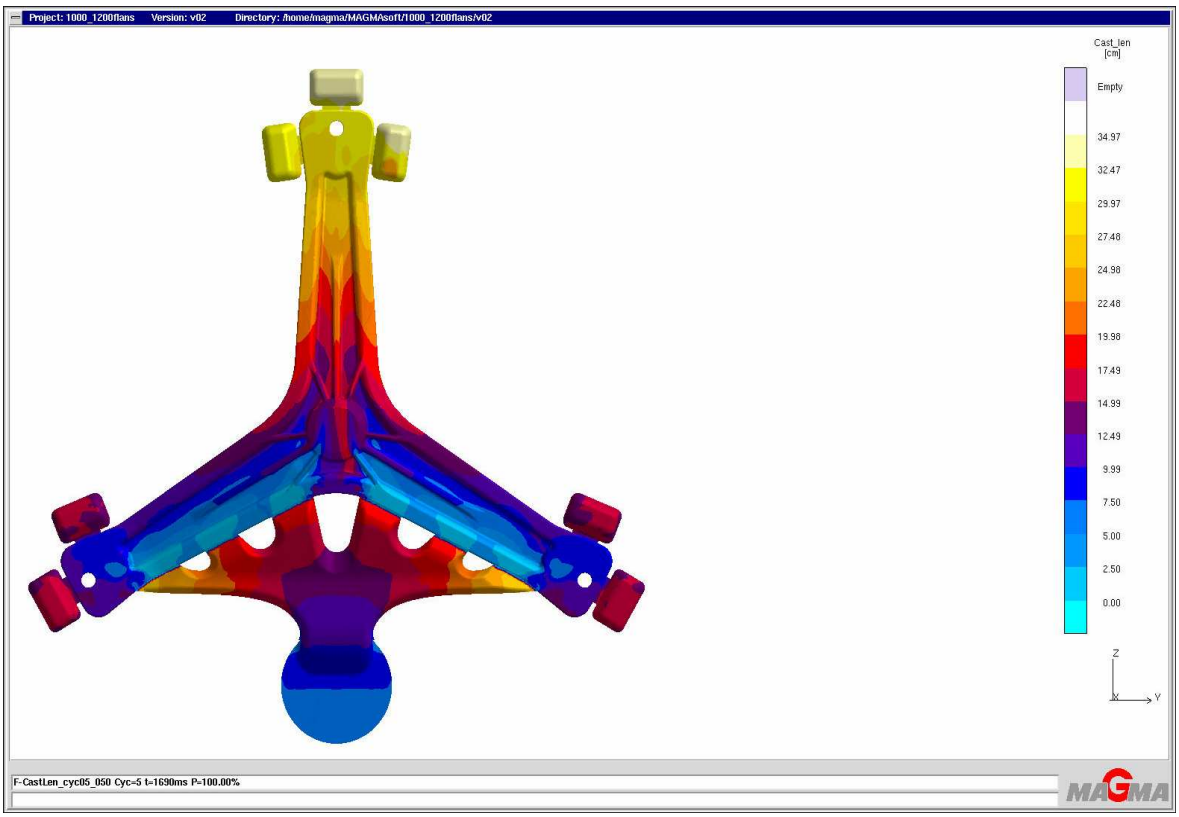

Figure 3.3.12. Filling cast lenght simulation result for 100% of filling at 1690 millisecond for five cycles

The cast lenght of the blue zone in the casting just after the ingate is 5 cm. Then, the cast lenght of the dark blue zone in the casting is 9.99 cm. Then, the cast lenght of the purple zone in the casting is 14.99 cm, the red zone in the casting is 19.98 cm, the orange zone in the casting is 24.98 cm, the yellow zone at the top of the casting is 32.47 cm. And the longest filling cast lenght is 34.97 cm shown with light yellow in the two top overflows as seen in the Figure 3.3.12.

Only one directional flow from biscuit to casting was seen in the filling flow lenght simulation of the figure 3.3.11, but two directional flow from biscuit to ingate and from ingate to casting is seen in the filling cast lenght simulation of the figure 3.3.12 since the casting part starts just after the ingate.

3.3.12. The Simulation Results For the filling Wall-Contact

In the Figure 3.3.13, the filling wall-contact simulation result for 100% of filling at 1690 millisecond is seen. The filling wall contact simulation picture explains about the liquid metal rubbing against the wall of the mould. Thus, wall contact is about wearing away of the mould. Additionally, wall contact is also about the turbulence relatively since there is less turbulence in the liquid metal side which crashes to the wall of the mould.

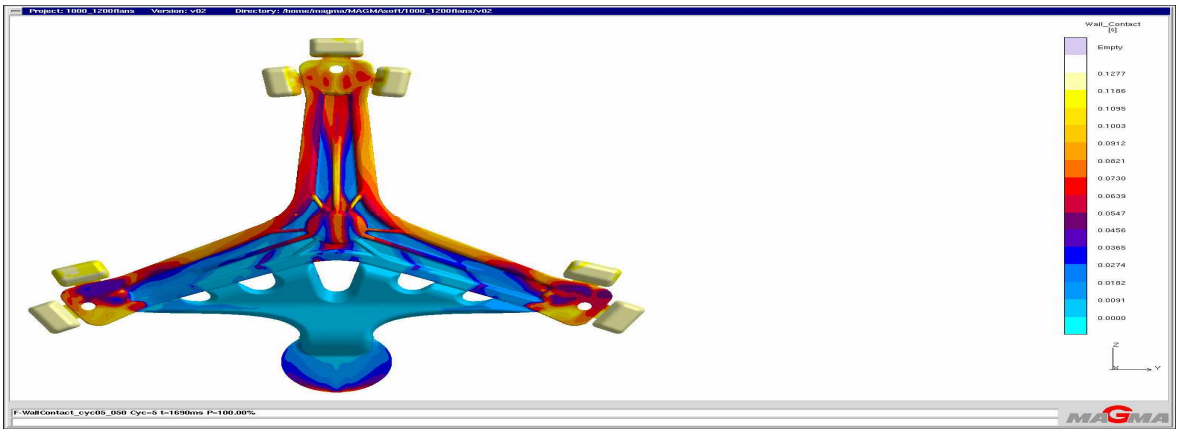

Figure 3.3.13. Filling wall-contact simulation result for 100% of filling at 1690 millisecond for 5 cycle

It is observed from the Figure 3.3.13 that wall contact for the shortest time is in the light blue colored gating and in the exits of the top four ingates for 0.0091 second by comparing with the wall contact scale with respect to second on the right side of the figure. It is also observed that wall contact for the longest time is in the light yellow colored overflows for 0.1277 second.

After the overflows, wall contact for long time is in the two edges of the casting shown with light orange for 0.1003 second. It is seen from the figure that the wall contact time is getting shorter away from the wall of the casting. The wall contact time for these regions can be understood by comparing their color with the wall contact time scale. For instance, wall contact time for dark blue regions is 0.0365 second, for purple regions is 0.0456 second, for red regions is 0.0730 second, and for orange regions is 0.0912 second and etc.

Furthermore, filling wall contact time in the biscuit changes from 0.0091 second to 0.0639 second step by step. Besides, the ununiform flowing in the navel of the casting is due to the geometry. Moreover, it can be said that the filling wall contact is happening very quickly with the help of the observations from the Figure 3.3.13.

3.3.13. The Simulation Results For The Filling Material Age

In the Figure 3.3.14, the filling wall-contact simulation result for 100% of filling at 1690 millisecond is seen. The youngest material is 1.458 second old in the top four runners shown with blue. The material is getting older from this side to up and down. The liquid metal, which came from the biscuit firstly, started to fill the mould so it does not stay in the biscuit. However, the liquid metal in the biscuit can not move after the mould was filled entirely. The unique movable liquid metal zone is the inner side of the mould. Since the edges of the mould was filled, the material in the bottom side of the biscuit and in the outer edges of the mould seem at the same age in the Figure 3.3.14.

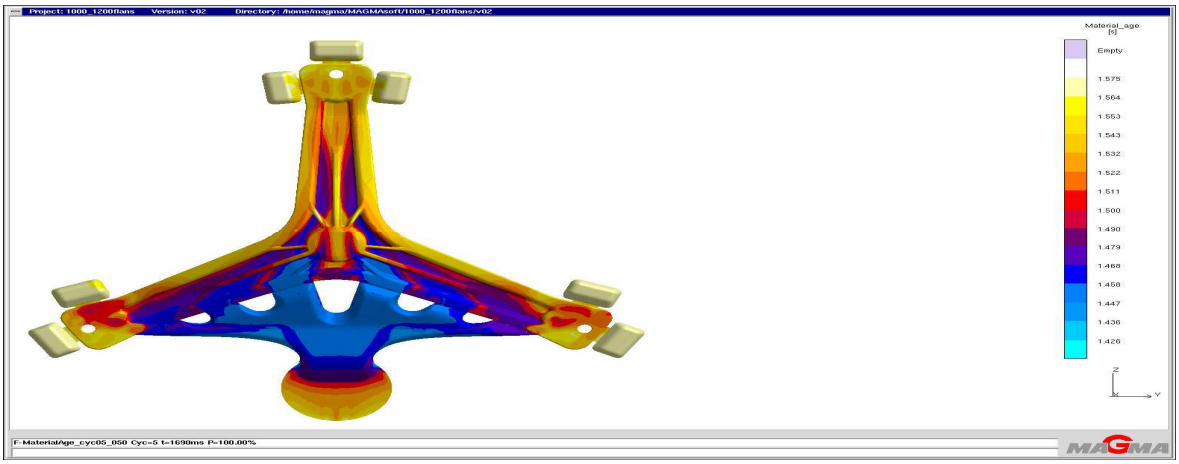

Figure 3.3.14. Filling material age simulation result for 100% of filling at 1690 millisecond for 5 cycles

The oldest material is 1.575 second old in the overflows shown with light yellow. After the overflows, the old material is in the edges, corners, navel, and thin sections of the casting colored with dark yellow, which represents 1.553 second. The age of other sides can be learned by comparing their color with the material age scale with respect to second on the right side of the Figure 3.3.14. For instance, the material age changes from 1.490

second to 1.564 second from top of the biscuit to the bottom of the biscuit. Although the age difference in the whole material is little, this difference might be because of flowing, and geometry. Consequently, it can also be said that this process is very fast.

3.3.14. The Simulation Results For The Solidification

In the Figure 3.3.15, the solidification time simulation result for 100% of filling for 1 cycle is seen. 1 cycle means casting is done for only one time, and 5 cycles mean casting is done for five times respectively. The simulation for one cycle was only done for observing whether filling of the mould was accurate or not; since a faulty simulation is not wanted to be done. As simulation takes very much time, only solidification time and solidification temperature simulations were carried out for one cycle. Thus, there is no gating for one cycle simulation. This serves as a guideline in order to find the spots that solidify last and find the suitable area for constructing the gating system later on. Entering the information only about solidification time and temperature to Magmasoft software in spite of whole information takes less time and the simulation works more quickly; therefore the simulation results in less time in order to check the accuracy of the simulation. Those functions that are typical for the MAGMAhpdc module are not yet used within this one cycled version.

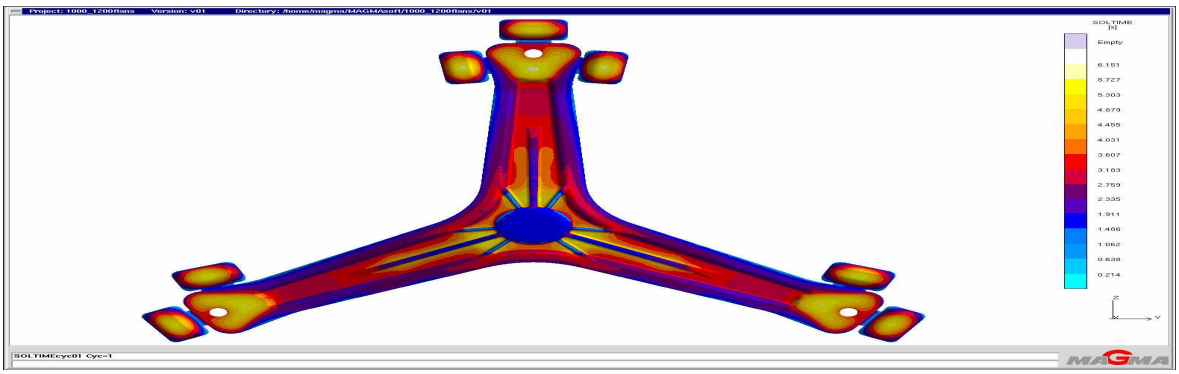

Figure 3.3.15. Solidification time simulation result for 100% of filling at 6.151 second for 1 cycle

It is seen from the Figure 3.3.15 that the solidification for 1 cycle is completed in 6.151 second wholly. Thus, this solidification process is rather fast. The regions, which

solidify lastly in 6.151 second, are the center of overflows, the corners of the casting, and the vicinity of the navel shown with light yellow. Besides, the regions which solidify early are the outer edges of the casting, outer edges of the overflows, the navel, the thin sections connected to the navel colored with blue corresponding to 1.911 second approximately. Solidification is a bit earlier in the thin sections because heat transfer is faster in the thin sections. Thick sections solidify later than thin sections.

The solidification time of the other regions can be understood by comparing their colors with the solidification time scale with respect to second on the right side of the Figure 3.3.15. For instance, purple colored regions solidified in 2.335 second, dark purple colored regions solidified in 2.759 second, dark red colored regions solidified in 3.183 second, red colored regions solidified in 3.607 second, orange colored regions solidified in 4.031 second, and etc.

In the Figure 3.3.16, the solidification temperature simulation result for 1 cycle is seen. The overflows, corners of the casting, the thin sections around the navel colored with turcoise have the lowest solidification temperature 529°C. The other white colored regions have the highest solidification temperature 570°C. The dark purple regions at the center of the turcoise regions have 546.6°C solidification temperature. The small red regions around the navel have 552.4°C solidification temperature. The solidification temperature of all regions can be learned by comparing the colors of the regions with the temperature scale seperated with colors with respect to °C on the right side of the Figure 3.3.16.

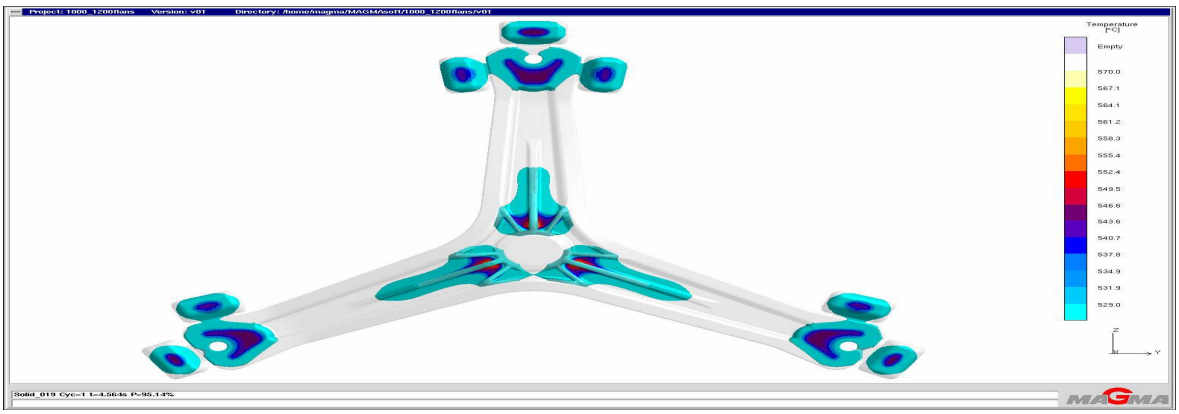

Figure 3.3.16. Solidification temperature simulation result for 1 cycle

According to these solidification temperature and solidification time results for one cycle, this draft is not only very accurate, but also any problem about casting is not seen from these simulations for one cycle. Therefore, this draft is valid to apply for five cycles. Casting for five cycles represents continous casting like the real casting in the high pressure die casting machines. The importance of casting simulation for five cycle is to be able to observe corrosion of the mould, warmness of the mould, and the other parameters. Thus, all of the parameters are entered to Magmasoft software for five cycle analyzing. Therefore, completing all of five cycled simulations about all the parameters lasts for days.

In the Figure 3.3.17, the solidification time simulation result for 100% of filling for 5 cycles is seen. This simulation result picture in the figure 3.3.17 is very similar to the solidification time simulation result for one cycle in the figure 3.3.15. It is observed from the figure 3.3.17 that the solidification for five cycles is completed in 7.002 second entirely. Therefore, it can be said that this solidification process of high pressure die casting alloy AlSi12Cu is rather fast.

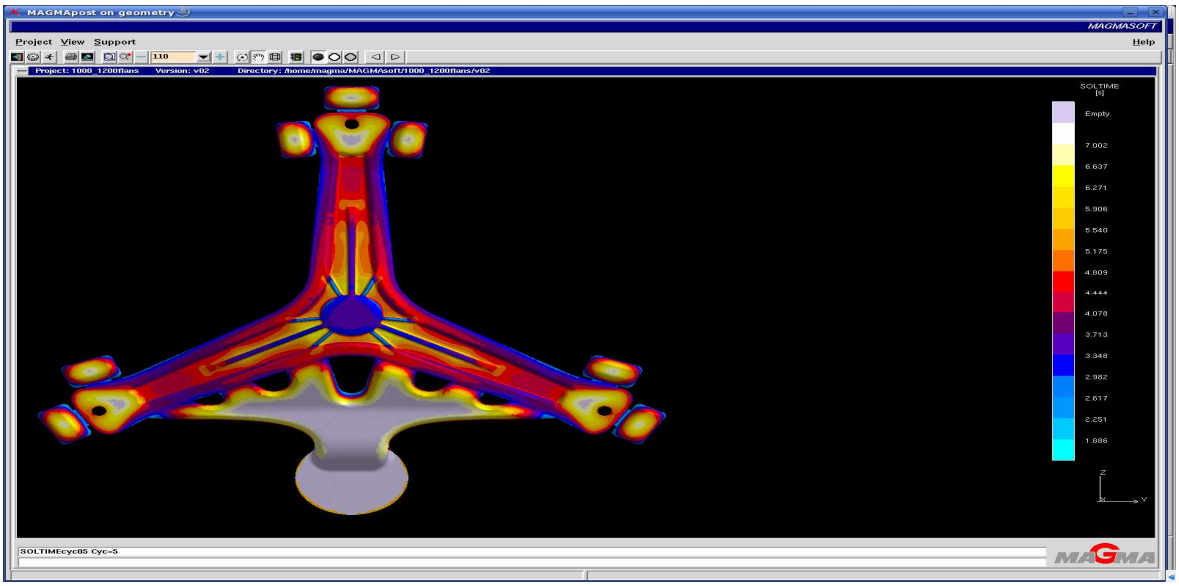

Figure 3.3.17. Solidification time simulation result for 100% of filling for 5 cycles

The regions, which solidify lastly in 7.002 second, are the center of overflows, the corners of the casting, the vicinity of the navel, and the gating shown with light yellow. Besides, the regions which solidify early are the outer edges of the casting, outer edges of

the overflows, the edges navel, the thin sections connected to the navel colored with blue corresponding to 2.982 second approximately. It is generally seen that thick sections in the mould solidify slowlier and so later, yet thin sections solidify faster and so earlier since heat transfer is faster in the thin sections.

The solidification time of the other regions can be understood by comparing their colors with the solidification time scale with respect to second on the right side of the Figure 3.3.17. For instance, purple colored zones solidified in 3.713 second, dark purple colored zones solidified in 4.078 second, dark red colored zones solidified in 4.444 second, red colored zones solidified in 4.809 second, orange colored zones solidified in 5.175 second, yellow colored zones solidified in 6.637 second, and etc. The solidification time is getting shorter from the runners to the ingates step by step from 7.002 second to 4.078 second for the gating since solidification time is approximately 7.002 second in the biscuit and approximately 4.078 second in the ingates.

The solidification temperature simulation result when 50.26% of casting operation was completed at 5.357 second for 5 cycles is seen in the Figure 3.3.18. Turcuise color is seen at most of the parts of the casting, which corresponds to the lowest solidification temperature 529°C. Other small parts of the casting such as dark red colored corners of the casting have 549.5°C. The dark blue colored zones around these dark red colored parts have 540.7°C.

There is stepped temperature increase seen from 529°C to 555.4°C at the three sides of the navel shown with color change from turcuise to dark orange. Furthermore, the general temperature is also 529°C in the overflows shown with turcuise. However, temperature change from 529°C to 549.5°C is observed at the center of the overflows with the color change from turcuoise to dark red for 50.26% of casting.

The hottest region with 570°C in the Figure 3.3.18 for 50.26% of casting is the small zone of the biscuit shown with light yellow. The temperature in the biscuit changes to 537.8°C from this small zone at the top of the biscuit to the bottom of the biscuit. By the way, 564.1°C is generally seen at the most of the biscuit.

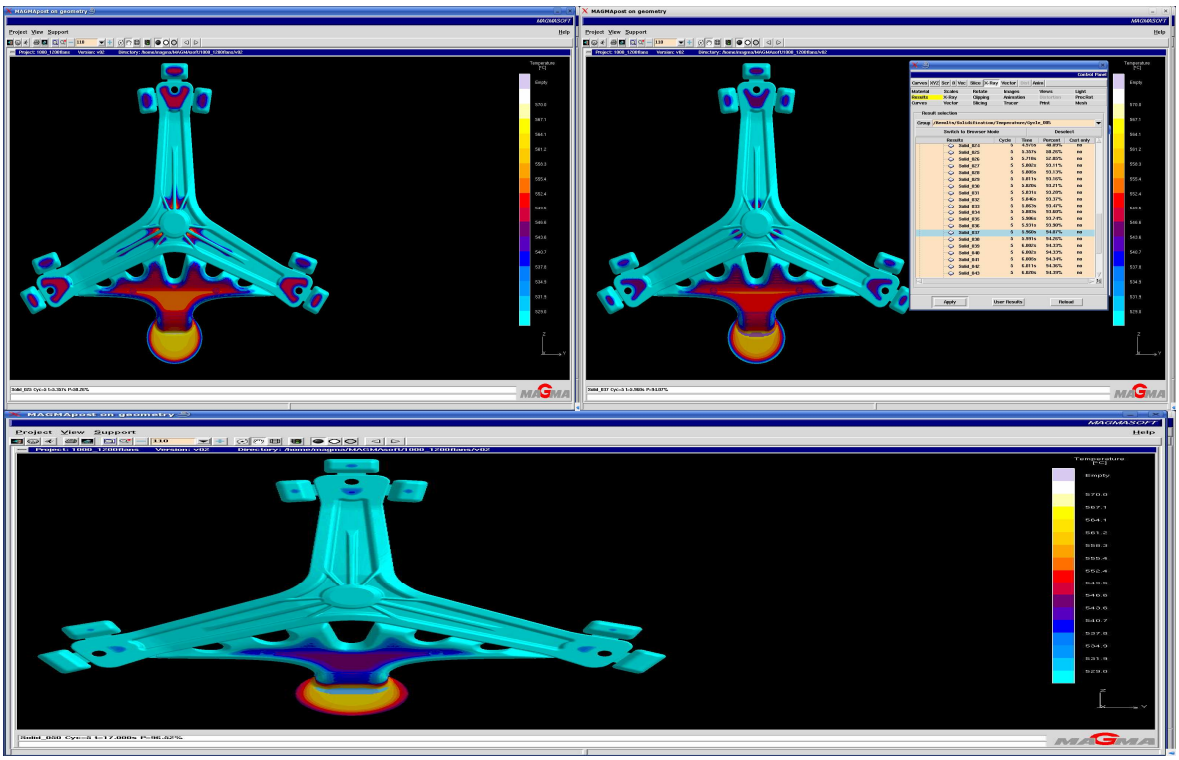

Figure 3.3.18. Solidification temperature simulation result when 50.26%, 94.07%, and 96.52% of casting operation was completed for 5 cycles, respectively

The solidification temperature 555.4°C represented with dark yellow is observed at the most of the runner. From this zone temperature decreases to 546.6°C step by step up and down. All the solidification temperature values can be understood by comparing the colors of the zones with the temperature scale seperated with colors on the right side of the figure. All the ingates have also turcuoise color. Therefore, solidification temperature for 50.26% of casting is 529°C in the ingates.

The solidification temperature simulation result when 94.07% of casting operation was completed at 5.960 second for 5 cycles is also seen in the Figure 3.3.18. This result for 94.07 percentage is like the continuation of the result for 50.26 percentage. It is observed that the temperature of some regions is colder than the previous image as the solidification increases.

The general temperature is 529°C, which is the lowest solidification temperature, at most parts of the casting represented with turcuise color. However, the temperature at the

small dark purple colored parts at the corners of the casting is 546.6°C. There is also a temperature change at the three very small sides of the navel from 529°C to 549.5°C for 94.07% of casting.

The general temperature in the most parts of the overflows shown with turcuoise is also 529°C. However, the temperature in the center of the overflows is 546.6°C shown with dark purple. Additionally, the temperature in the very small dark blue zone around this purple zone is 540.7°C with respect to the temperature scale.

The yellow colored center of the biscuit has 561.2°C solidification temperature. Temperature decreases to 531.9°C step by step from this side to the bottom of the biscuit shown with blue. The general temperature in the runner is 552.4°C represented with red. However, this temperature decreases to 529°C through the ingates since the temperature in the ingates is 529°C represented with turcuoise. There is also 555.4°C solidification temperature at the center of the runner in the thin orange zone. Moreover, all of the other temperature values in the gating can be understood from the temperature scale on the right side of the Figure 3.3.18 for 94.07% of casting .

It is also seen in this figure for 94.07% of casting how this simulation result picture was taken from the control panel in the ‘‘Magmasoft postprocessor on geometry’’ stage. In order to view the result picture, ‘‘result’’ option under ‘‘X-Ray’’ heading in the ‘‘control panel window’’ is clicked. Then, ‘‘/Results/Solidification/Temperature/Cycle_005’’ group was selected from the result selection mode. Thus, any solidification temperature result at different times of casting operation can be applied to view with the ‘‘Apply’’ button at the left bottom of the control panel window. The other results was also taken with the same procedure.

The solidification temperature simulation result when 96.52% of casting operation was completed at 17 second for 5 cycles is also seen in the Figure 3.3.18. This result for 96.52 percentage is like the continuation of the result for 94.07 percentage. It is observed that the temperature of some regions is colder than the previous image since the solidification increases.

Turcuoise color is seen at most of the parts of the casting, which corresponds to the lowest solidification temperature 529°C. It is seen that the three corners of the casting and the center of the overflows for 96.52 percentage have lower solidification temperature than the 94.07 percentage and the 50.26 percentage, which demonstrate the progress of the solidification.

Apart from the 529°C, there is also 537.8°C temperature at the very small points in the three corners of the casting and the center of the overflows shown with blue for 96.52% of casting. As the solidification progresses, temperature decrease and these blue points turn to turcuoise.

Temperature is also decreased in the runner comparing with the previous figures 3.3.34 and 3.3.33. The temperature at the center of the runner is 546.6°C represented with dark purple for 96.52% of casting. But, 546.6°C changes to 529°C step by step through the ingates since the temperature in the ingates is also 529°C.

The hottest temperature 564.1°C represented with yellow is still in the biscuit due to the piston behind the biscuit. Yet, this is not important since biscuit, gating, ingate and overflows will be cut after casting operation was completed. Thus, the real important part casting has generally turcuoise color representing the lowest temperature according to the temperature scale. Therefore, solidification progress is homogenesus and without any problem.

3.3.15. The Simulation Results For the feeding

Feeding is very crucial for a sound casting since many voids can occur in the casting part if feeding is not done properly. And these voids might cause the casting part to be broken. Additionally, these voids can be determined with the help of x-ray and metallographic inspections. Magmasoft programme can calculate the feeding and possible cooling shrinkage voids after completely feeding of the mould filling with some analytical approximations related to temperature, thickness of the part, viscosity of the melt, properties of the mould especially about heat transfer.

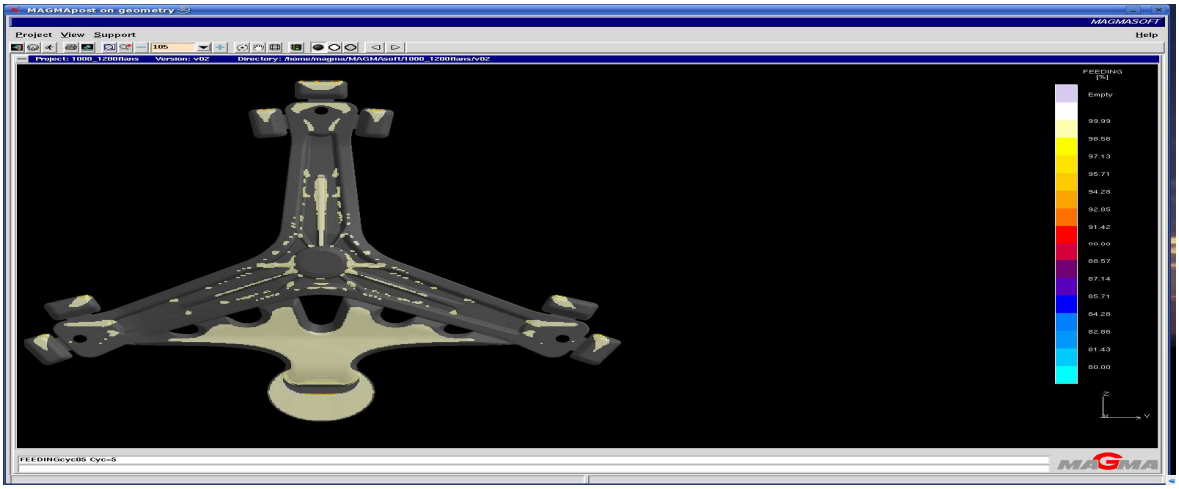

Figure 3.3.19. Feeding simulation result for five cycles

In the Figure 3.3.19, the feeding simulation result for five cycles is seen. Figure 3.3.19 demonstrate the feeding with the help of the ‘FEEDING’ criterion in the whole casting. This simulation result picture was taken from the ‘Magma postprocessor on geometry’ stage by screen shot. It is seen from the figure that all the colored points are light yellow which demonstrate 99.99% feeding, according to the feeding percentage scale differs between light blue 80% and light yellow 99.99% on the right side of the Figure 3.3.19. There is only 98.56% feeding in the small yellow zones of the overflows and the biscuit; but this is not important because these overflows, biscuit, and gating, ingate are cut and thrown away after casting was finished completely. Thus, the feeding of the casting is very sound.

3.3.16. The Simulation Results For The Hot Spots

In the Figure 3.3.20, the solidification hot spots simulation result for five cycle is seen. Hot spot means lately solidified regions due to excessive warming. Excessive warming might be because of the segregation in the casting part after solidification. Hot spots might cause shrinkage voids. Hot spots are generally parallel to feeding since the zones, which can not be fed by feeding, solidify lastly. Additionally, hot spots are generally seen in the thick sections. The Figure 3.3.20 shows the hot spots on the basis of the 'HOTSPOT' criterion.

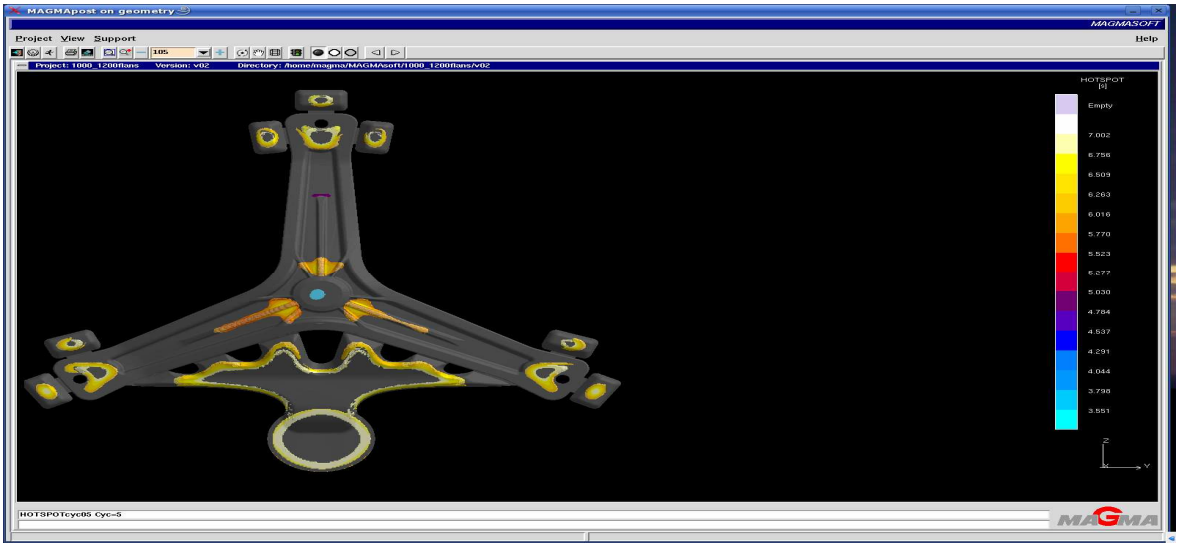

Figure 3.3.20. Solidification hot spot simulation result for five cycles

The yellow toned hotspots are around the biscuit, around the gating, at the center of the three corners of the casting, at the center of the overflows is seen in the Figure 3.3.20. In these regions, the light yellow tone represents hotspot for 7.002 second, the yellow tone represent hotspot for 6.756 second, and the dark yellow tone represent hotspot for 6.509 second. Moreover, there is more light yellow hotspot in the biscuit. But, casting part is more crucial than the biscuit and the gating parts.

There is a small light blue hotspot representing 3.798 second at the center of the casting. There are three orange hotspots representing 6.016 second in the three sides of the navel of the casting. There are also a small dark purple hotspot representing 5.030 second,

and a very small purple hotspot representing 4.784 second in the casting. However, these hotspots are not so dangerous because their periods are not so long. Furthermore, it is seen from the hot spot simulation result that the hot spots are in the same points as the feeding simulation result.

3.3.17. The Simulation Results For The Porosity

Porosity is areas of the mold that absorbed some of the casting material leaving the cast object with a rough, granular surface. Porosity is related to shrinkage voids due to feeding. Porosity is a unwanted casting parameter which can be calculated mathematically. Thus, Magmasoft programme is able to calculate the porosity theoretically with entering the parameters such as casting temperature, solidification range, alloy properties, shape of casting part and etc. Although theoretically calculated porosity might be different than the real porosity values, the Magmasoft porosity simulation result gives information about the possible porosity which can occur.

In the Figure 3.3.21, the solidification porosity simulation result for five cycles is seen. According to this simulation picture, the possible porosity percentage which might occur in the light purple colored corners of the casting, and in the thin sections of the casting is 1% since light purple color represent 1% porosity according to the porosity scale with respect to percentage on the right side of the Figure 3.3.21. 1% porosity is also seen in some parts of the overflows and in many parts of the gating but porosity in these regions is not so important because overflows and gating will be cut away after casting.

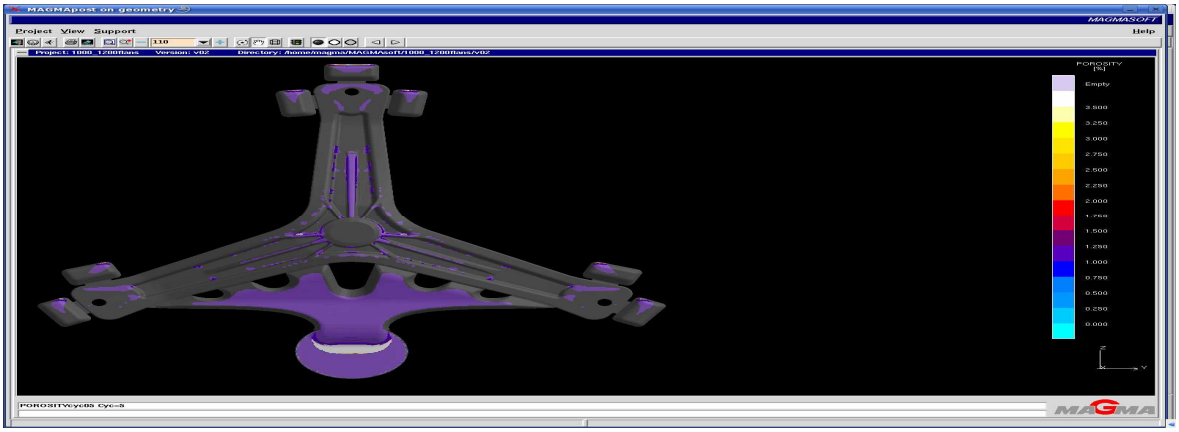

Figure 3.3.21. Solidification porosity simulation result for five cycles

4. EXPERIMENTAL STUDY

4.1. High Pressure Die Casting Practice Of The Simulated AlSi12Cu Flange

Firstly, AlSi12Cu alloy was melted at 700°C in the main melting furnace. Then, this AlSi12Cu melt was sent to the resting furnace near the high pressure die casting machine IP550 with the help of carrying pot after taking gas of the melt.

After spraying the mould, which was connected to the high pressure die casting machine at the temperature interval between 200°C and 240°C, with the seperating grease; the vice of the high pressure die casting machine IP550 was closed. The ladle,which waited in the liquid metal at the resting furnace, took the AlSi12Cu melt according to the adjusted amount and the ladle left the melt into the sending case of the high pressure die casting machine. The high pressure die casting machine made the injection pin move and the liquid metal was pressed by the piston in front of the pin in mould.

After solidification time was completed , the vice was opened at the adjusted time. After pushing, the Flange was taken by operator. After waiting for about five minutes to cool the Flange, Flange was trimmed in order to get rid of the gating, ingate, and the (risers) overflows (air pockets). After checking the Flange (without overflows, ingate, and gating) by eye, it was put into the case of the sound parts.

Table 5.1. High Pressure Die Casting Machine Adjusting Parameters

First phase velocity	0.2 m/s
Second phase velocity	3.8 m/s
Third phase pressure	280 bar
Point of passing to the third phase	320 mm
Vice time	8 s
Pump pressure	150 bar
Temperature of the liquid metal	680°C-695°C
Mould temperature	200°C

4.1.1. Tensile Testing of the AlSi12Cu Flange Casting

According to the simulation data, the Flange, which is a washing machine part, was casted in the Çelikel Company with high pressure die casting machine IP550_SC. In order to analyze the tensile strength of the casted flansh, tensile testing was applied to the specimens, which were taken from the biscuit part of the flange. Tensile testing specimens were machined to a standard size for tensile testing according to TS 138 as seen in the Figure 5.1.

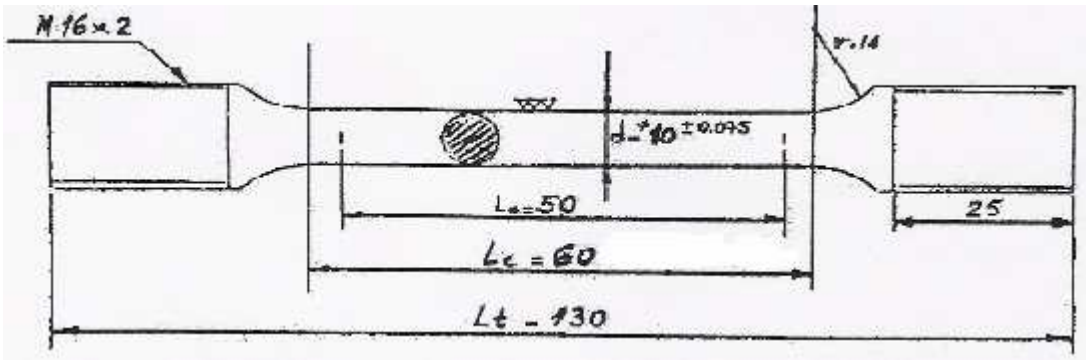

Figure 5.1. Dimensions of the tensile test specimen

The specimens were fractured in a tensile testing machine in İMES-KOSGEB.

Figure 5.2. Photo of high pressure die casted tensile test specimens

The load-extension data were recorded to evaluate the tensile properties. The tensile testing results data demonstrate very good agreement with data in the literature.

4.2. Estimation of the Solidification Time of AlSi12Cu Before Experimental Study

Chvorinov Equation is solved according to the casting values of AlSi12Cu (Etial 150) alloy in order to estimate solidification behavior of the alloy before experimental study.

Chvorinov Equation is [26]:

$$t = B.\left(\frac{V}{A}\right)^2 \tag{4.1}$$

$$B = \left(\frac{\rho\sqrt{\pi\alpha}\left[L_M + C_M\left(T_D - T_1\right)\right]}{2K\left(T_1 - T_o\right)}\right)^2 \tag{4.2}$$

$B = [2.66^2*\pi*13.9*[389+0.963(700-649)]^2] / [4*51.9^2*(649-300)^2] = 0.04519128$ (4.1)

$t = 0.04519128*(72.649352/ 4.90874)^2 = 9.898698 \approx 10$ second (4.2)

Table 4.1. Squeeze casting temperature values

In order to calculate B (mold constant) in the Chvorinov equation	
Melt temperature	700 °C
Die temperature	300 °C
Punch temperature	300 °C

After the third squeeze cast sample the die and punch temperature were increased to 400°C. Thus T_1 value changes from 300 to 400. So;

$B = [2.66^2*\pi*13.9*[389+0.963(700-649)]^2] / [4*51.9^2*(649-400)^2] = 0.0887783$ (4.1)

$t = 0.0887783*(72.649352/ 4.90874)^2 = 19.445999 \approx 20$ second (4.2)

4.3. Squeeze Casting Practice Of AlSi12Cu

The Etial 150 (AlSi12Cu) alloy in the Figure 5.3 was molten in a furnace set at 750°C, and the die and punch were heated in a second furnace which was set at 350 °C as seen in the Figure 5.4. The squeeze casting pressure applied was 100 MPa.

Figure 5.3. Some of the cut Etial 150 pieces before squeeze casting

After pouring the molten Etial 150 in to the die , the die was placed into the press in the Figure 5.5 and allowed to cool down to 300 °C . The punch was placed on the molten alloy in the die and then, squeezing pressure was applied for about two minutes.

Figure 5.4. The Etial 150 alloy in the pot is moltening in the furnace on the left and the die is being heated in the other furnace on the right.


Figure 5.5. Squeeze casting equipment (hidrolic press) is on the left and the die with micrometer in order to measure the temperature is on the right

The press load (force) necessary to deliver a pressure of 100 MPa on to the freezing alloy is calculated as follows:

Table 5.2. Calculation of the pressure on the mould

Hydraulic Press Pressure	63,73	kg/cm^2	6,25	MPa	62,50	Bar
Hydraulic Press Piston Diameter	100	mm		10	cm	
Mould Piston Diameter	25	mm		2,5	cm	
Hydraulic Press Piston Surface Area	7853,98	mm^2		78,54	cm^2	
Mould Piston Surface Diameter	490,87	mm^2		4,91	cm^2	
P=F/A	$P(kg/cm^2)$	F(kg)		$A(cm^2)$	P(Mpa)	
Hydraulic Press	63,73	5005,34		78,54	6,25	
Mould	1019,68	5005,34		4,91	100,00	

Four specimens were squeeze cast. The die and punch temperature were increased to 400 °C after the third squeeze cast sample. Additionally, six specimens were not squeezed and cast to the die at the temperature of 400 °C. Moreover, six specimens were not squeezed and cast to the cold die at the room temperature of 20 °C.

Figure 5.6. Squeeze casted four specimens are seen on the left, six specimens unsqueezed in the hot die are seen in the middle, and four of the six unsqueezed in the cold die specimens are seen on the right.

Table 5.3. Applied casting types

Cast no 1	High pressure die casted
Cast no 2	Squeezed under 100 MPa
Cast no 3	Not squeezed in the die at 400 °C
Cast no 4	Not squeezed in the cold die

4.4. Tension and Hardness Tests

The tension test samples were machined from the castings according to the TS 138 (EN 10002 - 1:1990) standard and tested in İMES. Table 5.5, 5.6, and 5.7 include the tension test sample dimensions (i.e. initial radius and initial length), tensile load applied, elongation at fracture (ε_f), yield strength (σ_{YS}), tensile strength (σ_{TS}), and Brinell Hardness (HB) where the ball diameter and load used were 2.5 mm and 62.5 kg, respectively. The load-extension curves obtained from each tension test are collected in the Appendix. However, a sample curve from each group are also given below.

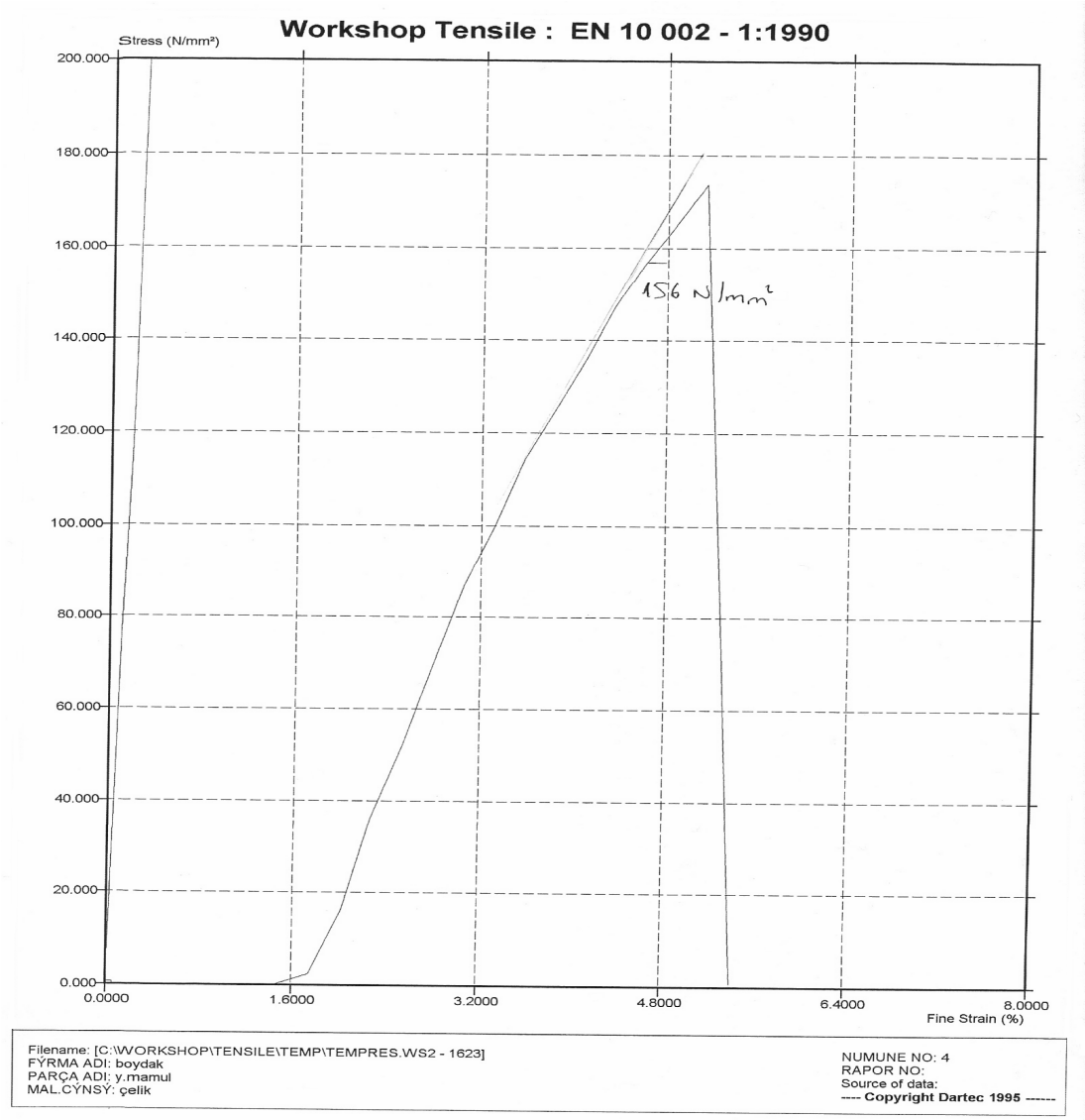

Figure 5.7. Stress-strain curve of the fourth not-squeezed sample

Table 5.4. Mechanical test results obtained from the not-squeezed ETIAL 150 (AlSi12Cu) castings

Sample No	$D_0/2$ (mm)	L_0 (mm)	Load (N)	ε_f (%)	σ_{YS} (N/mm^2)	σ_{TS} (N/mm^2)	HB
1	10	50	13960	-	-	178	76
2	10	50	14190	1	146	181	74
3	10	50	10990	-	-	140	74
4	10	50	13640	0.4	156	174	71
5	10	50	12680	0.4	151	161	77
6	5	25	1141	-	-	58.1	76

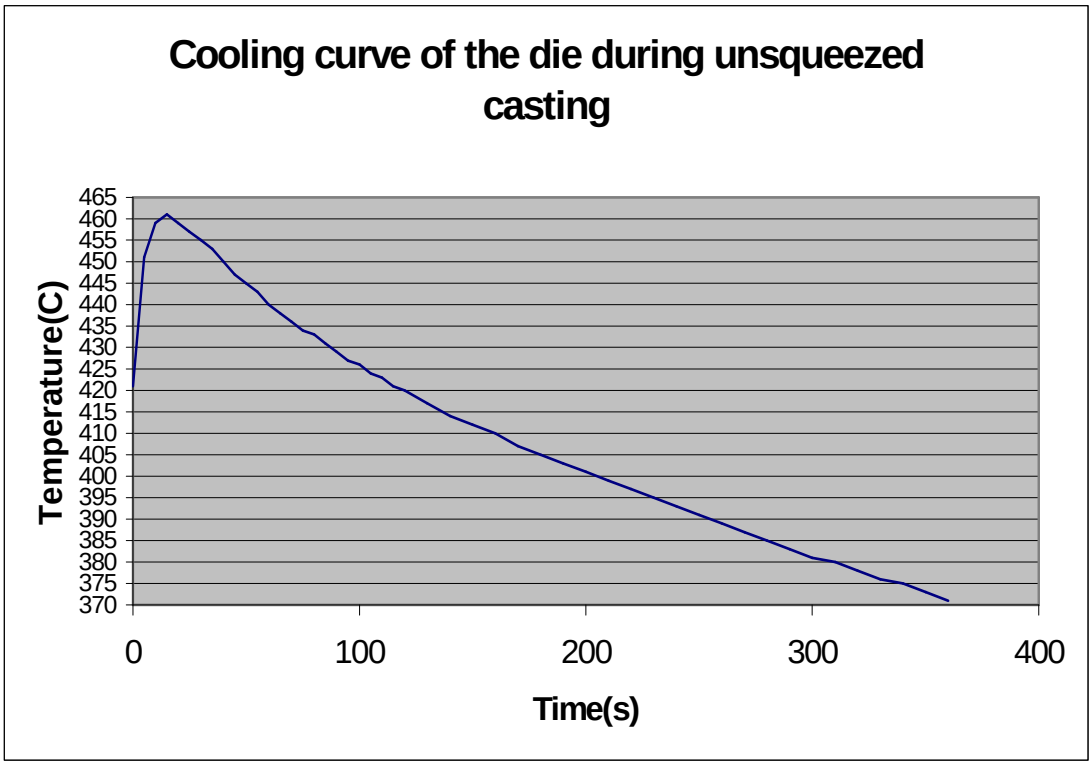

Figure 5.8. Cooling curve of the die during unsqueezed casting for the first sample

The slope of the cooling curve, which is 0.2609 $°Cs^{-1}$, gives the cooling rate of the not-squeezed casting as seen in the Figure 5.8.

Table 5.5. Mechanical test results obtained from the squeezed ETIAL 150 castings

Sample No	$D_0/2$ (mm)	L_0 (mm)	Load (N)	ε_f (%)	σ_{YS} (N/mm^2)	σ_{TS} (N/mm^2)	HB
7	10	50	13140	-	-	167	
8	10	50	16390	1.2	202	209	
9	10	50	15430	1.2	179	196	
10	10	50	13320	0.8	157	170	

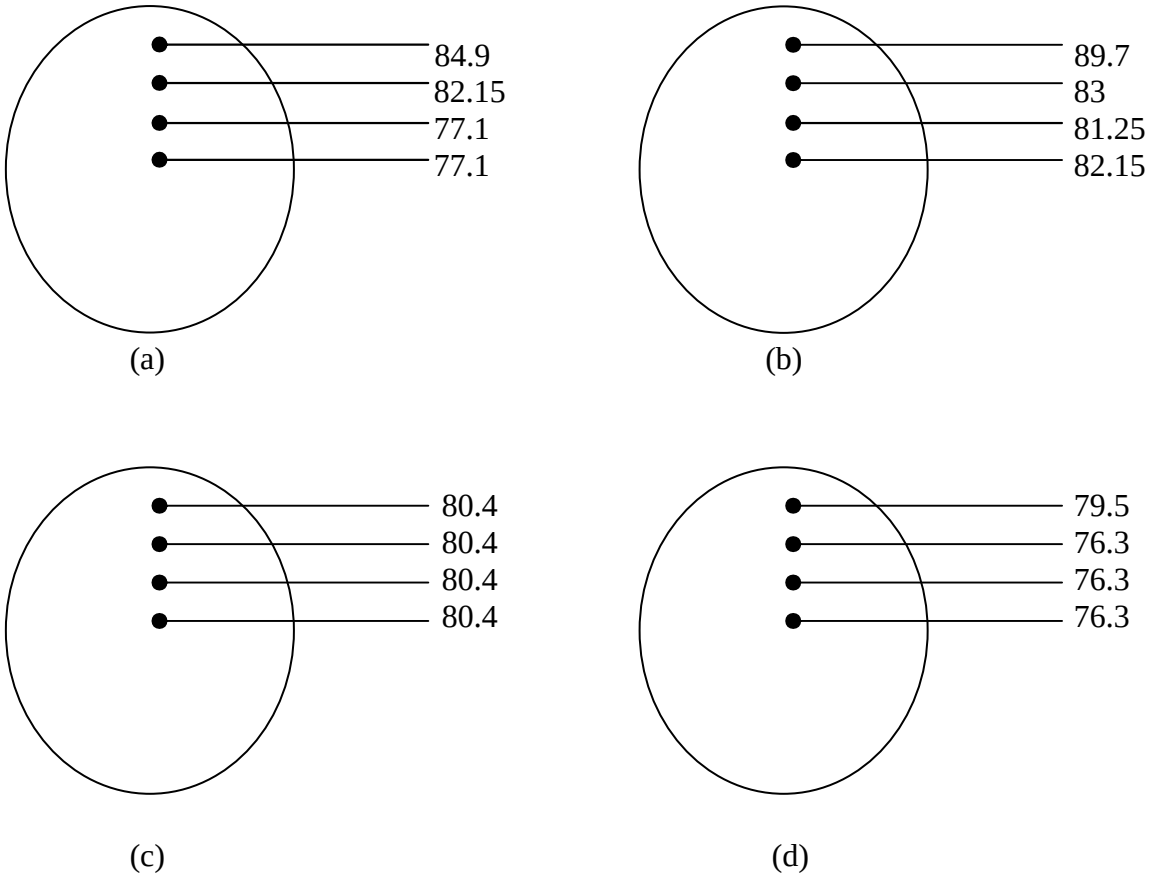

Figure 5.9. Brinell hardness values of four different points of the squeezed Etial 150 castings. (a): The values of the seventh sample (b). The values of the eigth sample, (c): The values of the nineth sample, (d): The values of the tenth sample.

Figure 5.10. Photo of hardness specimens of squeeze castings

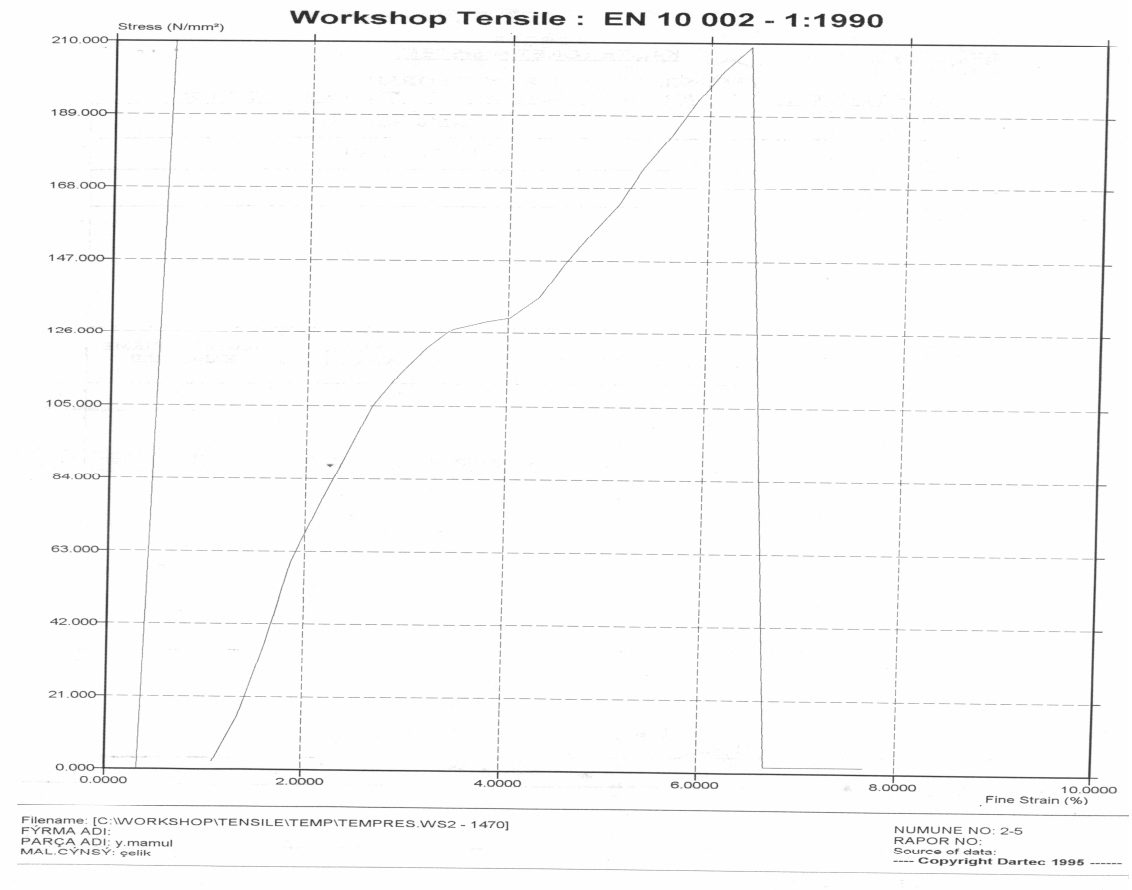

Figure 5.11. Stress-strain curve of the number ten squeezed specimen

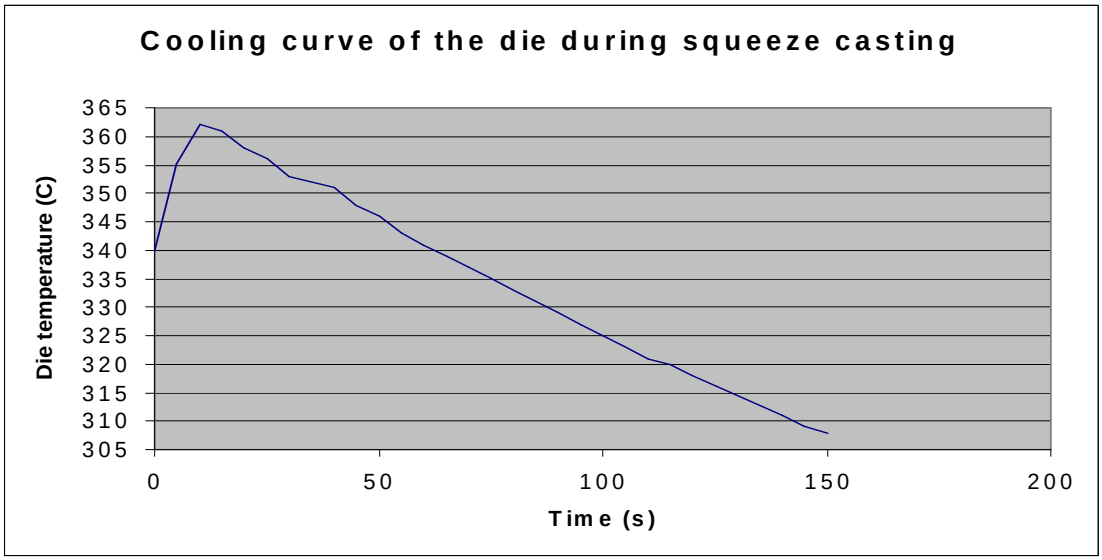

Figure 5.12. Cooling curve of the die during squeezed casting for the eigth sample

The cooling rate of the squeezed casting is 0.3857 $°Cs^{-1}$, which is the slope of the cooling curve in the Figure 5.12. It is noted that the die heats up and cools down more quickly during squeeze casting. This is a result of more efficient heat transfer from the freezing alloy to the die due to pressure application.

Table 5.6. Mechanical test results obtained from the high pressure die cast ETIAL 150 Flansch

Sample No	$D_0/2$ (mm)	L_0 (mm)	Load (N)	ε_f (%)	σ_{YS} (N/mm^2)	σ_{TS} (N/mm^2)	HB
11	6	30	4052	2.3		143.3	89.7
12	6	30	2773	1		98.1	89.7
13	6	30	2804.8	-		99.2	87.75

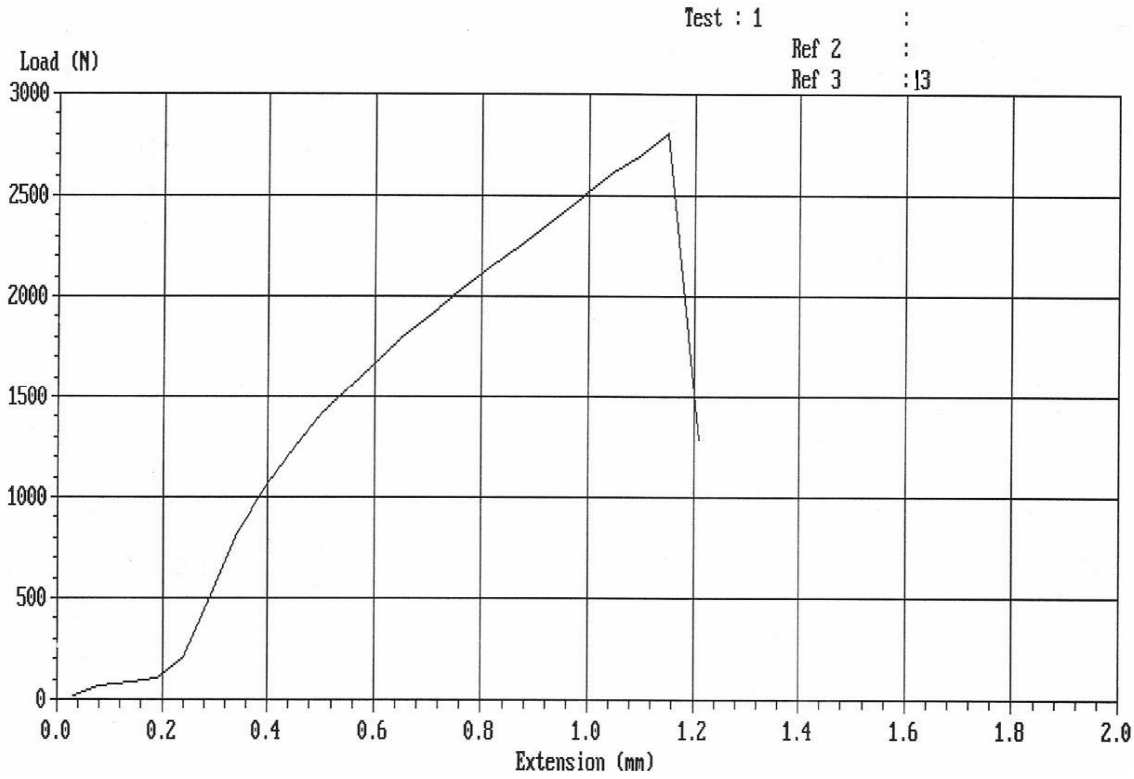

Figure 5.13.Load-extension diagram of the number thirteen high pressure die cast specimen

When the tensile strengths of all casting types are compared, it is seen that squeeze casting provides the highest tensile strength value. However, the Brinell hardness and elongation values of the high pressure die casting is the largest.

Figure 5.14. Remainings of the tensile tested six unsqueezed in the hot die specimens on the left, four squeezed specimens in the middle, and three high pressure die casted specimens on the right.

Table 5.7. Mechanical test results obtained from the not-squeezed ETIAL 150 castings to the cold die

Sample No	$D_0/2$ (mm)	L_0 (mm)	Load (N)	ε_f (%)	σ_{YS} (N/mm^2)	σ_{TS} (N/mm^2)	HB
14	5	50	5360	0.4	-	68	85.85
15	5	50	14240	3.41	-	181	83.95
16	5	50	9250	2	-	118	87.75
17	5	50	11810	2.54	-	150	87.75
18	5	50	14280	3.73	-	182	87.75
19	5	50	15930	3.69	-	203	87.75

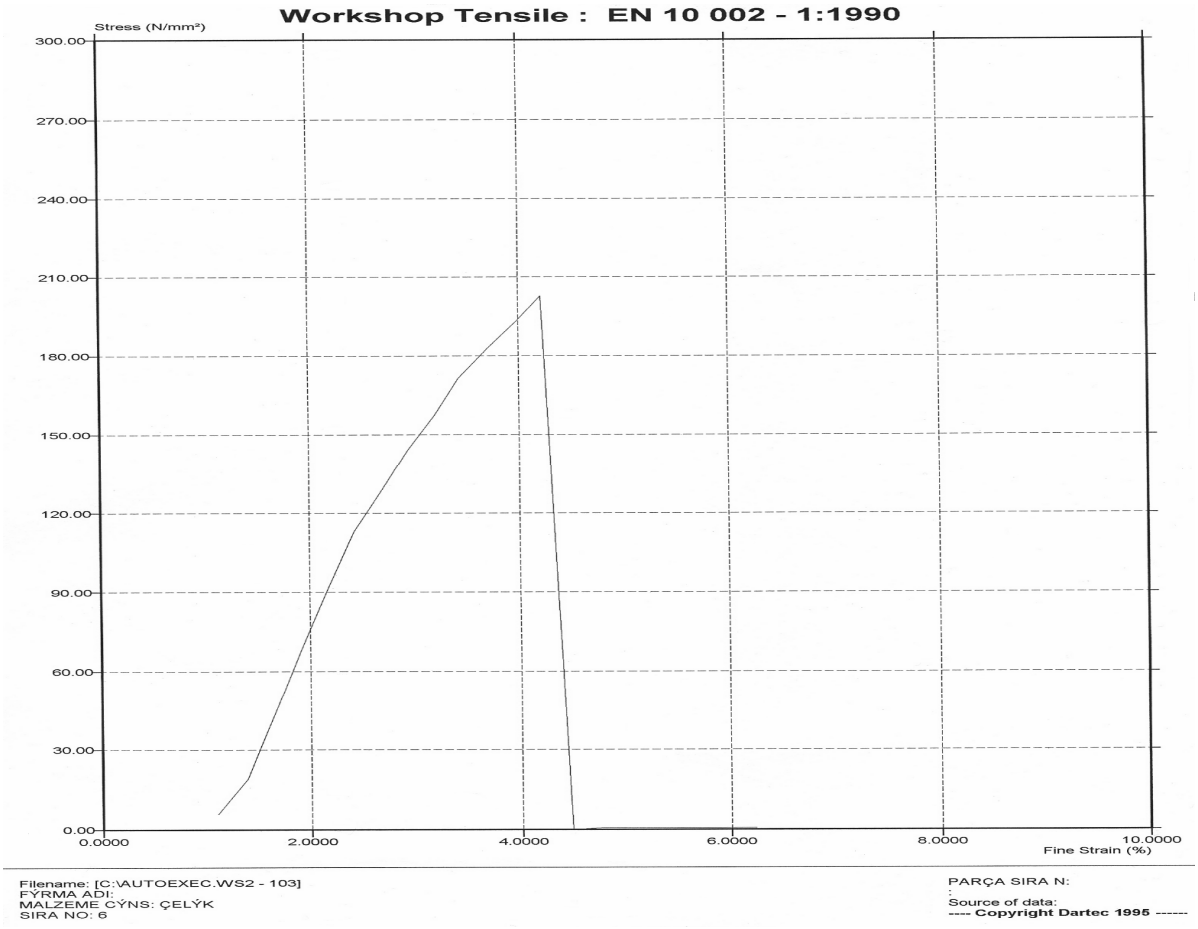

Figure 5.15. Stress-strain curve of the number nineteen not-squeezed cast to cold die sample

According to the mechanical test result table in the Table 5.8 and the stress-strain graph in the Figure 5.15, the unsqueezed cold die specimens are brittle.

Figure 5.16. Six tensile testing specimens of unsqueezed in the cold die casting; before tensile testing on the left and after tensile testing on the right photo

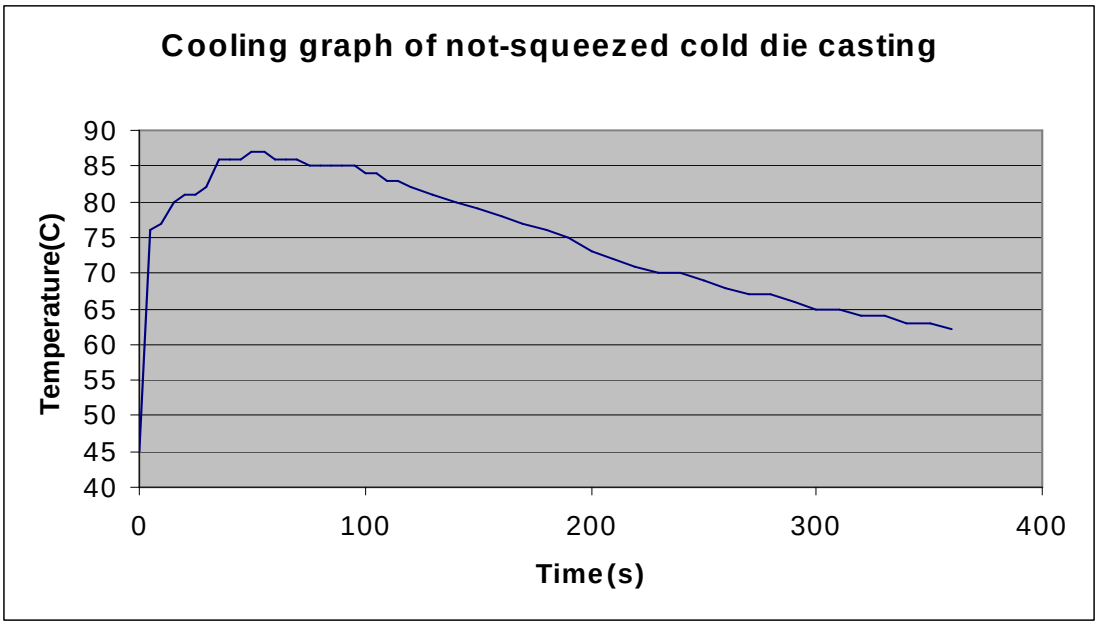

Figure 5.17. Cooling curve of the die during unsqueezed casting to cold die for the eighteenth sample

The cooling rate of the squeezed casting is 0.0943 $°Cs^{-1}$, which is the slope of the cooling curve in the Figure 5.17.

4.5. Microstructural Analysis

The micrographs of the not-squeezed in the hot die, squeezed, high pressure die cast, and not-squeezed in the cold die samples were taken in the IMES. Some examples of these micrographs of the cast samples are seen below.

Figure 5.18. Polished six unsqueezed specimens for microstructural analysis

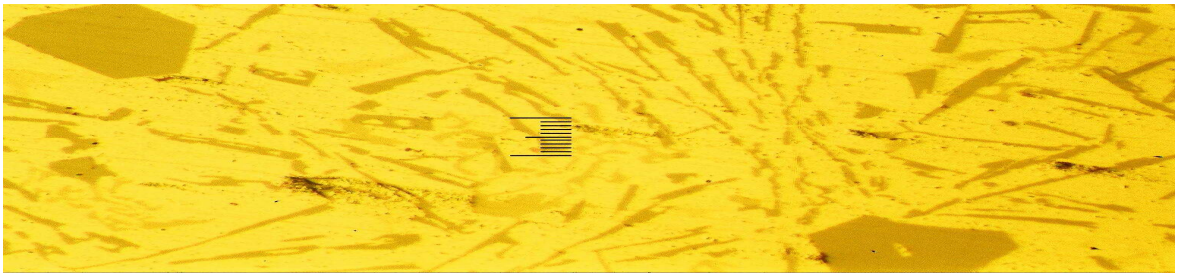

Figure 5.19. The microstructure of the second not-squeezed sample under ×500 magnification

It is seen that the silicon flakes are coarsed and faceted silicon primaries are also present in Figure 5.19.

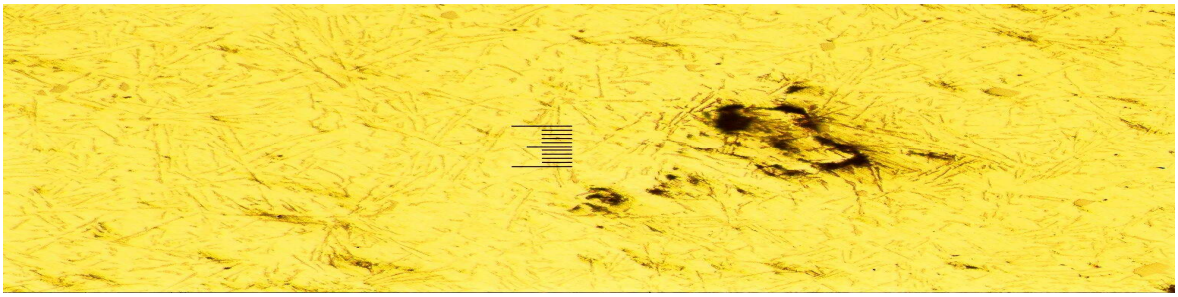

Figure 5.20. The microstructure of the fourth not-squeezed sample, ×100

Porosity is seen in the Figure 5.20. Moreover, Aluminum rich phase shrinks while Silicon rich phase expands upon cooling as seen in Figure 5.20.

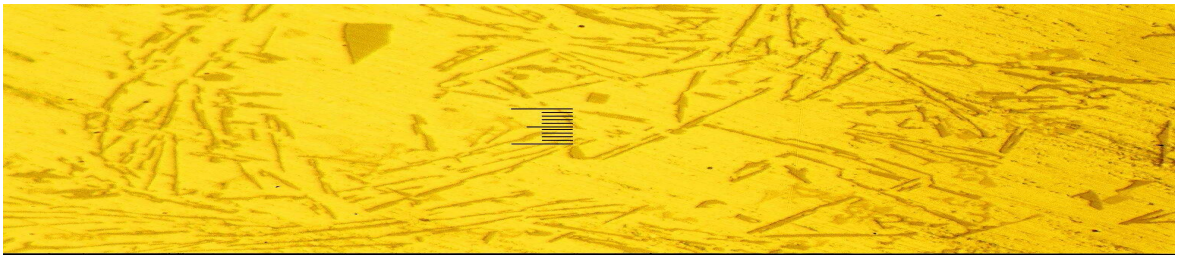

Figure 5.21. The microstructure of the sixth not-squeezed sample, ×500

Coarse silicon flakes and Chienese script are seen in the Figure 5.21. The spacing is about 15 μm between the silicon flakes.

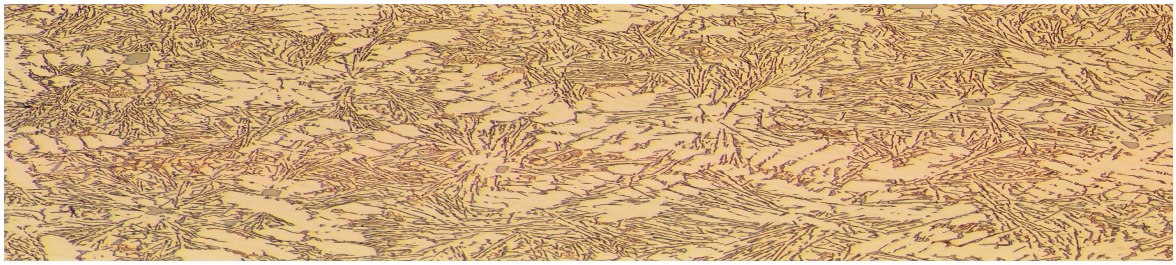

Figure 5.22. The microstructure of the number five squeezed (dağlanmış) sample, ×100

Figure 5.22 demonstrates that porosity is eliminated. Aluminum rich dendrites, which are seen in the microstructure, means casting cooled quickly. Spacing between Silicon flakes are reduced.

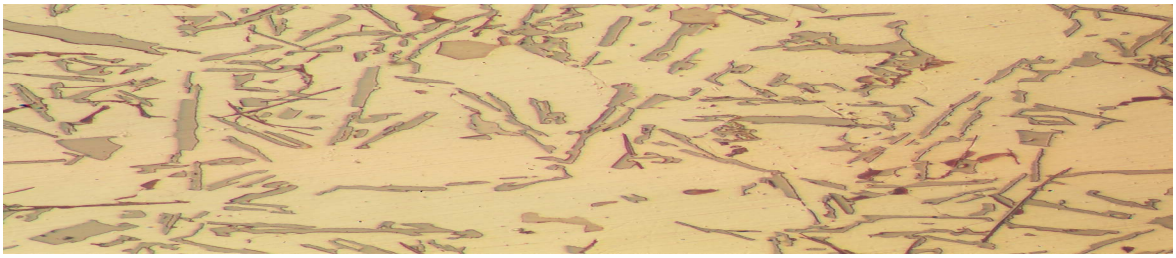

Figure 5.23. The microstructure of the number twelve high pressure die cast (dağlanmış) sample, ×500

Figure 5.23 shows that both silicon flakes and also faceted primaries are refined. Moreover, porosity is eliminated.

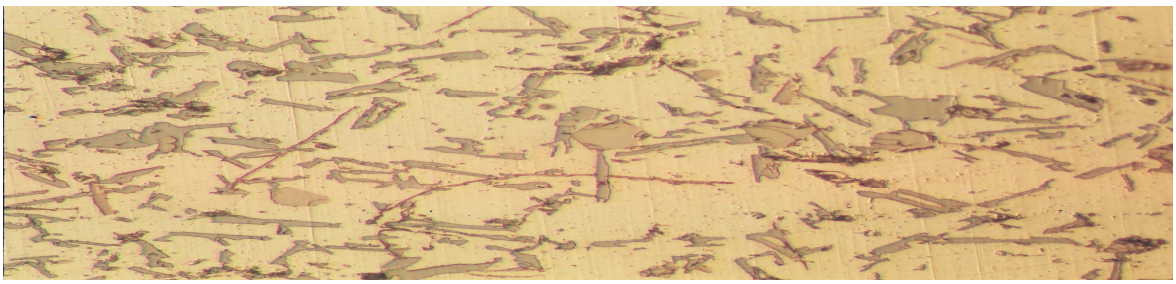

Figure 5.24. The microstructure of the number thirteen high pressure die cast (dağlanmış) sample, ×500

It is seen in the Figure 5.24 that faceted silicon primaries still present. However, they are refined as compared to the not-squeezed casting. Furthermore, no porosity is present in the Aluminum rich matrix.

5. CONCLUSIONS

- Simulation results are in good agreement with experimental findings.
- Simulation is a very efficient way to optimize casting quality. It is also very economical and practical, since one can change every parameter (die temperature, casting temperature, pressure, mould design etc.) in the computer simulation very easily and then go on to try the results in real casting. This helps to reduce time spent on trial and error experiments.
- For optimum and reliable results, minimum 5 cycles needed to be carried out in simulation software.
- One of most important parameters in casting quality is the porosity. Main reason for product rejection is due to the porosity (either gas or shrinkage). Since simulation can reveal this and helps to minimize this defect, the use of computers in casting process increases the casting quality significantly.
- Depending on the cast quality specified, high prssure die casting or squeeze casting procedures can be applied readily to the Etial 150 (AlSi12Cu) alloy.

APPENDIX A: LOAD-EXTENSION CURVES OBTAINED FROM EACH TENSION TESTS

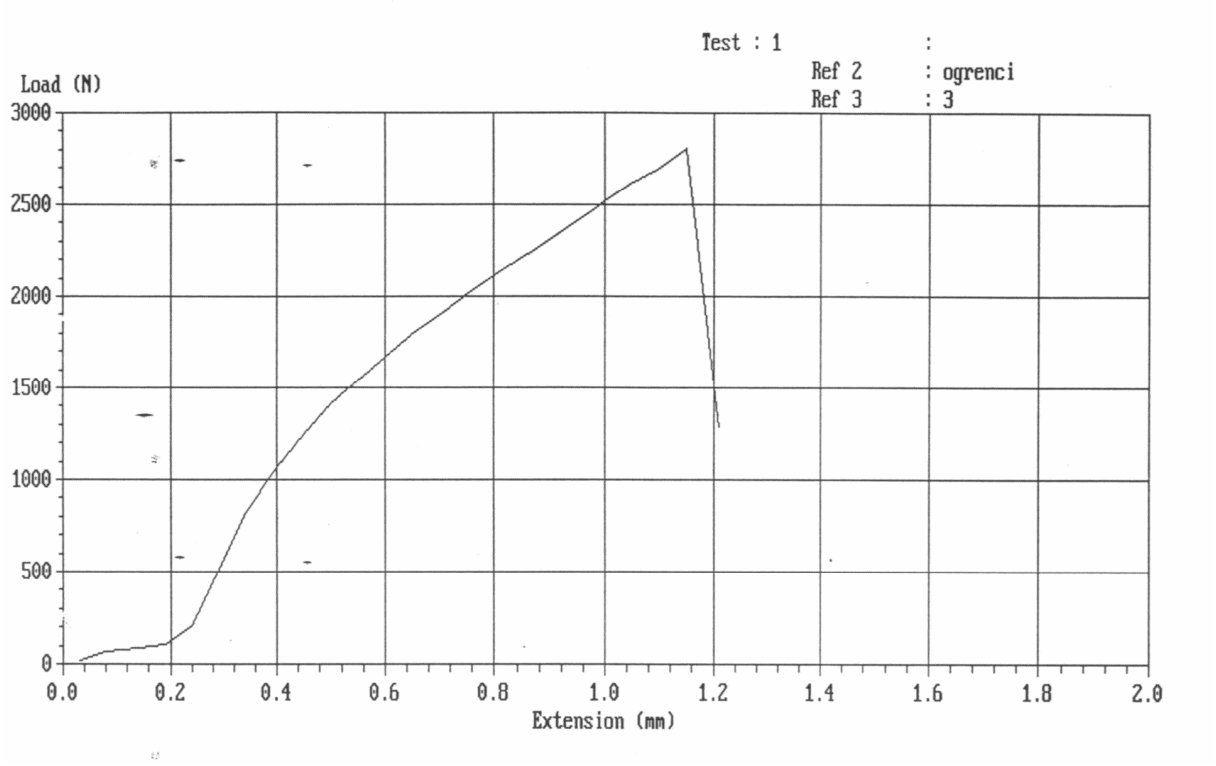

Figure A.1. Load-extension curve of the first high pressure die casting sample

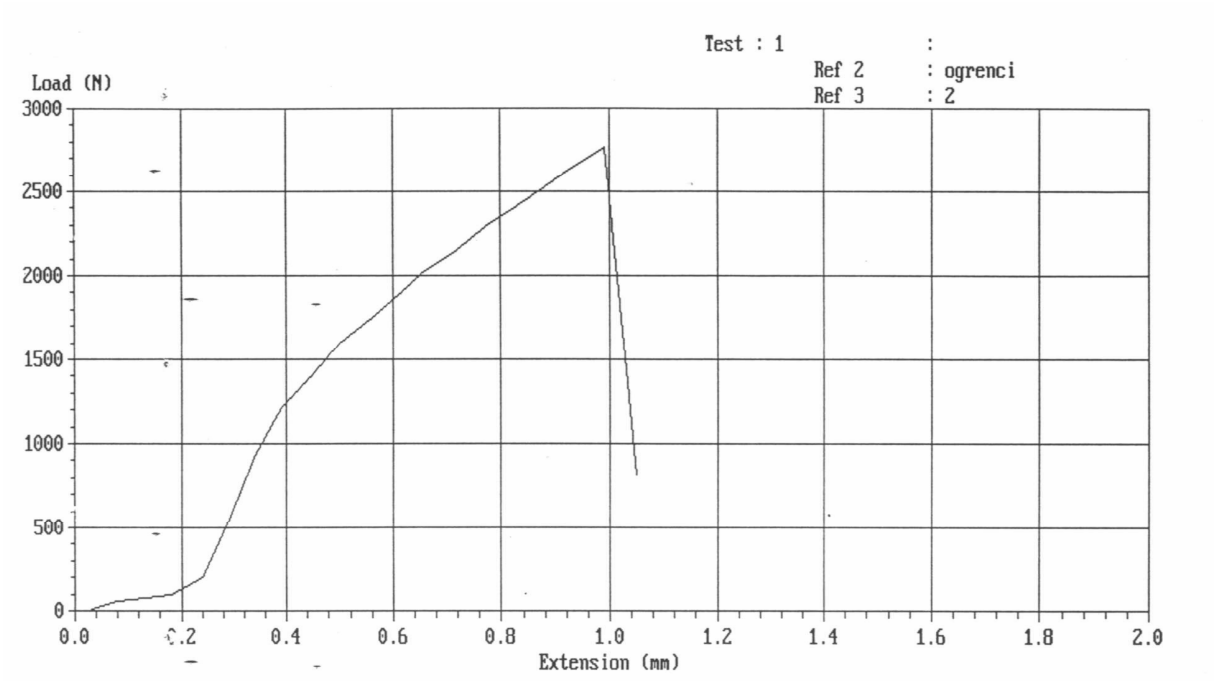

Figure A.2. Load-extension curve of the second high pressure die casting sample

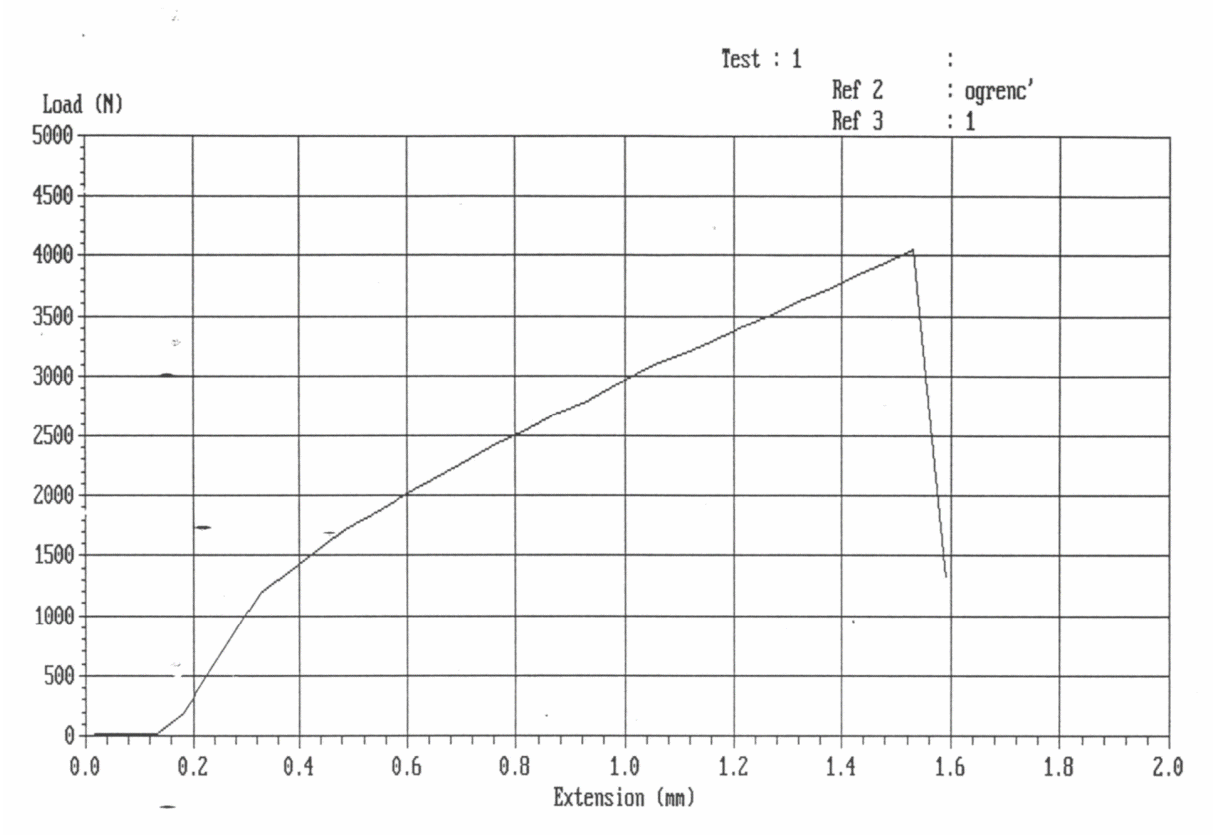

Figure A.3. Load-extension curve of the third high pressure die casting sample

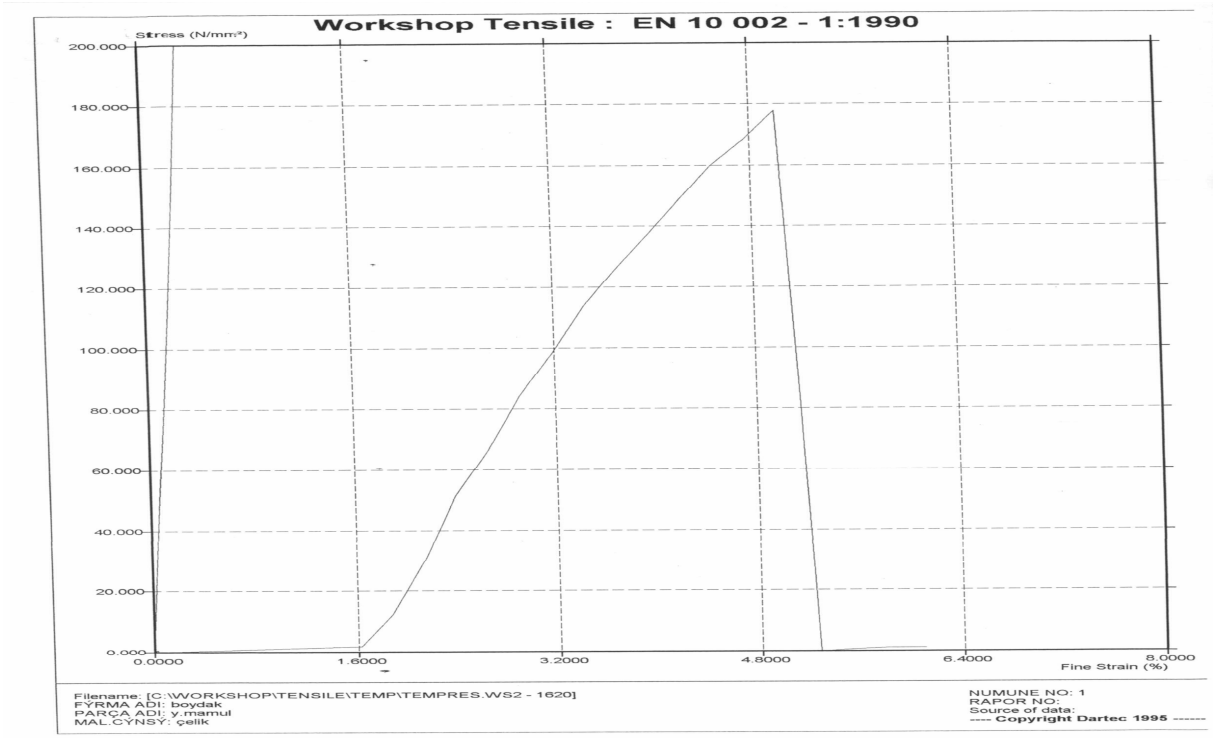

Figure A.4. Stress-strain curve of the first not-squeezed sample

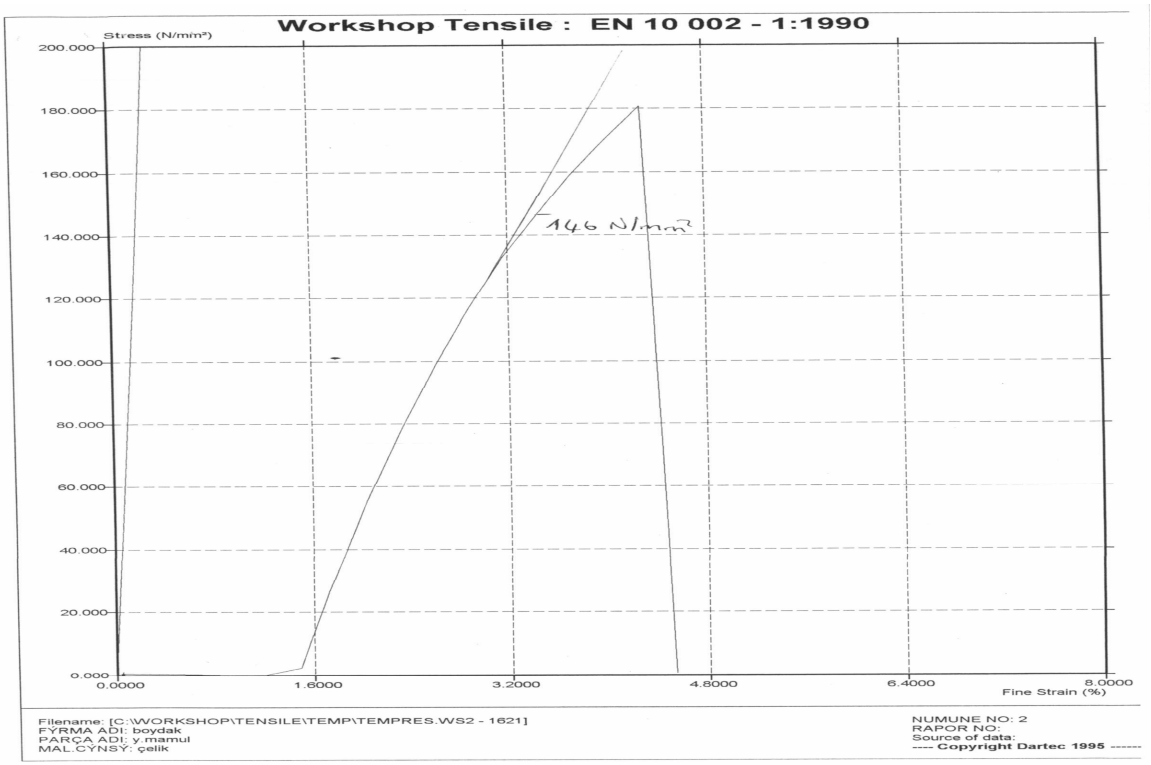

Figure A.5. Stress-strain curve of the second not-squeezed sample

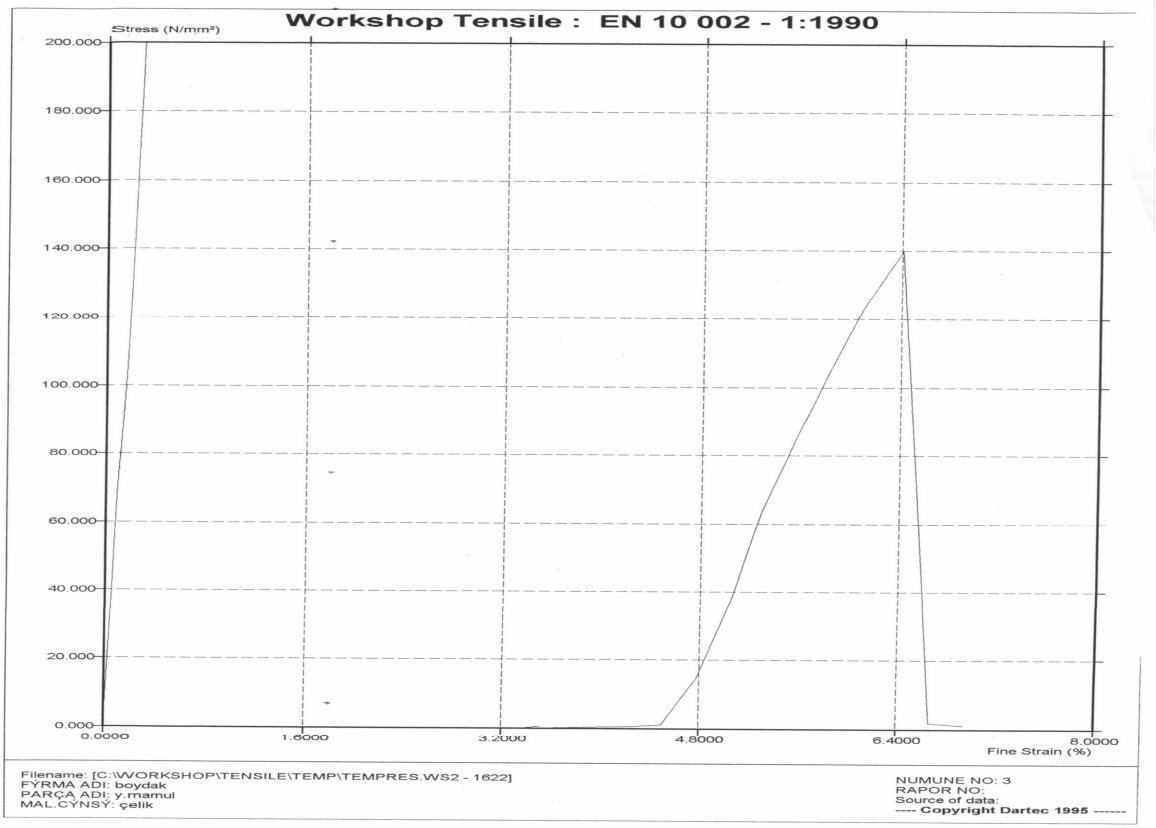

Figure A.6. Stress-strain curve of the third not-squeezed sample

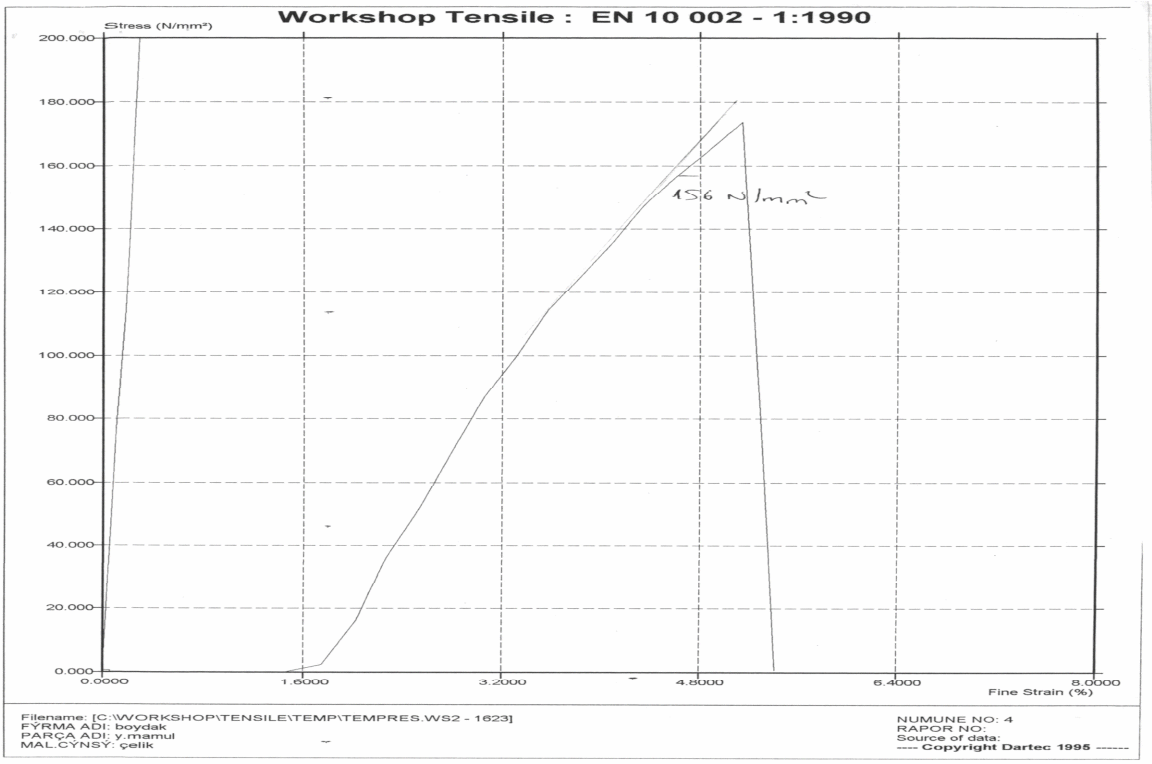

Figure A.7. Stress-strain curve of the fourth not-squeezed sample

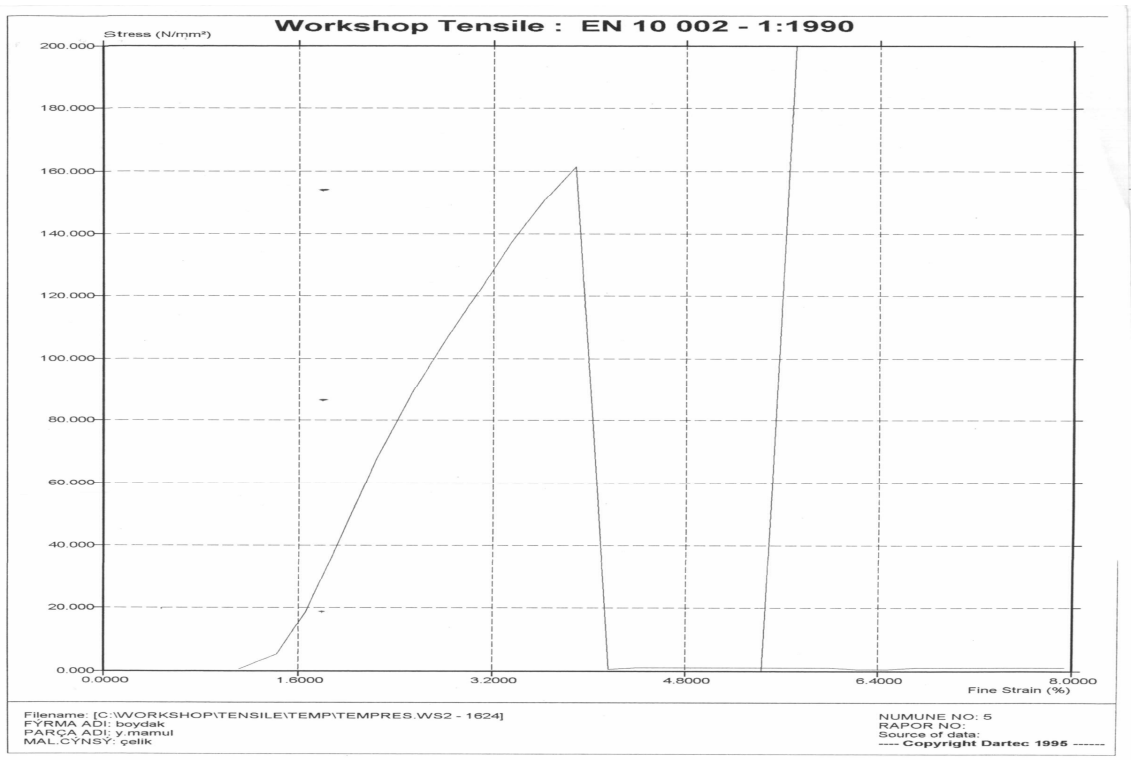

Figure A.8. Stress-strain curve of the fifth not-squeezed sample

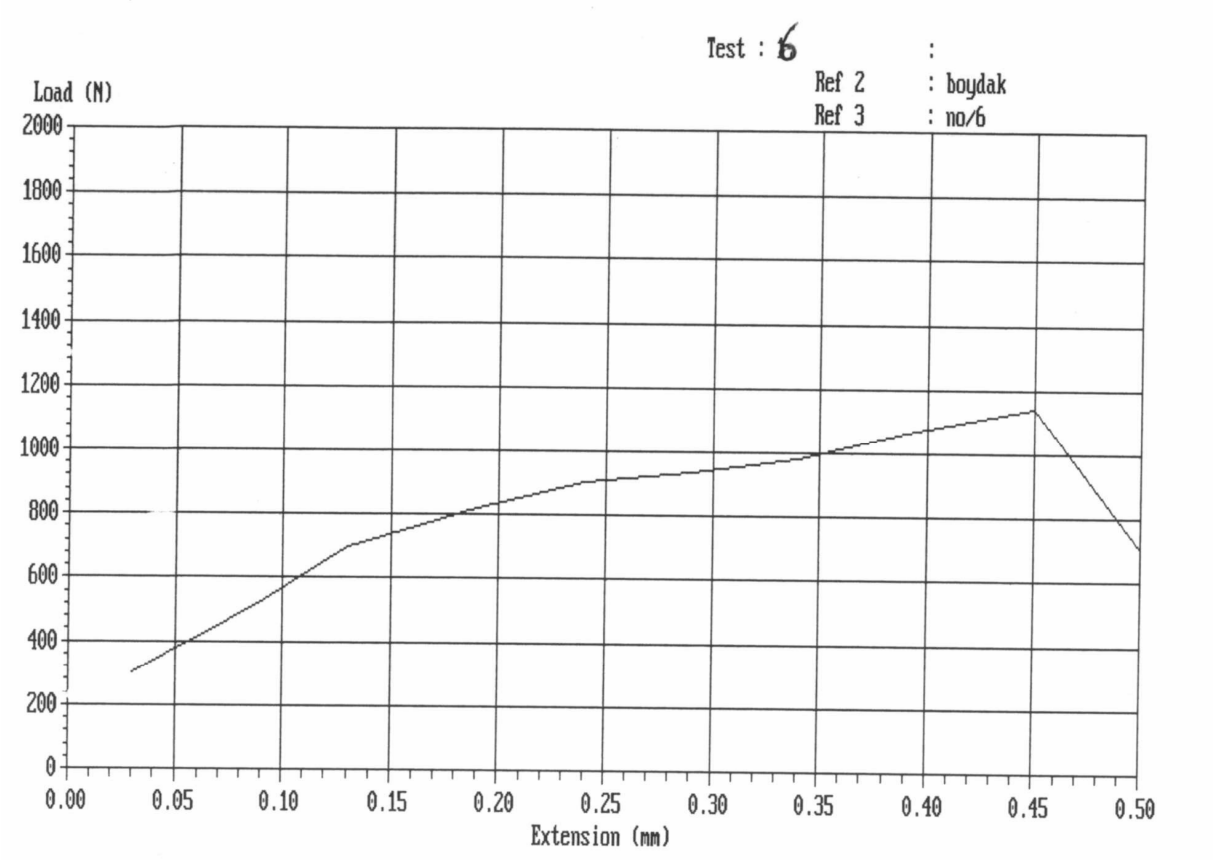

Figure A.9. Stress-strain curve of the sixth not-squeezed sample

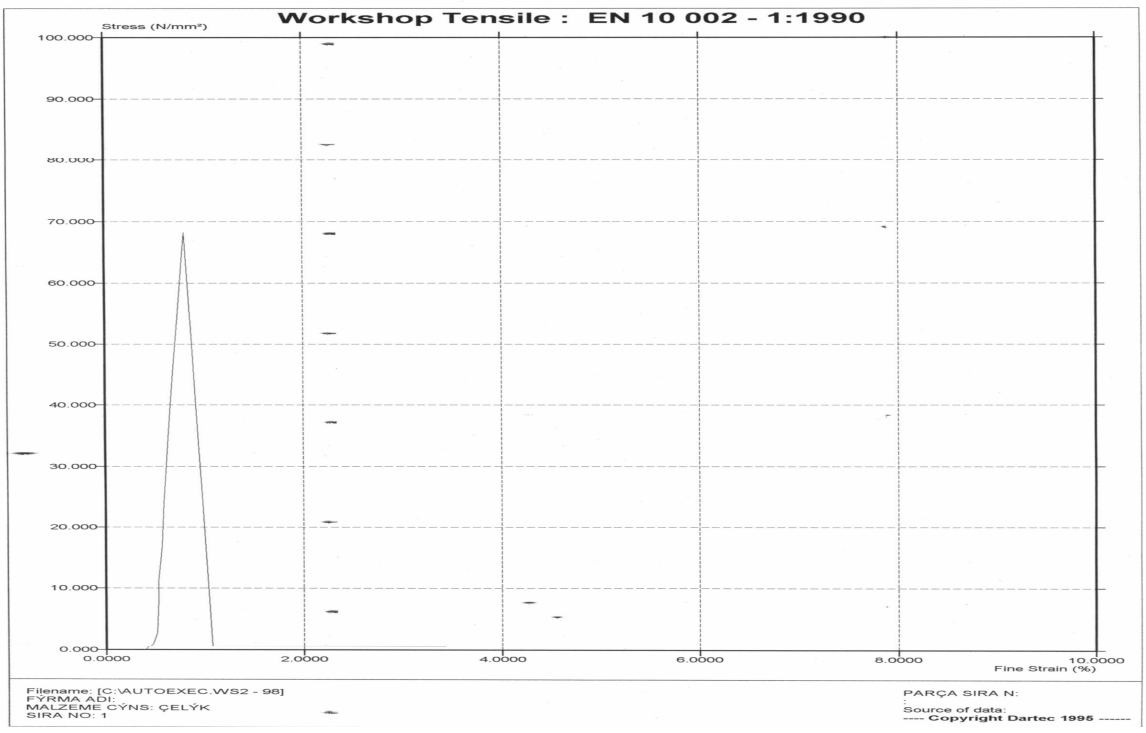

Figure A.10. Stress-strain curve of the firsth not-squeezed in the cold die sample

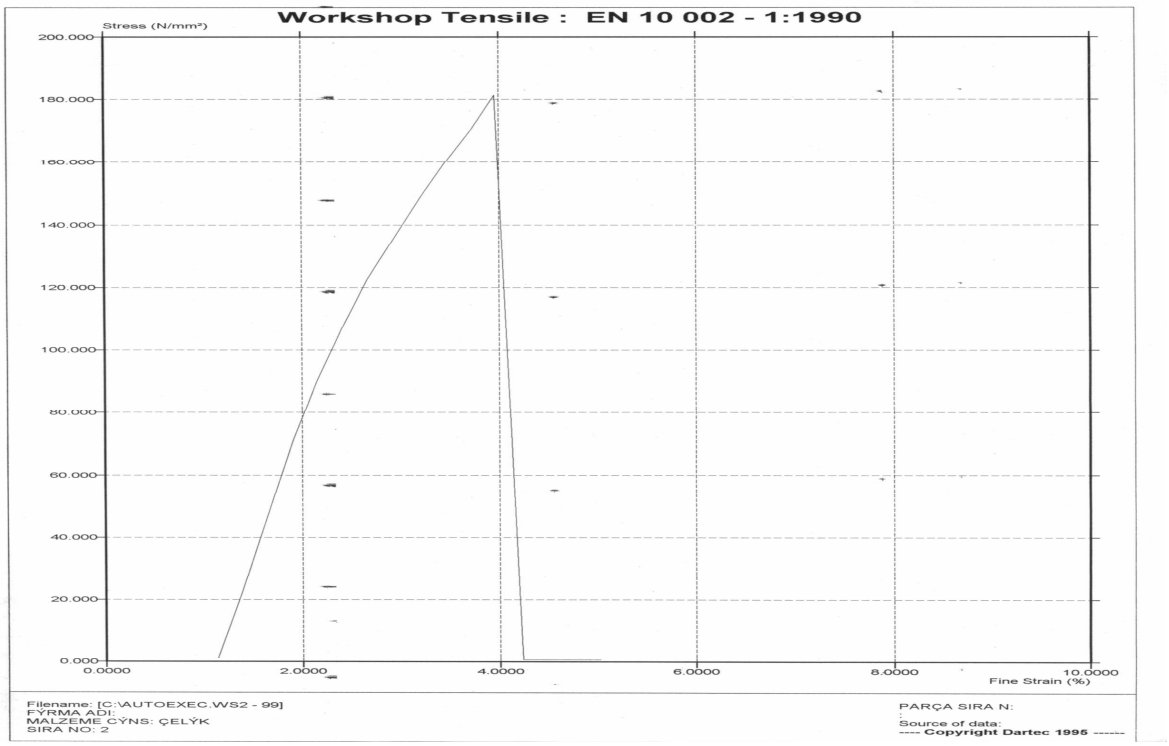

Figure A.11. Stress-strain curve of the second not-squeezed in the cold die sample

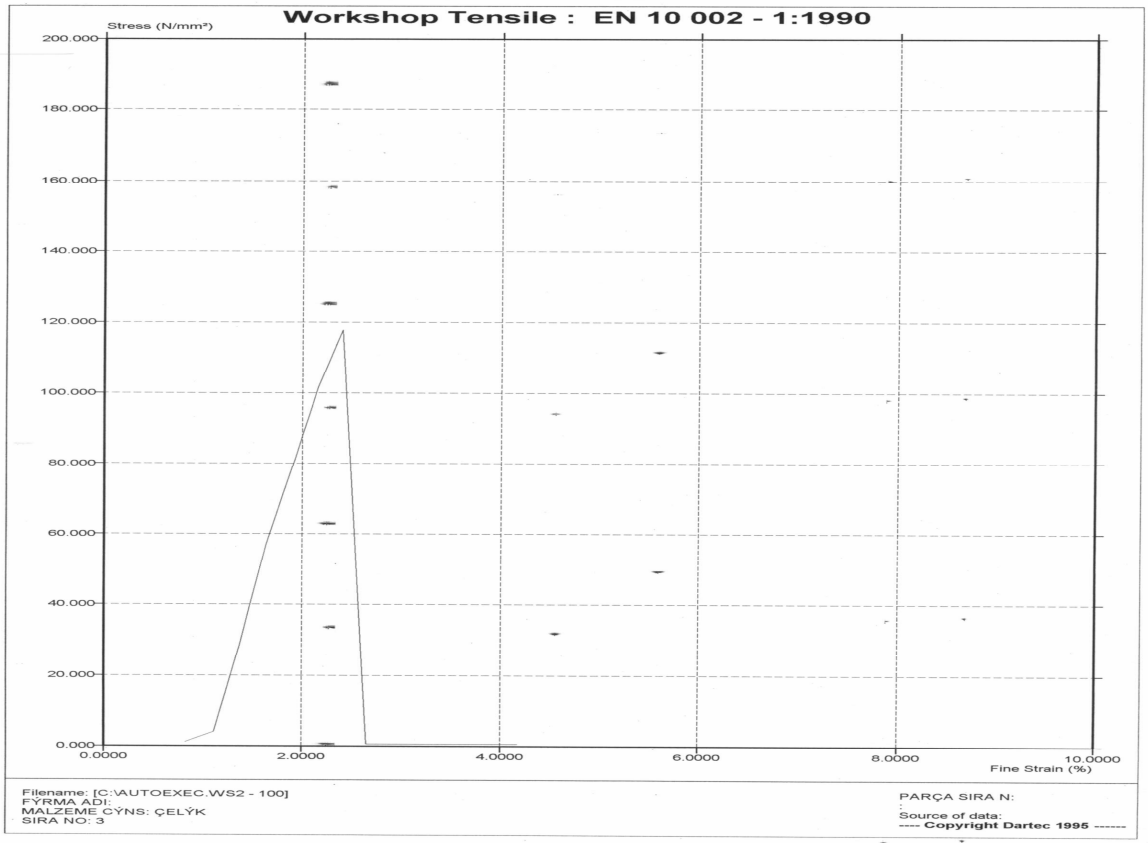

Figure A.12. Stress-strain curve of the thirth not-squeezed in the cold die sample

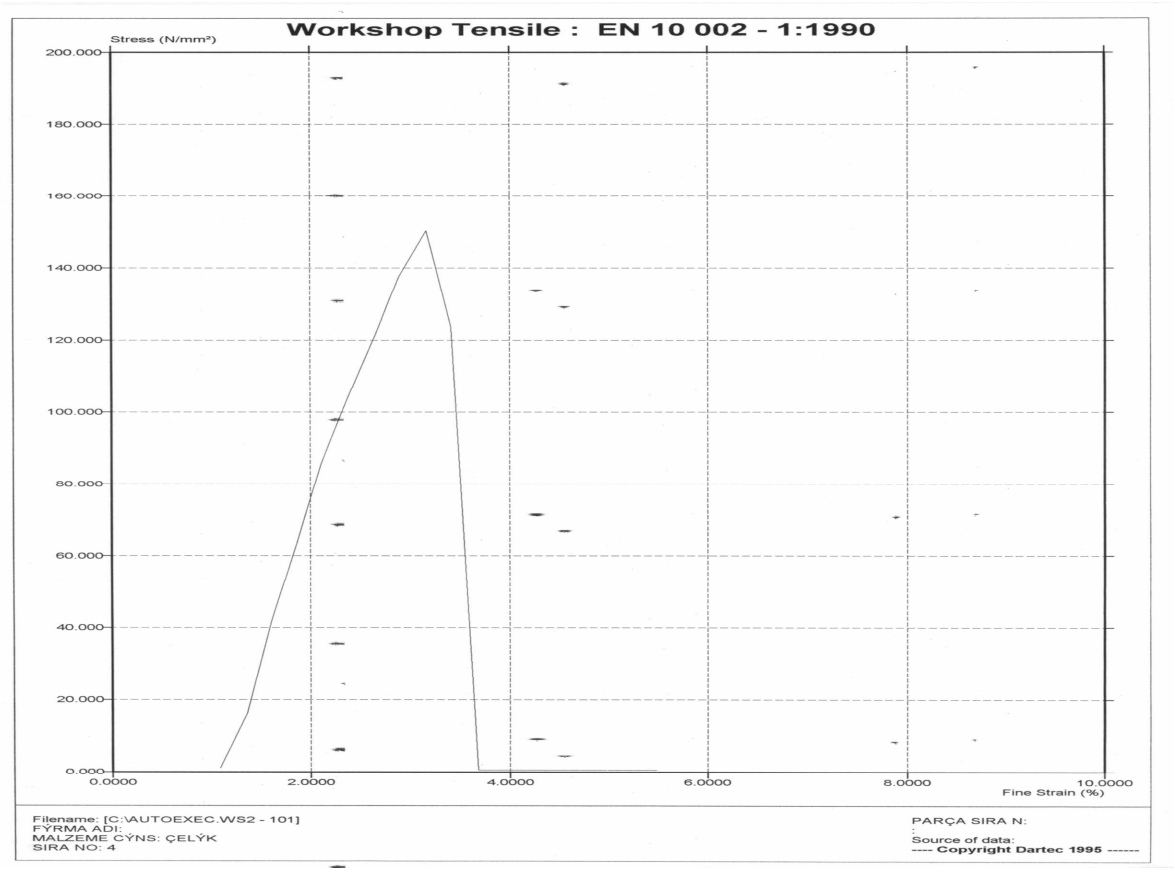

Figure A.13. Stress-strain curve of the fourth not-squeezed in the cold die sample

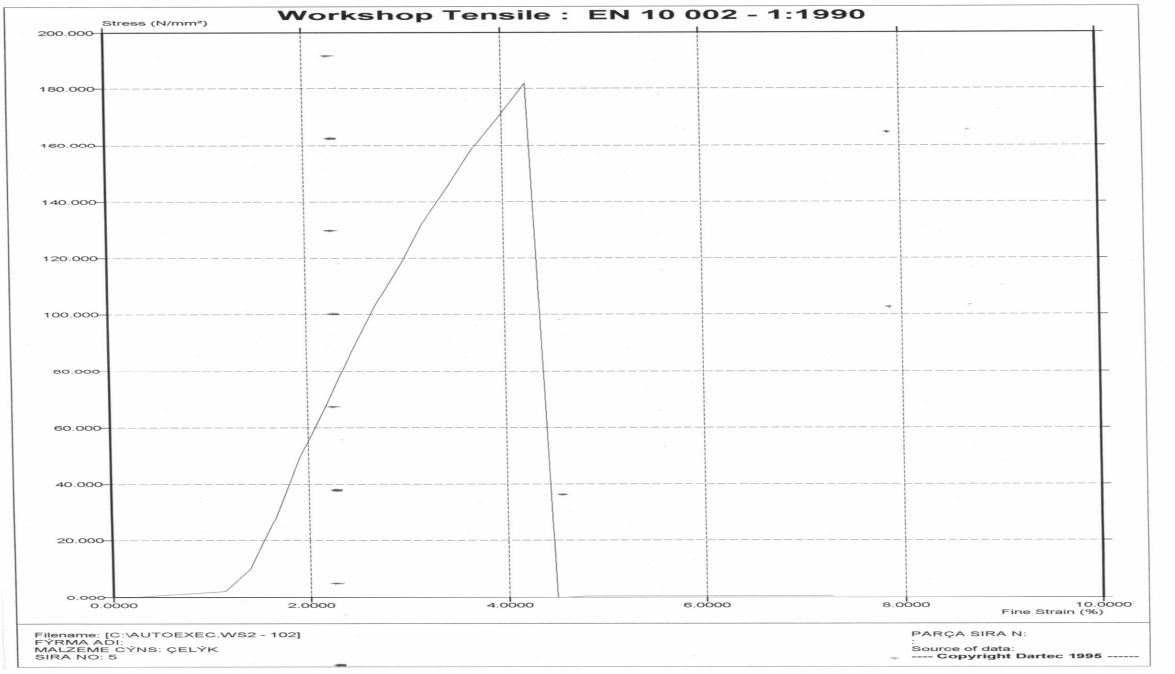

Figure A.14. Stress-strain curve of the fifth not-squeezed in the cold die sample

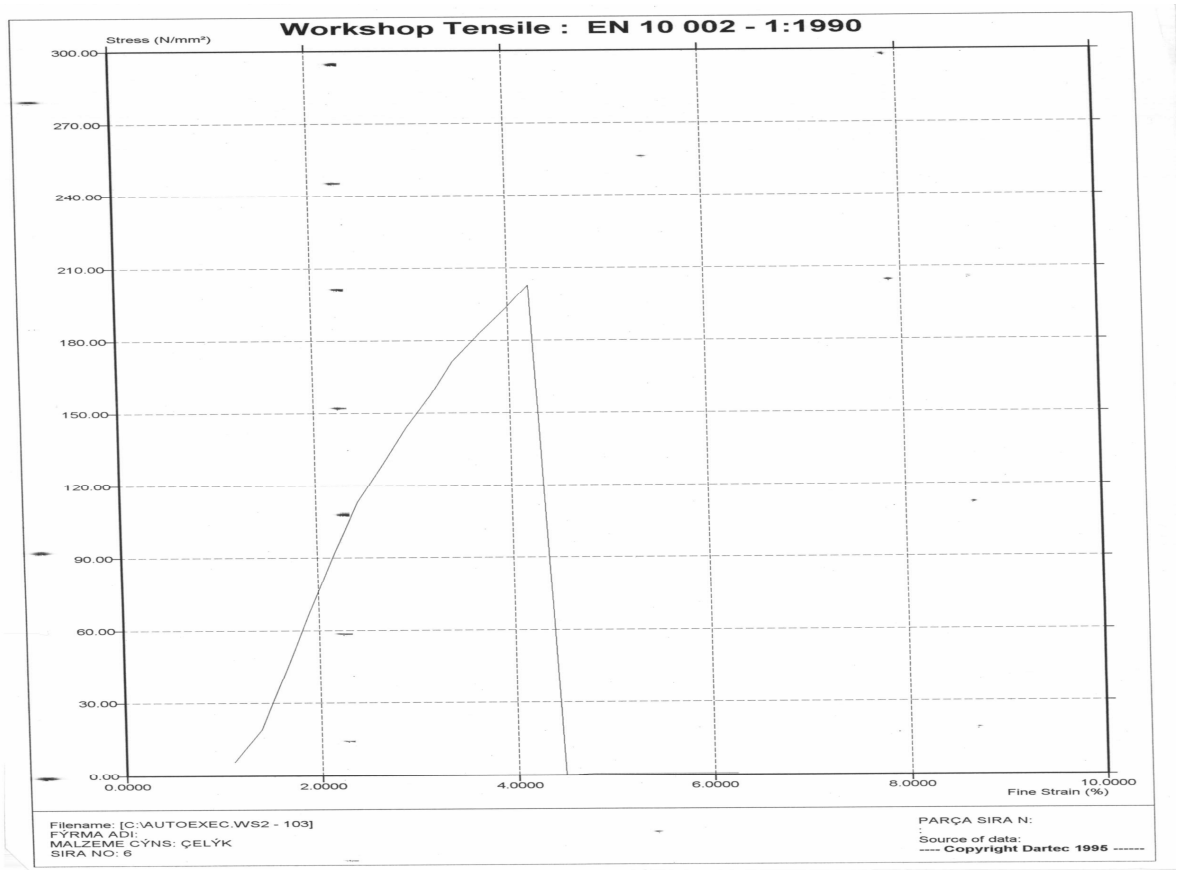

Figure A.15. Stress-strain curve of the sixth not-squeezed in the cold die sample

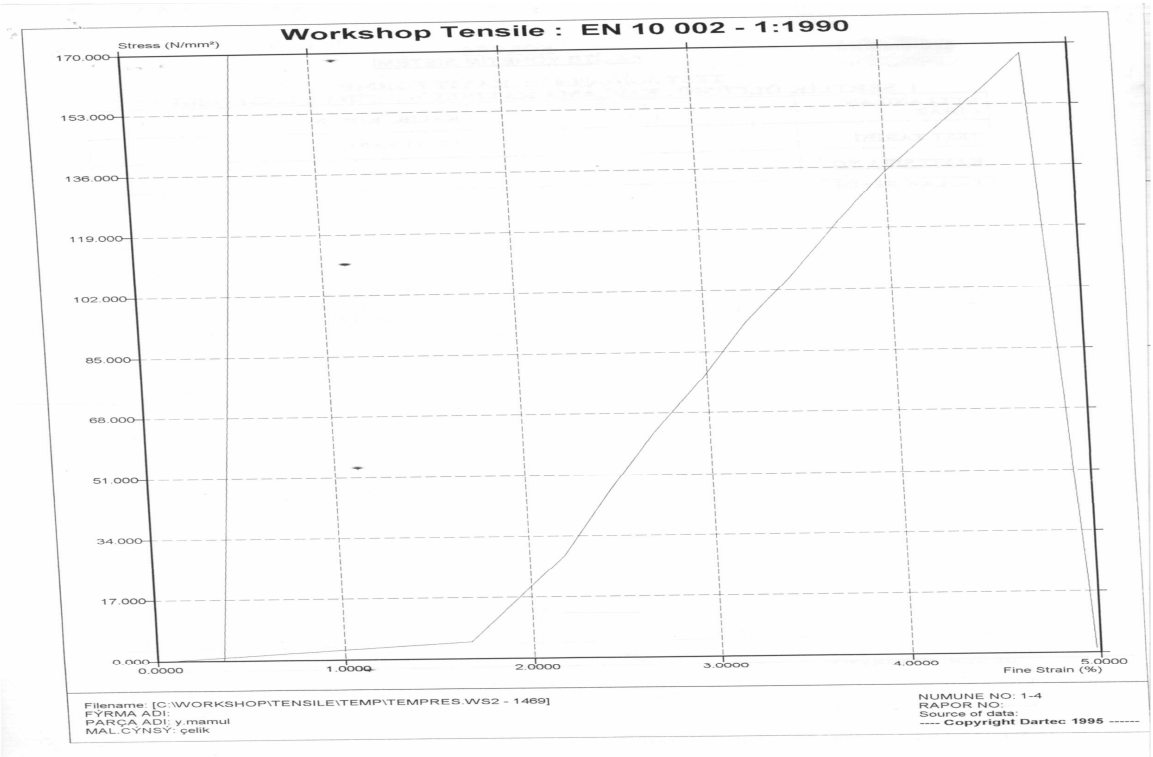

Figure A.16. Stress-strain curve of the first squeezed sample

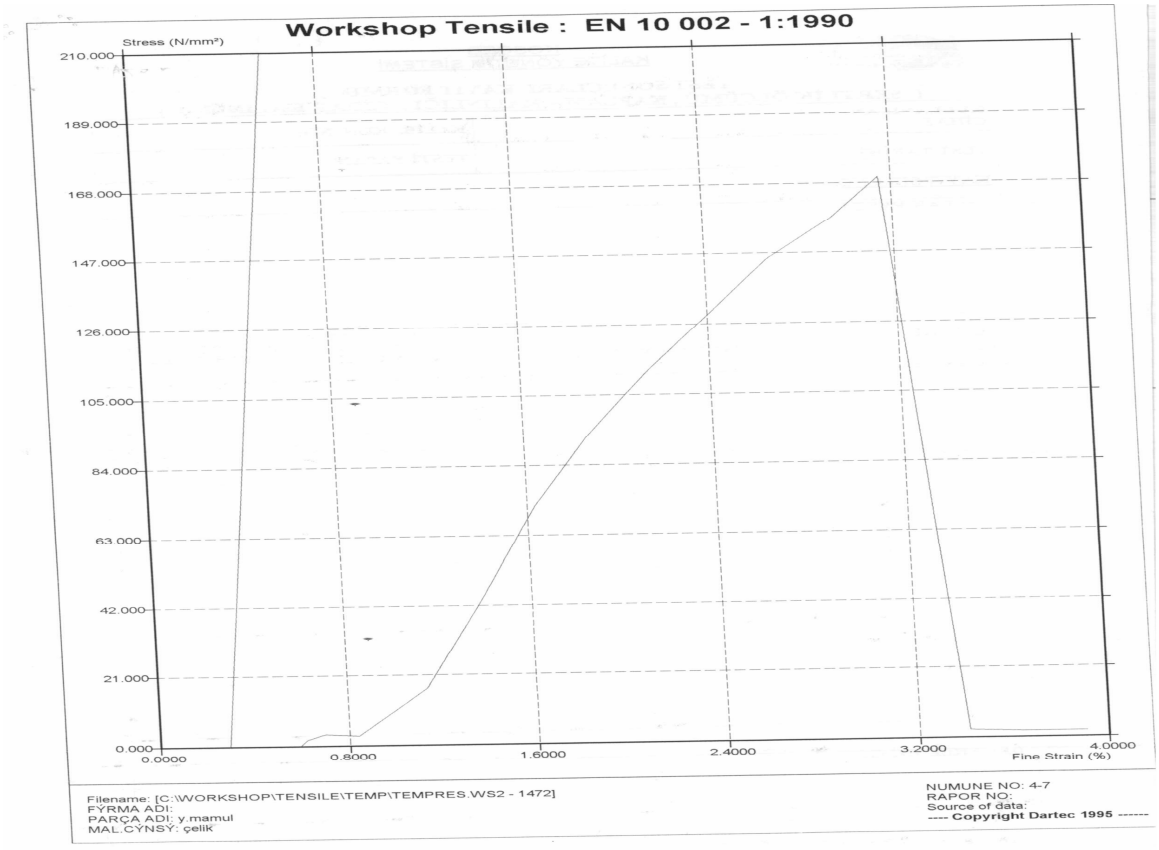

Figure A.17. Stress-strain curve of the second squeezed sample

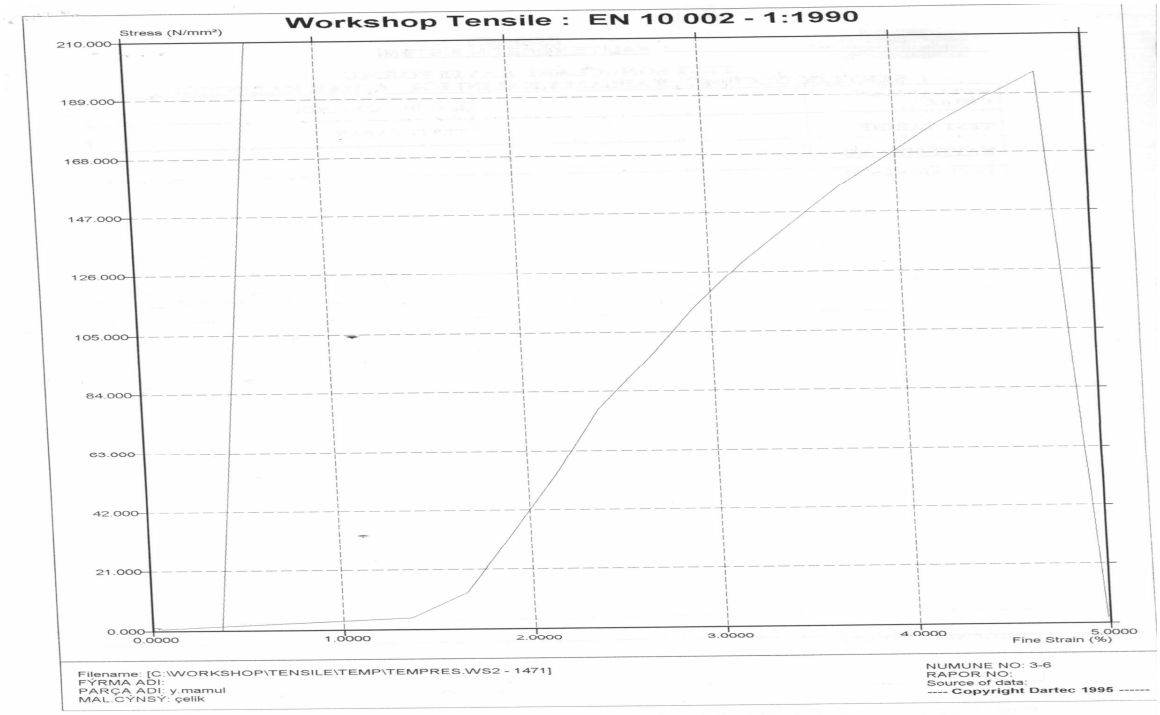

Figure A.18. Stress-strain curve of the thirth squeezed sample

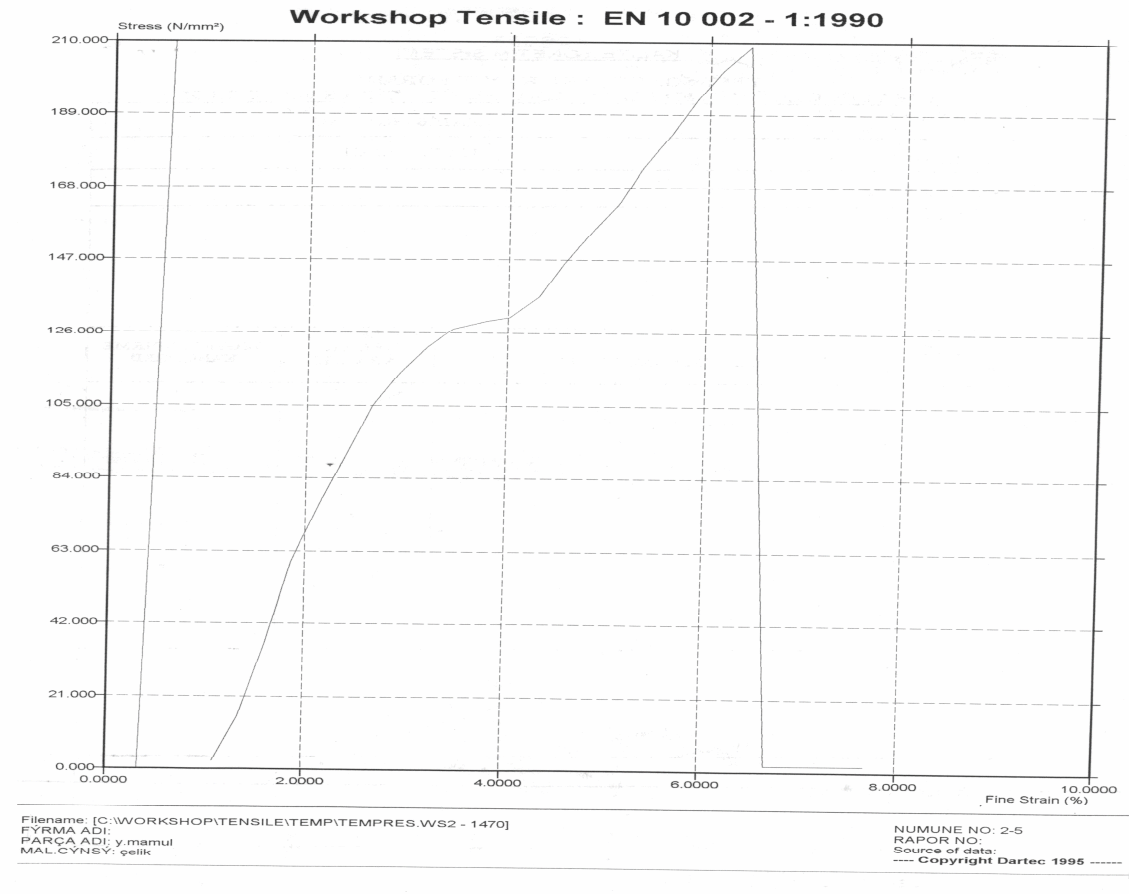

Figure A.19. Stress-strain curve of the fourth squeezed sample

REFERENCES

1. Vinarcik, E. J., ‘‘High Integrity Die Casting Process’’, John Wiley & Sons, New York, 2003.

2. Saçlı, O., ‘‘A Numerical And Quantitative Analysis of An Al-Si Alloy’’, M.S. Thesis, Boğaziçi University, 2001.

3. Sturges, ‘‘First Manually Operated Machine For Casting Printing Type’’, Patent, 1849.

4. New York, N.Y.: The New Jersey zinc company, ‘‘Practical Considerations in Die Casting Design’’, 1955.

5. Savaş, M. A. and S. Altıntaş, ‘‘Control of Mechanical and Wear Properties of a Commercial Al-Si Eutectic Alloy’’, Journal of Materials Science, Vol. 27, pp. 1255-1260, March, 1992.

6. Schey, J. A., ‘‘Introduction to Manufacturing Processes’’, McGraw-Hill,1987.

7. Niu X.P., H. Hu, I. Pinwill and H. Li, ‘‘Vacuum assisted high pressure die casting of aluminium alloys’’, *Journal of Materials Processing Technology, Volume 105, Issues 1-2, Pages 119-127, 7 September 2000.*

8. Chadwik G. A. and T. M. Yue, ‘‘Principles and applications of squeeze castings’’, Met. Mater. 5 (1), pp.6-12, 1989.

9. Ghomashchi M. R. and A. Vikhrov, ‘‘Squeeze casting: an overview’’Journal of Materials Processing Technology, vol. 101, pp. 1-9, 2000.

10. New York, N.Y. : The New Jersey zinc company, ‘‘Die Casting For Engineers’’, 1953.

11. Youn S. W., C. G. Kang, and P. K. Seo, ‘‘Thermal fluid/solidification analysis of automobile part by horizontal squeeze casting process and experimental evaluation’’, *Journal of Materials Processing Technology*, vol. 146, pp. 294-302, 2004.

12. http://www.osti.gov/bridge/servlets/purl/801193-l6DxFj/native/801193.pdf, ‘‘Optimization of the squeeze casting process for aluminum alloy parts’’, D.Schwam, J.F. Wallace, Q.Chang, Y.Zhu.

13. L.J. Yang ‘‘The effect of casting temperature on the properties of squeeze cast aluminium and zinc alloys’’, *Journal of Materials Processing Technology, Volume 140, Issues 1-3, , Pages 391-39, 22 September 2003.*

14. Dr.-Ing. G. Hartmann, ‘‘Integration of Casting Simulation into the Design Process Structural Chain.pdf’’ TCN CAE Conference *by* North American Die Casitng Association, Sardigna, Italy , October 2-5, 2003.

15. Qingyou Han and Hanbing Xu, ‘‘Fluidity of alloys under high pressure die casting conditions’’, *Scripta Materialia, Volume 53, Issue 1, Pages 7-10, July 2005.*

16. Z. W. Chen, ‘‘Skin solidification during high pressure die casting of Al–11Si–2Cu–1Fe alloy’’, Materials *Science and Engineering A, Volume 348, Issues 1-2,* Pages145-*153, 15 May 2003.*

17. http://www.magmasoft.com/conpresso/: ‘‘Modeling and simulation in high-pressure die casting’’, Dr.-Ing. E. Flender, Dr.-Ing. G. Hartmann, MAGMA GmbH.

18. http://www.magmasoft.com/conpresso/: ‘‘Application of Simulation As A Front-End Design Tool.pdf’’, Winston Sequeira, Steve Sikorski, MAGMA Foundry Techn., Inc., Matt Brown, Port City Group.

19. Shuhua Yue, G. Wang, F. Yin, Y. Wang and J. Yang, ‘‘Application of an integrated CAD/CAE/CAM system for die casting dies’’, *Journal of Materials Processing*

Technology, Volume 139, Issues 1-3, Pages 465-468, 20 August 2003.

20. Paul W. Cleary and Joseph Ha, ‘‘Three-dimensional smoothed particle hydrodynamics simulation of high pressure die casting of light metal components’’, *Journal of Light Metals, Volume 2, Issue 3, August 2002, Pages 169-183.*

21. Paul Cleary, Joseph Ha, Vladimir Alguine and Thang Nguyen, ‘‘Flow modelling in casting processes’’, *Applied Mathematical Modelling, Volume 26, Issue 2, February 2002, Pages171-190.*

22. D. H. Lee , P. K. Seo and C. G. Kang, ‘‘Die design by filling analysis of semi-solid injection forging process and their experimental investigation’’, *Journal of Materials Processing Technology, Volume 147, Issue 1, 30 March 2004, Pages 45-50*

23. Matthew S. Dargusch, G. Dour, N. Schauer, C.M. Dinnis and G. Savage, ‘‘The influence of pressure during solidification of high pressure die cast aluminium telecommunications components’’, *Journal of Materials Processing Technology,* vol. xx (2006), pp. xx-xx, article in press

24. C. G. Kang, Y. I. Son and S. W. Youn, ‘‘Experimental investigation of semi-solid casting and die design by thermal fluid-solidification analysis’’, *Journal of Materials Processing Technology, Volume 113, Issues 1-3, 15 June 2001, Pages 251-256*

25. Spada A. T., 2004, Modern Casting

26. Carl B. Rundmann, ‘Metal Casting’